Volume 49
Number 9
7 May 2020
Pages 2525–2844

Chem Soc Rev

Chemical Society Reviews

rsc.li/chem-soc-rev

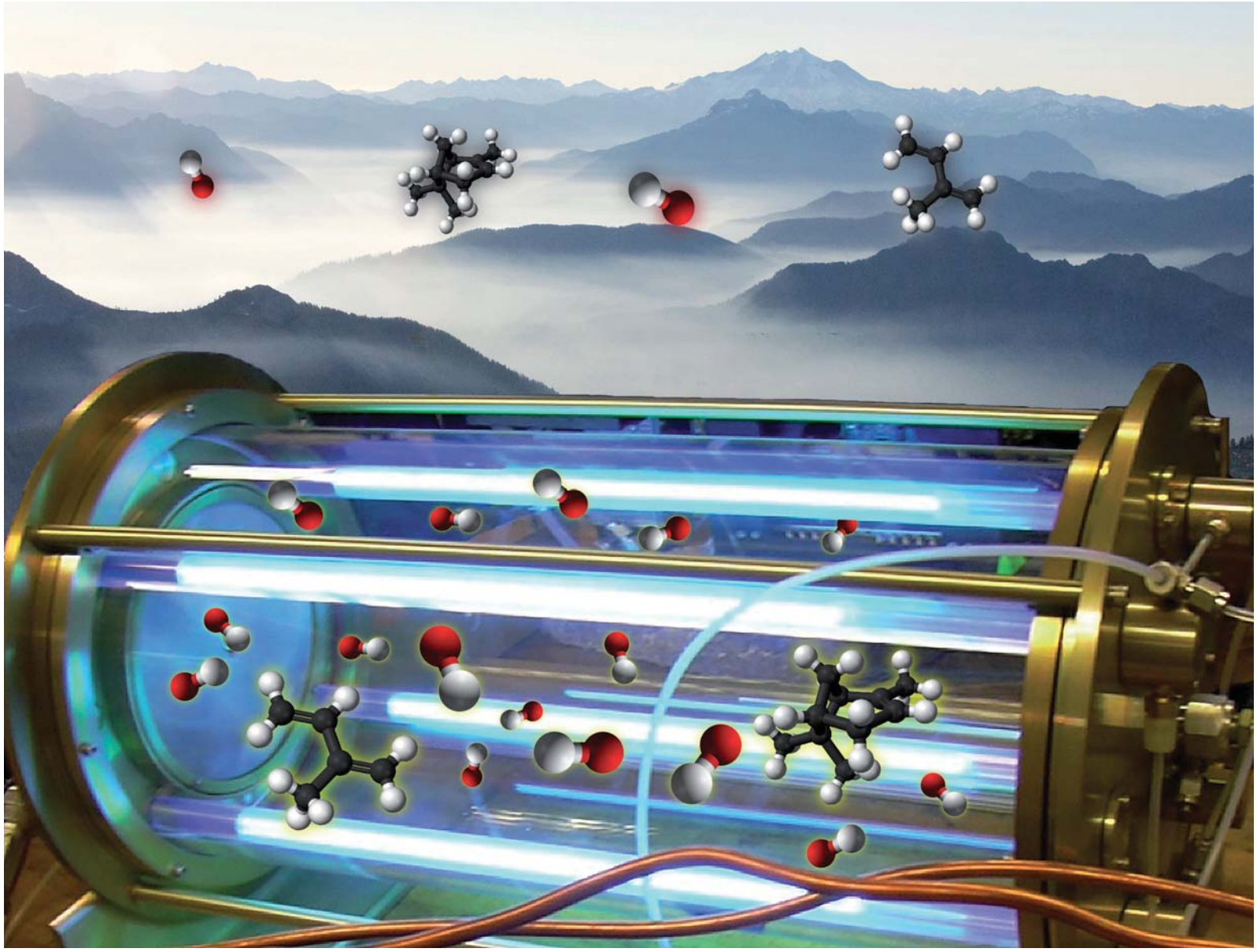

ISSN 0306-0012

ROYAL SOCIETY OF CHEMISTRY

REVIEW ARTICLE

Zhe Peng and Jose L. Jimenez

Radical chemistry in oxidation flow reactors for atmospheric chemistry research

Chem Soc Rev

REVIEW ARTICLE

View Article Online
View Journal | View Issue

Cite this: *Chem. Soc. Rev.*, 2020, **49**, 2570

Radical chemistry in oxidation flow reactors for atmospheric chemistry research†

Zhe Peng * and Jose L. Jimenez *

Environmental chambers have been playing a vital role in atmospheric chemistry research for seven decades. In last decade, oxidation flow reactors (OFR) have emerged as a promising alternative to chambers to study complex multigenerational chemistry. OFR can generate higher-than-ambient concentrations of oxidants *via* H_2O, O_2 and O_3 photolysis by low-pressure-Hg-lamp emissions and reach hours to days of equivalent photochemical aging in just minutes of real time. The use of OFR for volatile-organic-compound (VOC) oxidation and secondary-organic-aerosol formation has grown very rapidly recently. However, the lack of detailed understanding of OFR photochemistry left room for speculation that OFR chemistry may be generally irrelevant to the troposphere, since its initial oxidant generation is similar to stratosphere. Recently, a series of studies have been conducted to address important open questions on OFR chemistry and to guide experimental design and interpretation. In this Review, we present a comprehensive picture connecting the chemistries of hydroxyl (OH) and hydroperoxy radicals, oxidized nitrogen species and organic peroxy radicals (RO_2) in OFR. Potential lack of tropospheric relevance associated with these chemistries, as well as the physical conditions resulting in it will also be reviewed. When atmospheric oxidation is dominated by OH, OFR conditions can often be similar to ambient conditions, as OH dominates against undesired non-OH effects. One key reason for tropospherically-irrelevant/undesired VOC fate is that under some conditions, OH is drastically reduced while non-tropospheric/undesired VOC reactants are not. The most frequent problems are running experiments with too high precursor concentrations, too high UV and/or too low humidity. On other hand, another cause of deviation from ambient chemistry in OFR is that some tropospherically-relevant non-OH chemistry (*e.g.* VOC photolysis in UVA and UVB) is not sufficiently represented under some conditions. In addition, the fate of RO_2 produced from VOC oxidation can be kept relevant to the troposphere. However, in some cases RO_2 lifetime can be too short for atmospherically-relevant RO_2 chemistry, including its isomerization. OFR applications using only photolysis of injected O_3 to generate OH are less preferable than those using both 185 and 254 nm photons (without O_3 injection) for several reasons. When a relatively low equivalent photochemical age ($< \sim 1$ d) and high NO are needed, OH and NO generation by organic-nitrite photolysis in the UVA range is preferable. We also discuss how to achieve the atmospheric relevance for different purposes in OFR experimental planning.

Received 6th November 2019

DOI: 10.1039/c9cs00766k

rsc.li/chem-soc-rev

1. Introduction

Oxidation processes play a central role in the chemistry occurring in Earth's atmosphere.[1] Volatile organic compounds (VOCs) and inorganic gases (*e.g.* CO, SO_2 and NO_x (= NO + NO_2)) emitted by biological and human activities into the atmosphere are oxidized by ambient oxidants such as hydroxyl radicals (OH) and O_3.[2,3] Those processes alter the radical balance in the atmosphere and are the fundamental cause of atmospheric self-cleaning.[1] On the other hand, they also contribute to the formation of O_3[2,3] and secondary aerosols[2,4–7] in the troposphere, both of which are major air pollutants and deleterious to human health.[8–10] In addition, secondary aerosols are also a major source of uncertainty in the radiative balance of the atmosphere and thus the Earth's climate modeling.[11]

Atmospheric chemists started to address these challenges more than seven decades ago. Since the pioneer Haagen-Smit's[2] generation, environmental chambers have been a vital tool in atmospheric chemistry research, particularly for one of its three pillars, laboratory studies.[12,13] Chambers have been widely used in the research of crop damage due to air pollution,[2] kinetics of atmospherically relevant gas-phase reactions,[14] simulation of VOC oxidation and secondary organic aerosol (SOA) formation,[15–17]

Cooperative Institute for Research in Environmental Sciences and Department of Chemistry, University of Colorado, Boulder, Colorado 80309, USA.
E-mail: zhe.peng@colorado.edu, jose.jimenez@colorado.edu

† Electronic supplementary information (ESI) available. See DOI: 10.1039/c9cs00766k

new particle formation,[18] atmospheric multiphase chemistry,[19] ice nucleation[20] and many other atmospheric chemistry-related topics.

Chambers to study atmospheric oxidation processes generally use actinic wavelength ($>\sim$300 nm) light sources (*e.g.* black-lights and sunlight), the emitted photons of which also exist in the troposphere. The photon absorption by molecules initiates the photochemistry in the chamber by generating radicals and major oxidants (most commonly, OH).[15,16] With light sources of similar wavelength range and intensity as the sunlit troposphere, chambers usually sustain OH radicals in them at levels similar to or slightly higher than the troposphere (10^6–10^7 molecules cm^{-3} *vs.* average ambient OH concentration: 1.5×10^6 molecules cm^{-3}).[21] With other precursor concentrations also similar to ambient values, rates of most of processes occurring in chambers can be relatively easily kept comparable to those in the troposphere. This enhances the atmospheric relevance of chamber experiments and is one of the main advantages of chambers. This feature also implies that for a mixture of species to reach a certain integrated oxidant exposure, the reaction/aging time that the mixture needs in chambers is also similar to that in the atmosphere (a.k.a. "photochemical age").

In last decade, chamber wall effects have been gaining a lot of attention.[22–25] Reactive gases and aerosols are substantially lost (adsorbed) to Teflon chamber walls typically in 15 min.[22–24] Stainless steel chamber walls can catalyze some reactions.[25] Particles are also lost to walls by diffusion and electrophoresis.[26] Wall losses alone can usually prevent chamber experiments from being longer than 1 d, and thereby from achieving photochemical ages that significantly higher than 1 d. However, many atmospheric oxidation process lifetimes are much longer than 1 d, *e.g.* reaction of benzene with OH[27] and heterogeneous oxidation of organic aerosols.[28]

Oxidation flow reactors (OFR),[29,30] defined in this Review as flow reactors using oxidants with substantially (often orders of magnitude) higher concentrations than in the atmosphere to accelerate the oxidation chemistry in them, have emerged as an alternative to traditional chambers. OFRs can have high oxidative capacity (*e.g.* a photochemical age of a day or more can be reached in a few minutes), and hence short needed residence times (minutes) and reduced wall effects.[31,32] Besides, OFR are generally much smaller (volume typically in L) than chambers (volume typically in m^3). This logistical advantage allows OFR to go beyond laboratory applications, *e.g.* be deployed to field,[31,33–35] aircraft[36] and source studies.[37–39]

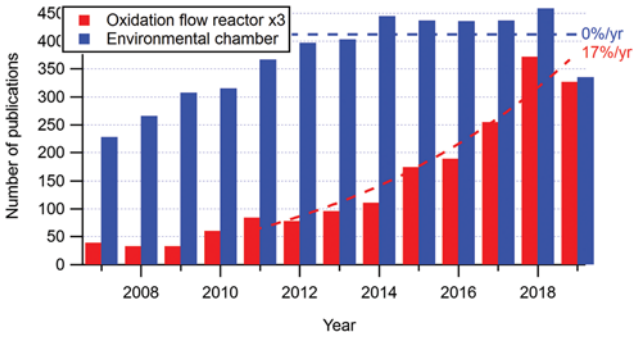

Fig. 1 Annual numbers of the publications concerning OFR and environmental chambers. The data are based on Google Scholar search (as of September 4, 2019) with the search string (*"oxidation flow reactor" OR "potential aerosol mass" OR "Toronto photo-oxidation flow tube" OR "Caltech photo-oxidation flow tube") AND "organic aerosol"* for OFR and the search string (*"smog chamber" OR "environmental chamber") AND "organic aerosol"* for chamber. A few ($\leq$4 year^{-1}) additional papers for OFR that are well-known in the OFR field but cannot be identified in the Google Scholar search are also taken into account. The growth curves are fitted with the data between 2011 and 2019 using exponential functions.

Due to these advantages of OFR, they have been rapidly gaining popularity. In the last decade, the annual number of publications concerning OFR has increased from very small to $\sim$1/3 of those using chambers for organic aerosol studies (Fig. 1), and is still increasing exponentially. Despite the growing popularity of OFR, concerns over the atmospheric relevance of the radical chemistry and hence gas and aerosol products in OFR has persisted, in particular due to the very strong oxidative capacity of OFR (up to several orders of magnitude stronger than

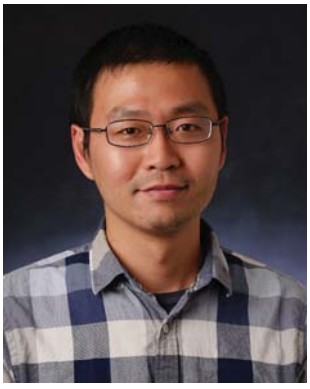

Zhe Peng

Zhe Peng is a Research Scientist at the Cooperative Institute for Research in Environmental Sciences (CIRES) and Department of Chemistry, University of Colorado-Boulder. He received BS from Wuhan University, China and PhD from Université Paris-Sud, France, both in Chemistry. Since 2014, he has been working in the group of Prof. Jose L. Jimenez at CIRES, with understanding the chemistry in oxidation flow reactor being one of his research foci. His current interests include modeling of volatile organic compound oxidation and aerosol formation in both the atmosphere and laboratory experiments.

Jose L. Jimenez

Jose Luis Jimenez is a Professor of Chemistry and a Fellow of CIRES at the University of Colorado-Boulder. He received an MS from the Universidad de Zaragoza, Spain, and the Université de Technologie de Compiègne, France in 1993, and a PhD from Massachusetts Institute of Technology in 1999. His group develops and applies advanced mass spectrometric techniques for atmospheric aerosols. He is a Highly Cited Researcher and a Fellow of the American Association for Aerosol Research and the American Geophysical Union.

the atmosphere) and the distinct radical generation methods (see Section 2).[40–44] A series of recent studies has addressed the atmospheric relevance of OFR chemistry.[45–50] These studies have provided detailed characterizations of the radical chemistry in various types of OFR, and thereby laid down the foundation of a meaningful planning of OFR experiments by clarifying the conditions that lead to atmospherically relevant results and those that do not.

In this Review, we summarize the various types of OFR and their operation modes (Section 2) and summarize prior studies of OFR chemistry (Section 3). Based on the current knowledge about OFR chemistry, we also comprehensively discuss its atmospheric relevance in a wide range of conditions (Section 4) and OFR experimental planning (Section 5).Finally, we will conclude with a summary and provide our outlook to the future research directions in this field (Section 6).

2. OFR for atmospheric chemistry research

In this section we summarize all OFR operation modes and corresponding reactors in use that have been developed so far (Table 1 and Fig. 2). As OH is the most important oxidant in the atmosphere, OFR with OH as the main oxidant is by far the most common type of OFR. This section, as well as other sections of this Review, will have an emphasis on OH OFR, while discussing OFR with other species as the main oxidant when appropriate.

2.1. OH OFR under low NO conditions

The early OH OFR development focused on OH production and did not consider the perturbation of the radical chemistry in OFR by nitrogen oxides ($NO_x = NO + NO_2$).[29,30] NO concentration is an important quantity in OFR, and more generally in atmospheric chemistry, because it regulates the fate of organic peroxy radicals (RO_2), a type of radical intermediates that are almost always formed upon reactions of VOCs with OH and thereby play a central role in atmospheric organic chemistry (VOC oxidation, SOA formation *etc.*).[51] In this Review, we adopt the terminology proposed by Wennberg,[52] in which ''high-NO'' and ''low-NO'' conditions refer to those under which the dominant fate of RO_2 is reaction with NO and other reactions (*e.g.* reactions with HO_2 or another RO_2, or isomerization), respectively.[51,53] Urban atmospheres are often high-NO environments, because of high NO emissions from vehicles and other combustion and industrial sources,[54] while remote and pristine areas usually have low-NO atmospheres due to low influence of anthropogenic NO emissions. Following the development sequence, we will also first discuss OH OFR under low NO_x conditions.

2.1.1. OFR254. One of early and widely known OFR used for comprehensive speed-up of chemistry, the Toronto Photo-Oxidation Flow Tube (TPOT),[29] was operated in a mode currently

Table 1 Summary of OFR operation modes and corresponding reactors in practical use

Main oxidant	Oxidant generation (NO generation)	Operation mode notation	Reactor(s) in use	Representative reference
OH	O_3 photolysis at 254/266 nm (including initial NO injection)	OFR254/266	TPOT	29
			PAM	56
			LBNL FTR	76
			TSAR	83
			MIT quartz flow tube	81
			Go:PAM	39
			PEAR	84
			Unnamed reactor	82
	H_2O photolysis at 185 nm and O_3 photolysis at 254 nm (including initial NO injection)	OFR185	PAM	30
			LBNL CFSTR	85
			MSC	60
			CPOT	61
			F-OFR	68
	H_2O_2 photolysis by UVA or UVB		CPOT	61
	O_3 photolysis at 254 nm (NO generated by $N_2O + O(^1D)$)	OFR254-iN_2O	PAM	86
	H_2O photolysis at 185 nm and O_3 photolysis at 254 nm (NO generated by $N_2O + O(^1D)$)	OFR185-iN_2O	PAM	49
	H_2O photolysis at 185 nm and O_3 photolysis at 254 nm (NO continuously injected along the flow)	OFR185-cNO	PAM (only numerically evaluated)	49
	iPrONO photolysis at 369 nm (NO generated in the same manner)	OFR369-i(iPrONO)	PAM	87
	HONO photolysis at ~360 nm (NO generated in the same manner)		PhoFR	93
			Unnamed reactor	92
	Reactions of H produced from H_2/He microwave discharge with O_2 or NO_2		Harvard high-pressure flow system	96
			Unnamed reactor	95
O_3	Externally generated by O_3 generator		UCI aerosol flow system	102
			LBNL FTR	109
			PAM	101
			Unnamed reactor	103
NO_3	Decomposition of N_2O_5 injected from a cold trap		PAM	101
Cl	Cl_2 photolysis at 355 nm		Unnamed reactor	82

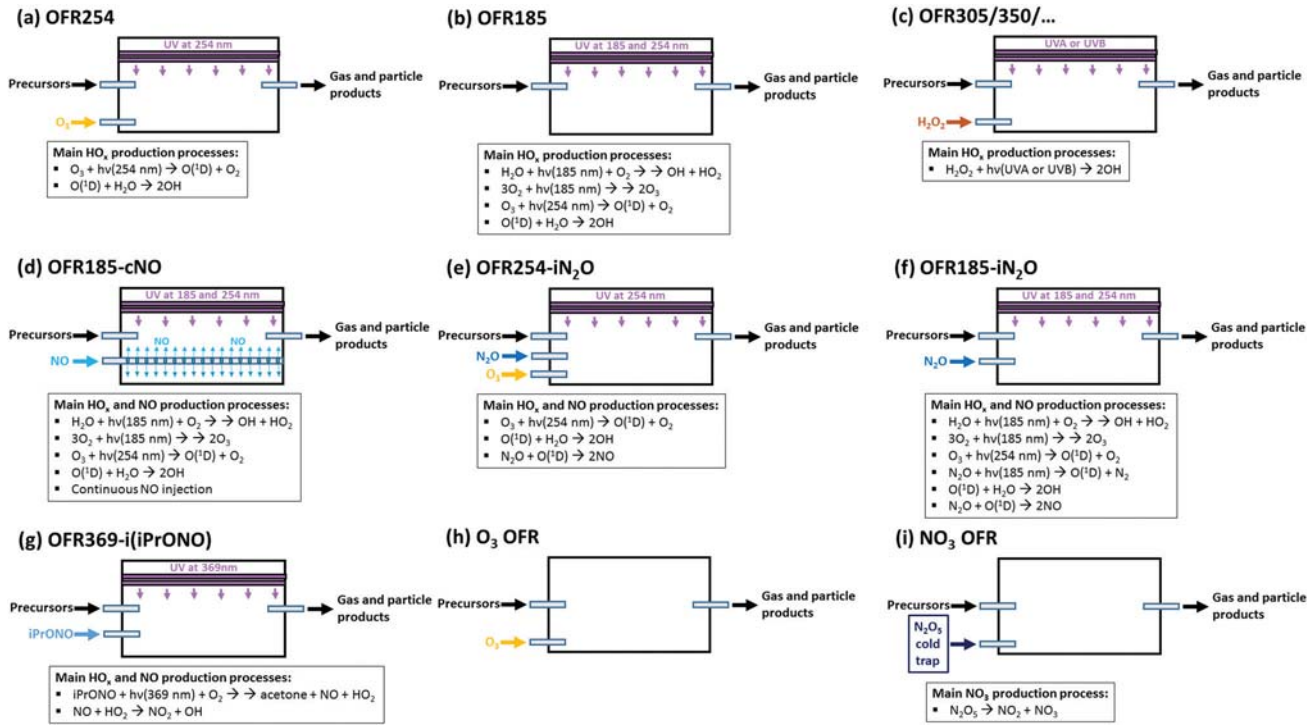

Fig. 2 Schematics of different operation modes summarized in the Review. Two consecutive arrows ("→ →") denotes that the corresponding reaction is not elementary and some elementary steps are omitted.

termed "OFR254", in which "254" stands for 254 nm UV light being the photochemistry initiator (Fig. 2a). UV at 254 nm is provided by low-pressure Hg lamps in most OFR and photolyzes O_3 that is externally generated and then injected into the reactor. This photolysis produces $O(^1D)$, which reacts with water vapor to generate OH. Many low-pressure Hg lamps also emit UV at 185 nm, which is always filtered (*e.g.* by quartz lamp sleeve)[30] in OFR254. Since 254 nm photons are not sufficiently energetic to photolyze any major air components (N_2, O_2, H_2O, CO_2 *etc.*) to produce radicals,[55] injection of externally formed O_3 is indispensable for OH production in OFR254.

2.1.2. OFR185. Another pioneering OFR for comprehensive oxidation chemistry acceleration, the Potential Aerosol Mass (PAM) reactor, though also able be to run in OFR254,[56,57] was first operated in the "OFR185" mode[58,59] and other later reactors were also designed to be able to run in this mode.[60,61] "185" in the naming notation means that UV at 185 nm is also used for OH generation (Fig. 2b). In this operation mode, 185 nm UV is also emitted by low-pressure Hg lamps, but not filtered as in the OFR254 mode. 185 nm photons are energetic enough to break H_2O molecules into H (which then recombines with O_2 to form hydroperoxy radical (HO_2)) and OH, and to dissociate O_2 into $O(^3P)$.[55] As water photolysis alone can produce OH, externally generated O_3 is no longer needed. In addition, $O(^3P)$ recombines with O_2, forming O_3, which is also able to produce OH with the help of 254 nm UV emitted by Hg lamps, as in OFR254. Without the need for an O_3 generator, OFR185 has a lower logistical burden and thus has been more often deployed outside the laboratory.[31,33,34,36,37,62–65]

2.1.3. Commonly used OFR(s) of this type. As OFR185 and OFR254 are the most basic operation modes and have undergone the longest development (since the first OFR were built), they are regarded as the most mature modes, and have been the most widely used modes as well. A number of OFR that can be operated in these modes (Table 1) have been designed. There have already been many publications using these reactors.[66]

Among them, the PAM OFR is far more popular than the others and the only one that has been commercialized so far (by Aerodyne Research, Inc., Billerica, Massachusetts, USA). More than 40 research groups worldwide are currently using PAM reactors. The PAM reactor is a cylindrical vessel with an internal diameter of ~20 cm and a volume of ~10 L and usually with a residence time of ~100–200 s. Low-pressure Hg lamps are installed inside the reactor. PAM has a few designs with different wall materials, of which the most common ones are quartz and aluminum. PAM has been used in laboratory (*e.g.* ref. 59), field (*e.g.* ref. 31), source (*e.g.* ref. 37) and aircraft (*e.g.* ref. 36) studies. While PAM has been mainly used for VOC oxidation and SOA formation studies, it has also been used to study organic aerosol (OA) aging (heterogeneous oxidation).[33] Two other OFR, Gothenburg Potential Aerosol Mass (Go:PAM)[35,39,67] and Field-Oxidation Flow Reactor (F-OFR),[65,68–70] can be considered as variants of PAM in terms of operation, chemistry and result interpretation, although their geometries are either longer and more tube-like (Go:PAM) or smaller (F-OFR).

TPOT[28,29,71–74] is the best-known representative of another OFR design, all of which have smaller volumes than PAM and are run in OFR254 mode and mainly for OA heterogeneous

oxidation. In addition to TPOT, this type of OFR includes the Lawrence Berkeley National Laboratory Flow Tube Reactor (LNBL FTR),[75–80] the MIT Quartz Flow Tube[81] and a flow tube designed by Smith *et al.* at the University of Georgia.[82] The other two OFR254 reactors are either much smaller (Tampere University of Technology Secondary Aerosol Reactor (TSAR))[83] or significantly larger than PAM (Photochemical Emission Aging flow tube Reactor (PEAR)).[84] TSAR is so small that it can be made into a tool box to identify emissions from mobile sources, while PEAR has a volume of 139 L for high-throughput SOA production for emission exposure studies.

In addition to PAM, three additional reactors have reported the use of the OFR185 mode, *i.e.* Mini Smog Chamber (MSC),[60] Caltech Photo-Oxidation Flow Tube (CPOT)[61] and the Lawrence Berkeley National Laboratory Continuous Flow Stirred Tank Reactor (LBNL CFSTR).[85] Similar to TSAR, MSC, with a very small volume (0.15 L), is used to monitor real-time SOA formation potential of combustion emissions. CPOT is much longer and larger (55 L) than PAM and specifically designed to have a well-controlled residence time distribution (RTD) close to that of laminar flow. Due to these features, CPOT has laboratory applications only. Note that CPOT can also adopt a traditional OH generation method used in chambers, *i.e.* H_2O_2 photolysis by blacklights (Fig. 2c). Although not discussed further here, we note that small reactor sizes and short residence times can lead to major losses of condensable vapors, especially under lower pre-existing aerosol concentrations.[31] The LBNL CFSTR is an even larger ($\sim$150 L) reactor equipped with an impeller ensuring that gases and particles are well-mixed in the reactor. This reactor does not aim for a laminar-like RTD but for good mixing in it, which can be useful in studies of heterogeneous and particle-phase chemistry.

2.2. OH OFR targeting high NO chemistry

As NO reacts relatively rapidly with both HO_x (= OH + HO_2) and O_3,[55] its lifetime was too short in the extremely oxidative environment of initially-developed OH OFR to have an impact on VOC oxidation and SOA formation.[45] This limited the initial OFR to simulate only low-NO conditions. To overcome this difficulty, several methods have been proposed and/or tested.[48,49,86,87] All of them require injection of N-containing species as direct or indirect (precursor) sources of NO. Although all these methods are always able to increase the NO concentration in OFR to some extent, they do not necessarily lead to a high-NO environment under all experimental conditions, as NO may not be sufficiently high to dominate RO_2 fate. Nevertheless, injection of a significant amount of NO or of its precursors always results in major oxidized nitrogen species (NO_y = NO_x + NO_3 (nitrate radical) + HNO_3 + HO_2NO_2 (peroxynitric acid) + ...) chemistry occurring (see Section 3.2).

2.2.1. OFR185/254-iNO. The simplest way to introduce a source of NO into OFR is a direct NO injection, denoted as OFR185/254-iNO, in which "iNO" refers to initial injection of NO (Table 1). This mode is also the one with the longest history that requires NO source/precursor injection.[38] Peng and Jimenez[48] showed that, despite fast reactions of NO with the main oxidants in OFR, meaningful high-NO conditions are difficult but possible to achieve in OFR185-iNO, while they are generally not possible for OFR254-iNO. Further details will be discussed in the following sections.

2.2.2. OFR185-cNO. Recently, Peng *et al.*[49] proposed a technique to maintain the NO level in OFR185 by continuously injecting NO through perforated tubes along the flow (Fig. 2d). "cNO" in the operation mode notation stands for continuous NO injection. Although this technique has not yet been experimentally validated, it has been numerically verified that cNO can be an effective method to maintain high-NO conditions, since NO destroyed by the oxidants can be quickly replenished by new injection along the flow.

2.2.3. OFR185/254-iN$_2$O. Lambe *et al.*[86] and Peng *et al.*[49] proposed initial injection of a very large amount (percent level) of N_2O into OFR254 (OFR254-iN_2O) and OFR185 (OFR185-iN_2O), respectively, to maintain high NO (Table 1 and Fig. 2e and f). The iN_2O technique has been shown to be effective experimentally by Lambe *et al.*[86] and numerically by Peng *et al.*[49] N_2O can react with $O(^1D)$ to produce NO, and N_2O (at percent level) can compete with water vapor in reacting with $O(^1D)$.[88] In OFR254-iN_2O, $O(^1D)$ is supplied by O_3 photolysis as discussed above; in OFR185-iN_2O, it is mainly produced by N_2O photolysis at 185 nm. Except for these reactions, N_2O is a quite inert gas, and thus can serve as a stable NO precursor supply without causing other experimental complications. In this Review, when OFR185/254 and OFR185/254-iN_2O are discussed as a whole (for a range of RO_2 fate from zero NO to high NO), they are denoted as OFR185/254(-iN_2O).

2.2.4. OFR369-i(iPrONO). This operation mode employs a different light source (UV at 369 nm) and OH and NO precursor (isopropyl nitrite (iPrONO)) (Table 1 and Fig. 2g). It is similar to a common method for the simultaneous generation of OH and NO in chambers, *i.e.* nitrite photolysis in the UVA range.[89,90] Its feasibility was first demonstrated through both experiments and modeling by Lambe *et al.*,[87] who tested several nitrites as precursors and found that iPrONO is the most chemically and economically viable one.

In this mode, OH is no longer generated by H_2O photolysis or reaction of $O(^1D)$ and H_2O, but by reaction of NO and HO_2.[55] NO is produced by photolysis of the nitrite, while HO_2 is formed by the H abstraction by O_2 from the alkoxy radical (RO),[7] the other product of nitrite photolysis.[91] Note that UV at 185 and 254 nm can also photolyze nitrite, but are not used in this mode because it is not necessary for nitrite photolysis and could introduce significant non-tropospheric chemistry (see Section 4).

2.2.5. Other OH-generation methods. There are other OH-generation methods. However, they often require more complex setups and thus are limited to laboratory applications. Here we discuss two examples. Similar to iPrONO, nitrous acid (HONO) can be used as a precursor of both OH and NO, through its photolysis in the UVA range.[92,93] HONO is produced by the reaction of HCl with $NaNO_2$. In addition, H_2/He mixture microwave discharge can also be a source of OH.[94] In the discharge, H atoms are generated then react with either NO_2[94,95] or O_2.[96] The former method produces OH and NO, while the latter generates HO_2, which reacts with subsequently added NO to form OH.

2.2.6. Commonly used OFR(s) of this type. To our knowledge, PAM is currently the only type of OFR using UVC as light source that has been used specifically to create OH oxidation environment with a significant presence of NO. Although such a goal is difficult to achieve,[48,49] efforts have been made to enable PAM for this application.[48,49,86,87] As these new modes were all recently proposed and/or evaluated, there has been only one published application to date.[97]

Despite its high instrumental complexity, the H_2/He microwave discharge system had more applications to study OH oxidation in the presence of NO than PAM.[95,98–100] All of those applications are however more traditional gas-phase chemical kinetics studies. The HONO photolysis method, to our knowledge, has not been applied in any atmospheric chemistry studies where NO plays an important role. H_2SO_4 particle formation through SO_2 oxidation by OH in a Photolytic Flow Reactor (PhoFR) used this technique,[93] but NO was not involved in the key oxidation process of interest.

2.3. OFR with other oxidants

In addition to OH oxidation, oxidation of VOCs by other oxidants, *e.g.* O_3 and NO_3, can also be studied in an OFR.[101,102] As O_3 and NO_3 are both externally generated and not involved in any chemistry except the VOC oxidation steps, O_3 and NO_3 OFR are conceptually and mechanistically simpler than the OH versions. Besides, as O_3 and NO_3 OFR do not require UV light to initiate chemistry, they are also conceptually more similar to chamber and traditional flow reactor experiments, with the main difference being higher concentrations of the oxidants. Therefore, many OFR in principle can also be used for this type of applications.[101–104] Oxidation by chlorine atoms, a method frequently used in chambers,[105] is also in principle accessible to OFR setups. Nevertheless, to our knowledge, it has only been experimentally demonstrated by Smith *et al.*,[82,92] whose flow tube uses the third harmonic (355 nm) of a pulsed Nd:YAG laser to photolyze Cl_2 and generate Cl atoms.

2.3.1. O_3 OFR. In this application, a large amount of O_3 is usually produced by an O_3 generator before being injected into the reactor (Table 1 and Fig. 2h). Then VOC ozonolysis occurs in the reactor under dark (no UV) conditions. Among the early (prior to TPOT and PAM) applications of O_3 OFR are studies of kinetics of heterogeneous and particle-phase O_3 reactions.[82,103,104,106–108] Palm *et al.*[101] used PAM to perform such ozonolysis experiments in a mountain forest. A much larger (1200 L) flow reactor has been employed to study SOA formed by VOC ozonolysis in the laboratory at UC Irvine.[102] Recently, a series of heterogeneous OA ozonolysis studies have been carried out using the LBNL FTR,[109–111] which is mainly used for heterogeneous OA oxidation. F-OFR has also been used in laboratory ozonolysis experiments.[70,112]

2.3.2. NO_3 OFR. Palm *et al.* also conducted NO_3 OFR experiments at the same field site as their ozonolysis experiments.[101] They used the thermal decomposition of N_2O_5 to generate NO_3 ($N_2O_5 \rightarrow NO_2 + NO_3$). N_2O_5 was synthesized and stored in a cold trap, before being warmed into a zero air flow and introduced into the reactor (Table 1 and Fig. 2i). There are some experimental complications that are not shared by OH and O_3 OFR, such as fast N_2O_5 and NO_3 wall loss.[101]

3. Radical chemistry in OH OFR

As discussed above, OH OFR are much more widely used than other types of OFR, and their radical chemistry is significantly more complex than for other oxidants (*e.g.* O_3 and NO_3 OFR). We thus focus on the radical chemistry in OH OFR below. First, we will discuss the chemistry of the main oxidants present in OH OFR, *i.e.* HO_x and O_3. This is followed by the discussions about the NO_y chemistry when significant amounts of NO_x and/or NO precursors are injected, and we examine whether high-NO conditions are really achieved. After the inorganic species, we will summarize the organic side of the radical chemistry of VOC oxidation in OFR, *i.e.* RO_2 production and fate. Finally, methods of oxidant quantification and related issues, both experimental and modeling, will be discussed.

3.1. HO_x and O_3 chemistry

We will only discuss the HO_x/O_3 chemistry for the two basic modes, *i.e.* OFR185 and OFR254, in this subsection. When this chemistry is coupled with other chemistries, *e.g.* NO_y chemistry and VOC oxidation, the influences of other chemistries can be treated as perturbations to the basic HO_x/O_3 chemistry.

3.1.1. OH control by its production and loss. As OH is a radical and has very short lifetimes (usually <1 s), Peng *et al.*[46] analyzed its chemistry using the steady-state (SS) approximation, under which a species concentration can be expressed in the following general form:

$$\text{Concentration} = P/L \quad (1)$$

where P and L are the total production rate (in molecules cm^{-3} s^{-1}) and the total first-order loss rate coefficient (in s^{-1}) of the species of interest, respectively. The specific expression for OH concentration is then

$$\text{OH} = \frac{P_{\text{OH}}}{\text{OHR}} \quad (2)$$

where OHR is the OH reactivity, *i.e.* the first-order loss rate coefficient of OH (and the inverse of the OH lifetime). OHR is, by definition, equal to the sum of the products between the concentrations of the species consuming OH (OH reactants) in the system and the second-order rate coefficients of their reactions with OH ($\text{OHR} = \sum_i k_i \cdot c_i$, where k_i and c_i are the reaction rate coefficient with OH and concentration of the ith OH reactant, respectively). The integral of OH over time, OH exposure (OH_{exp}), is an important measure of photochemical age. Hereafter, we will use "photochemical age" as the time that the averaged ambient OH concentration needs to achieve a certain OH_{exp}.

3.1.2. OH primary production. In many cases P_{OH} is dominated by primary production (see Fig. 3a and b),[46] which is the origin of strong oxidative capacity of OFR. In both OFR185 and OFR254, P_{OH} roughly linearly scales with both UV intensity (abbreviated as UV hereinafter) and water vapor concentration (abbreviated as H_2O hereinafter). It has been confirmed by Peng *et al.*[46] with a box

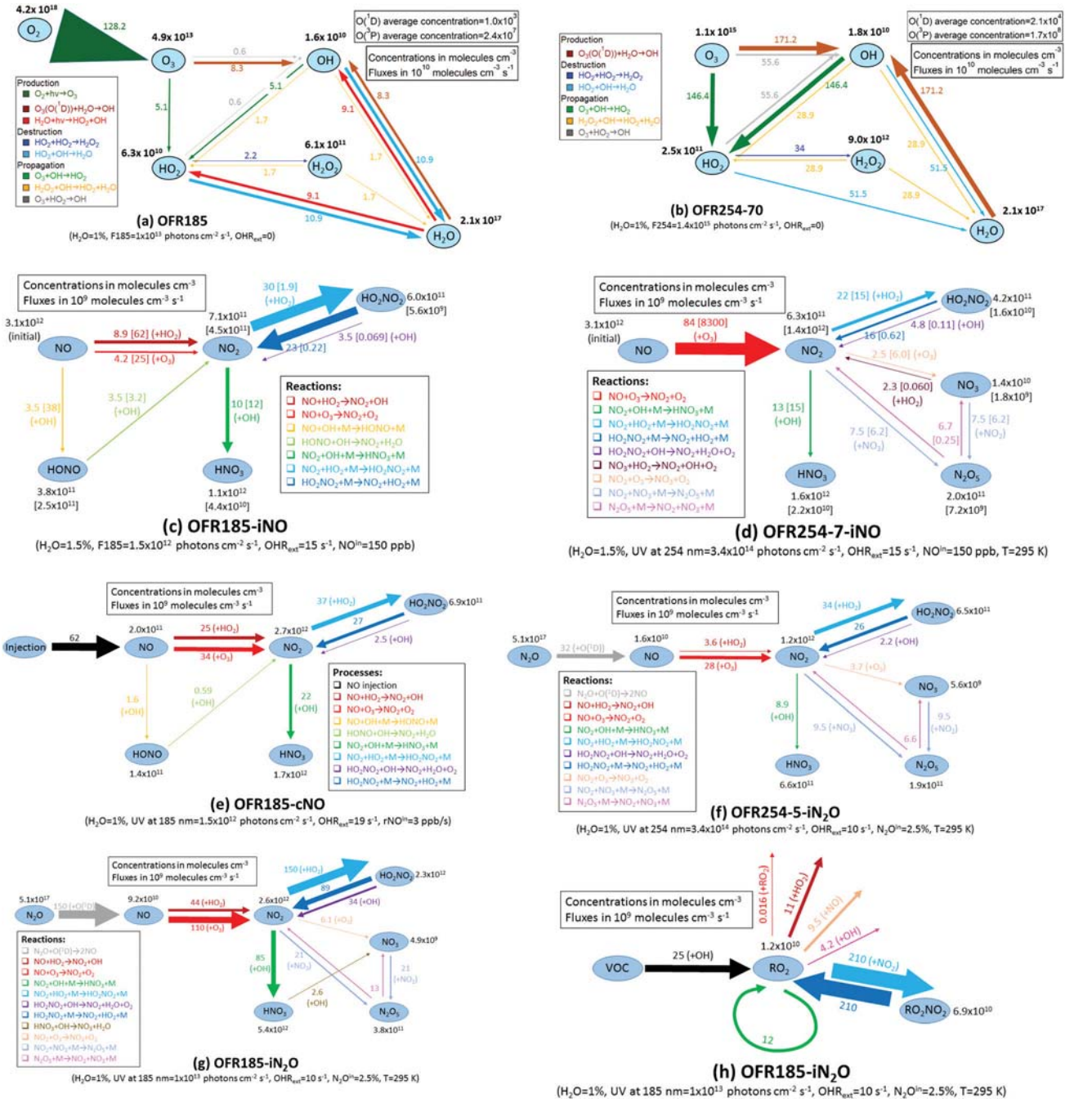

Fig. 3 Schematics of (a and b) HO_x and O_3 chemistry, (c–g) NO_y chemistry and (h) RO_2 chemistry under typical input conditions for several OFR operation modes discussed in this Review. Species average concentrations (in molecules cm^{-3}) are shown in black beside species names. Arrows denote directions of the conversions. Average reaction fluxes (in units of 10^{10} or 10^9 molecules cm^{-3} s^{-1}) are calculated according to the production rate, and shown on or beside the corresponding arrows and in the same color. Within each schematic, the thickness of the arrows is a measure of their corresponding species flux. Multiple arrows in the same color and pointing to the same species should be counted only once for reaction flux on a species. All concentrations and fluxes are average ones over the residence time and have two significant digits. (e–g) Reprinted with permission from ref. 49. Copyright 2018 American Chemical Society.

chemical kinetic model experimentally validated by Li *et al.*[45] in a very wide range of conditions. One of the two main OH production routes, $H_2O + h\nu$ (185 nm) → OH + H, is proportional to both UV intensity (in photons cm^{-2} s^{-1}) at 185 nm (abbreviated as F185 hereinafter) and H_2O (unitless water vapor mixing ratio). The other main OH production route in OFR185 and the only one in OFR254, $O(^1D) + H_2O \rightarrow 2OH$, also scales with H_2O. $O(^1D)$ is an extremely reactive species whose concentration is mainly controlled by its production ($O_3 + h\nu$ (254 nm) → OH + H) and the main loss pathway, *i.e.* collisional deactivation ($O(^1D) + M \rightarrow O(^3P) + M$), under the SS approximation. M can be any major component of the air and is usually effectively a constant. Thus, $O(^1D)$, and

thereby P_{OH} from that channel, also depends on F254 (UV at 254 nm). Li *et al.*[45] characterized the lamp emission at different lamp intensity settings (for Hg lamps model no. 82-9304-03, BHK Inc.) and found F185/F254 ratios in OFR185 to be around 1% with a slightly decreasing trend with lamp setting. Then, P_{OH} is roughly proportional to both F185 and F254 in OFR185.

3.1.3. OH loss. OHR is a combination of two types of contributors, *i.e.* internal (OHR_{int}) and external (OHR_{ext}) OH reactivities. OHR_{int} due to internal OH reactants, *i.e.* those formed in the reactor and/or injected as OH precursor(s); OHR_{ext} is due to external OH reactants, *i.e.* common OH-consuming species in ambient air (SO_2, CO, CH_4, NO_x, VOCs *etc.*). The internal OH reactants in OH OFR are O_3, HO_2, H_2O_2 and OH itself. They are a part of the reaction network of the HO_x and O_3 chemistry (Fig. 3a and b). From the typical cases shown in Fig. 3a and b, it can be found that $2OH + M \rightarrow H_2O_2 + M$ is negligible and $OH + H_2O_2 \rightarrow H_2O + HO_2$ is less important than $OH + O_3 \rightarrow HO_2 + O_2$ and $OH + HO_2 \rightarrow H_2O + O_2$. Thus O_3 and HO_2 are the main internal OH reactants. As they are also produced along with OH under different conditions or can be injected in various amounts, OHR_{int} can vary substantially, from a few to hundreds of s^{-1}.[46] All external OH reactants are introduced into the reactor, and their amounts are controlled by OFR users (for laboratory experiments), by ambient air concentrations, or by source air concentrations plus any applied source dilution. Thus OHR_{ext} can vary even more substantially, from <1 s^{-1} (air in pristine areas)[113] to $>10^5$ s^{-1} (undiluted combustion exhausts).[48]

O_3 production and loss are relatively simple. In OFR185, O_3 is exclusively formed by $O(^3P) + O_2 \rightarrow O_3$ and destroyed though its photolysis at 254 nm, *i.e.* $O_3 + h\nu(254\ nm) \rightarrow O_2 + O(^1D)$, and its reactions with OH and HO_2, *i.e.* $O_3 + OH \rightarrow O_2 + HO_2$ and $O_3 + HO_2 \rightarrow OH + 2O_2$. Note that most $O(^1D)$ converts back to O_3 *via* collisional deactivation to $O(^3P)$ followed by its recombination with O_2 and only $O(^1D)$ reacted with H_2O causes effective O_3 loss. The production rate is much higher than the loss rate (Fig. 3a). As a result, O_3 is always being accumulated during the whole residence time in OFR185. Under most conditions, O_3 increases approximately linearly with time in the reactor.[45,46] Only at relatively high H_2O ($>1\%$) and high lamp settings ($F185 > 1 \times 10^{13}$ photons cm^{-2} s^{-1}), where F254 is also high and a lot of HO_x radicals are created, can O_3 loss rate increase to a significant level compared to its production rate, as its concentrations increases with time. This O_3 increase with time is thus no longer linear in time. In most OFR254 conditions, little O_3 is consumed compared to its injected amount. Under high H_2O and UV, there can be a significant O_3 loss for the same reasons described for OFR185.

The production and loss of HO_2 are more complex than those of O_3. Nevertheless, they are still easy to understand in the absence of external OH reactants. In OFR185, it has a primary production pathway, *i.e.* reaction of H (produced by H_2O photolysis at 185 nm) with O_2, and a major secondary production pathway within the HO_x and O_3 scheme, *i.e.* $O_3 + OH \rightarrow O_2 + HO_2$ (Fig. 3a). This reaction is the only major internal HO_2 production pathway in OFR254 (Fig. 3b). Therefore, HO_2 concentration increases with OH production, because primary and internal secondary HO_2 production rates also increase. The internal HO_2 loss is due to its reactions with O_3, OH, and HO_2 itself ($2HO_2 \rightarrow H_2O_2 + O_2$).

3.1.4. OH suppression and HO_x recycling. As eqn (2) can be written as follows

$$OH = \frac{P_{OH}}{OHR_{int} + OHR_{ext}} \quad (3)$$

it can be expected that introducing OHR_{ext} into an OFR will reduce OH. This phenomenon is referred to as "OH suppression,"[45,46] especially for high values of OHR_{ext}, and is the key to understanding the chemistry of OH OFR systems. The ratio of the remaining OH after the introduction of OHR_{ext} to the original OH concentration in an otherwise-identical system without OHR_{ext} quantifies OH suppression. As discussed above, P_{OH} is mainly primary, and it is a reasonable approximation that P_{OH} does not vary with OHR_{ext}. If we also assume that OHR_{int} is not changed by adding OHR_{ext}, the OH fraction remaining after suppression can be simply estimated in the following manner

$$\frac{OH}{OH_0} = \frac{P_{OH}}{OHR_{int} + OHR_{ext}} \Big/ \frac{P_{OH}}{OHR_{int}} = \frac{OHR_{int}}{OHR_{int} + OHR_{ext}} \quad (4)$$

where OH_0 is the original OH concentration in the absence of OHR_{ext}. Eqn (4) indicates that the higher OHR_{int} (internal OH reactants also consume OH), the weaker OH suppression. Peng *et al.*[46] compared the remaining OH fraction after suppression estimated by eqn (4) and calculated by their full model for their OFR185 and OFR254 model cases across a wide range of conditions and a number of literature laboratory and source studies using OH OFR (Fig. 4). The estimates obtained from eqn (4) are in good agreement with the full model results, which validates the simple relationship described by eqn (4). Indeed it is observed that the higher OHR_{int}, the stronger resilience of the system to the perturbations by external OH reactants.[46] The modeling results have also been confirmed in the laboratory experiments of Li *et al.*[45] with SO_2 and CO as external OH reactants.

The discussions above have a few important implications. One is that in the presence of OHR_{ext} much higher than OHR_{int}, OH can be suppressed by orders of magnitude (Fig. 4). Using OH calibrated at low values of OHR_{ext} to analyze cases with high OHR_{ext} can be very misleading and lead to order-of-magnitude errors in the estimated OH_{exp}.

Another important role that O_3 plays is as a promoter of HO_x recycling.[46] $O_3 + OH \rightarrow O_2 + HO_2$ and $O_3 + HO_2 \rightarrow OH + 2O_2$ are both major secondary production pathways of HO_2 and OH, respectively (Fig. 3a and b). In OFR254, high O_3 injected governs this HO_x interconversion. A HO_x radical may be converted between the forms of OH and HO_2 by O_3 many times before going through a radical chain termination process. The other implication is that O_3, especially in OFR254 as it is injected in large amounts (*e.g.* 60 ppm (denoted as OFR254-60, with "60" for the injected O_3 amount), equivalent to an $OHR_{int} \sim 100\ s^{-1}$), can make the chemical system in OFR much more resilient to OH suppression through the reaction $O_3 + HO_2 \rightarrow OH + 2O_2$.[46] Lower amounts of O_3 (*e.g.* 6 ppm (OFR254-6), equivalent to an $OHR_{int} < \sim 10\ s^{-1}$) injected weaken this resilience in OFR254.

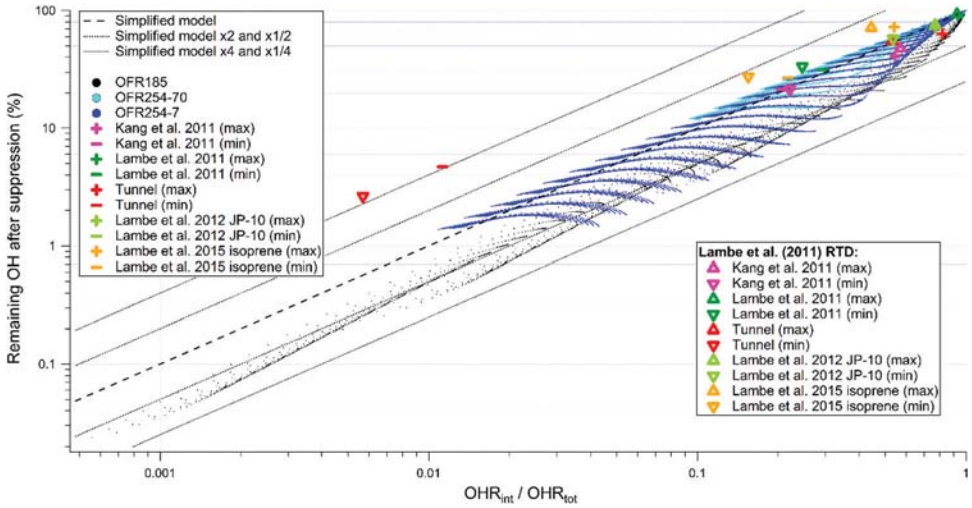

Fig. 4 Percentage of remaining OH after suppression in OFR185 (black dot), OFR254-70 (cyan dots), and OFR254-7 (blue dots) *vs.* the ratio between internal and total OH reactivities. The "simplified model" (eqn (4)) prediction as well as lines at ×2, ×4, ×1/2, and ×1/4 of the simplified model are also shown for comparison. The estimated ranges for laboratory experiments[57,59,203,226] and a source study in an urban tunnel[37] are also shown. These ranges are estimated by the models with plug flow and with the Lambe *et al.*[116] residence time distribution according to the experimental conditions in these studies.

Therefore, it is difficult to achieve a very low OH (10^8 molecules cm^{-3} or lower) in OFR254, even at low H_2O and lamp settings.[46]

HO_x interconversion can be also promoted by external OH reactants. For instance, the product of the reaction of SO_2 with OH, HSO_3, extremely rapidly undergoes H abstraction by O_2 to form SO_3 and HO_2,[55] while NO can directly convert HO_2 back to OH *via* NO + HO_2 → NO_2 + OH. VOC oxidation initiated by OH can often recycle HO_x radicals in downstream chemistry (*e.g.* ref. 51, 114 and 115), but recycling ratios (β, number of HO_2 molecules recycled per OH molecule consumed) vary substantially across types of VOCs and physical conditions.[51] As a consequence, external OH reactants may alter the HO_2-to-OH ratio established by internal HO_x and O_3 chemistry, particularly at high OHR_{ext} (hundreds of s^{-1}) in OFR185 (where usually less O_3 is present to promote the HO_x interconversion). The recycling ratio β in modeling will be discussed in more detail in Section 3.4.1.

3.2. NO_y chemistry

As NO is a critical species controlling the fate of RO_2 radicals and of much higher importance than other NO_y species, we first summarize NO chemistry prior to discussing a few other NO_y species.

3.2.1. NO production and loss. The steady-state concentration of NO can be estimated by eqn (5)

$$NO = \frac{P_{NO}}{L_{NO}}. \quad (5)$$

The NO sources are all different in iNO, cNO and iN_2O operation modes. We thus focus on L_{NO} first. NO can rapidly react with all major oxidants in OH OFR, *i.e.* OH, HO_2 and O_3 (Fig. 3c–g).[48,49,55] However, the NO lifetime ($\tau_{NO} = 1/L_{NO}$) can vary substantially depending on conditions. In OFR254 (including iNO, cNO and iN_2O modes), injected O_3 is rarely less than 2 ppm (see Sections 4 and 5 for discussions about the reasons). Consequently, the contribution of NO + O_3 → NO_2 + O_2 with 2 ppm O_3 alone to L_{NO} is ~1 s^{-1},[55] which translates to a τ_{NO} of 1 s or shorter. Such a short lifetime is of no practical interest, compared to OFR residence times of a few min. In contrast, under many OFR185 (including iNO, cNO and iN_2O modes) conditions, τ_{NO} can be much longer, as O_3 is not injected but internally formed and hence its concentration is typically much lower than in OFR254 modes. In the case shown in Fig. 3c, average O_3 is <200 ppb. With NO + OH + M → HONO + M and NO + HO_2 → NO_2 + OH also taken into account, the NO → NO_2 reactive flux is still much smaller than that of NO + O_3 → NO_2 alone in a typical OFR254-5-iNO case shown in Fig. 3d and τ_{NO} in the case of Fig. 3c is ~10 s.[48] This is still short compared to OFR residence times, but it is sufficiently long for some oxidation chemistry to occur with a substantial fraction of the initial NO surviving. In the case of Fig. 3a, during the first τ_{NO}, an OH exposure (OH_{exp}, integral of OH over time) of ~3 × 10^{10} molecules cm^{-3} s (equivalent to a photochemical age of ~6 h) can be reached. Such a photochemical age can already result in significant oxidation of some VOCs and even SOA formation.[34,116]

At lower F185, which produces even less O_3 (and HO_x as well) in OFR185, τ_{NO} can be even longer. In OFR185-iNO, an initial NO injection may lead to high-NO conditions with active radical chemistry[48] (see Sections 4 and 5 for discussions about the practical realization of these conditions). Note that at very low UV, OFR185-iNO can elevate OH with respect to similar OFR185 conditions with NO + HO_2 → NO_2 + OH as a major secondary OH source. Besides, the possibility of significant τ_{NO} also shows that the cNO operation mode may be a viable method to achieve sustained high-NO conditions (as opposed to NO always decaying as in OFR185-iNO).[48] However, this method has not yet been experimentally validated to our knowledge. A continuous NO injection rate (rNO^{in}) of a few ppb s^{-1} as P_{NO} can maintain a NO concentration of several ppb in an environment with L_{NO} ~ 1 s^{-1}, which does not result in high NO in OFR185-iNO (Fig. 3e).

In the iN$_2$O modes, N$_2$O mixing ratio needs to be as high as a few percent to allow N$_2$O + O(^{1}D) → 2NO to compete with H$_2$O + O(^{1}D) → 2OH.[49,86] Since the latter reaction is one of the main HO$_x$ production pathways, the NO production through the former reaction should be at least comparable to the OH production through the latter. Then RO$_2$ + NO will play a significant role in the RO$_2$ fate compared to RO$_2$ + HO$_2$, as the rate coefficients of these two reactions are similar.[7] When N$_2$O competes with H$_2$O in reacting with O(^{1}D), the reactive flux of N$_2$O + O(^{1}D) typically reaches the order of 10^{10} molecules cm^{-3} s^{-1} (*i.e.*, of the order of ppb s^{-1}; Fig. 3e–g), also a typical order of magnitude of OH production rate in OFR185 and OFR254 (Fig. 3a and b). As discussed for the cNO mode, it is realistic to achieve ppb of NO in the OFR-iN$_2$O modes.

In the OFR369-i(iPrONO) mode,[87] the organic nitrite usually needs to be as high as several ppm and the UVA (369 nm) light intensity should be very strong (on the orders of 10^{15-16} photons cm^{-2} s^{-1}) to achieve a strong nitrite photolysis that produces both NO and RO in order to achieve sufficient photochemical ages (at least eq. hours). RO (iPrO, *i.e.* isopropoxy radical, in this case) extremely rapidly reacts with O$_2$, forming HO$_2$ and a carbonyl species (acetone in this case). HO$_2$ + NO → NO$_2$ + OH is the main NO loss pathway in OFR369-i(iPrONO), as O$_3$ is not injected and barely photochemically formed (because of no 185 nm UV light) in this mode.

3.2.2. Formation of other NO$_y$ species. The direct products of the reactions of NO with the main oxidants in OFR, OH, HO$_2$ and O$_3$, are HONO (from OH oxidation) and NO$_2$ (from HO$_2$ and O$_3$ oxidation), respectively. HONO and NO$_2$ can also be rapidly oxidized by OH to form NO$_2$ and HNO$_3$, respectively, through HONO + OH → NO$_2$ + H$_2$O and NO$_2$ + OH + M → HNO$_3$ + M, respectively (Fig. 3c–g), and thus can significantly contribute to OHR$_{ext}$[48] (though OH-consuming, NO$_y$ was not included in the lumped OHR$_{ext}$ by Peng *et al.*[48–50] in their modeling as NO$_y$ was explicitly modeled). NO$_2$, as a node of the NO$_y$ reaction network, can form other NO$_y$ species, such as HO$_2$NO$_2$ through NO$_2$ + HO$_2$ + M → HO$_2$NO$_2$ + M, NO$_3$ though NO$_2$ + O$_3$ → NO$_3$ + O$_2$ and N$_2$O$_5$ through NO$_2$ + NO$_3$ + M → N$_2$O$_5$ + M, depending on operation modes and conditions (Fig. 3c–g). However, all these subsequent products do not significantly contribute to OHR$_{ext}$ (as they react with OH much more slowly (*e.g.* HNO$_3$ and HO$_2$NO$_2$) or are not sufficiently abundant (*e.g.* NO$_3$)). Therefore, in the iNO modes, where NO is not replenished, OHR$_{ext}$ due to NO$_y$ species will quickly decrease upon NO$_x$ oxidation. By contrast, in the cNO, iN$_2$O and i(iPrONO) modes, NO$_y$ species keep being produced from NO source/precursors during the entire residence time. This leads to accumulation of NO$_y$ species (and hence OHR$_{ext}$ due to them), although NO itself may be stable.[49] In particular, acetone is always being formed as a byproduct in the NO production scheme of OFR369-i(iPrONO) and also contributes to OHR$_{ext}$.[87] Fast accumulation of NO$_y$ species and other byproducts limits the maximum photochemical age that OFR369-i(PrONO) can reach to ~1 d.[87] This limitation prevents OFR369-i(PrONO) from simulating multi-day aging at high NO, which can occur for example in large regions with strong NO$_x$ emissions over the whole region, such as eastern China.[117] To achieve a longer photochemical age in OFR369-i(iPrONO) by reducing the OHR$_{ext}$ due to the byproducts, a fully deuterated iPrONO (iPrONO-d$_7$) and a highly fluorinated iPrONO (1,1,1,3,3,3-hexafluoroisopropyl nitrite) have been proposed as alternative precursors. The former, though much expensive, has been demonstrated to be successful (denoted as OFR369-i(iPrONO-d$_7$)), while the latter has not because of the difficulty in its synthesis.[87]

In addition to NO$_2$ + O$_3$ → NO$_3$ + O$_2$, NO$_3$ can also be formed through HNO$_3$ + OH → NO$_3$ + H$_2$O (Fig. 3g). At high O$_3$ in the OFR254 modes with major NO$_y$ chemistry (*i.e.* OFR254-iNO and OFR254-iN$_2$O) and/or high UV in the OFR185 modes with major NO$_y$ chemistry (*i.e.* OFR185-iNO, OFR185-cNO and OFR185-iN$_2$O), NO$_3$ can be produced in significant amounts through the oxidation chain NO → NO$_2$ (→ HNO$_3$) → NO$_3$, and may serve as another major VOC oxidant (see Section 4.2). The potential interference for VOC oxidation by NO$_3$ in OH OFR experiments needs to be taken into account in experimental planning and/or data interpretation.

HO$_2$NO$_2$ can be considered as a reservoir species of NO$_2$, as it decomposes to the reactants forming it at room temperature, *i.e.* NO$_2$ and HO$_2$ (Fig. 3c–g).[48] Nevertheless, its concentration do not often plateau in the modes able to maintain high NO, since its thermal decomposition lifetime is ~30 s,[118] and NO$_2$ is often accumulated. Even under the assumption of a fast equilibrium with NO$_2$ (NO$_2$ + HO$_2$ + M ↔ HO$_2$NO$_2$ + M), HO$_2$NO$_2$ can still increase with time. These features also largely hold for the interconversion between RO$_2$ + NO$_2$ and RO$_2$NO$_2$ (peroxy nitrate stable species) for non-acyl peroxy radicals, as HO$_2$ and non-acyl RO$_2$ have the same functional group (–OO$^\bullet$) and similar reactivities toward NO$_2$.

3.3. RO$_2$ chemistry

As RO$_2$ is a radical usually with a relatively short lifetime, it concentration can also expressed in the steady-state form with the production and loss terms

$$\mathrm{RO_2} = \frac{P_{\mathrm{RO_2}}}{L_{\mathrm{RO_2}}}. \quad (6)$$

For the production, the most common and dominant pathway in OH OFR is VOC oxidation by OH, which produces a hydrocarbyl radical (R) *via* either addition to double bonds, or *via* H abstraction (VOC + OH → R (+ H$_2$O)). R then usually extremely rapidly recombines with O$_2$ to form RO$_2$ (R + O$_2$ + M → RO$_2$ + M).[27] Therefore, RO$_2$ production is limited by the first step, *i.e.* VOC oxidation, and an approximate expression of the total P_{RO_2} for all RO$_2$ radicals in the system can be written as P_{RO_2} = OH$^\bullet$OHR$_{VOC}$, where OHR$_{VOC}$ is the total OH reactivity due to all VOCs (including their stable oxidation intermediates and products).

The RO$_2$ loss pathways are central to atmospheric organic chemistry. RO$_2$ can react unimolecularly (isomerization)[51,119] and bimolecularly with a variety of species (HO$_2$, NO, another RO$_2$, NO$_2$, OH, O$_3$ and NO$_3$)[7,51,120] and can be photolyzed,[121] which lead to highly compositionally complex products (Table 2 and Fig. 3h).[51] Peng *et al.*[50] found that except under some conditions of no experimental interest (*i.e.* atmospherically irrelevant; see Section 4), both RO$_2$ photolysis and reactions

Table 2 Rate coefficients [in cm^3 $molecule^{-1}$ s^{-1} except for isomerization (in s^{-1})]/cross section (in cm^2) and product(s) of RO_2 loss pathways. Only organic species are listed for product(s). Copyright 2019 Copernicus Publications

RO_2 loss pathway	Rate coefficient/cross section	Product(s)
$RO_2 + HO_2$	1.5×10^{-11} [a]	Mainly ROOH for most RO_2[a]
$RO_2 + NO$	9×10^{-12} [a]	RO, $RONO_2$[b]
$RO_2 + RO_2$	Primary: $\sim 10^{-13}$ [a] Secondary: $\sim 10^{-15}$ [a] Tertiary: $\sim 10^{-17}$ [a] Substituted: can be up to 2 orders of magnitude higher[b] Acyl: $\sim 10^{-11}$ [b]	ROH + R(=O), RO + RO, ROOR[a]
$RO_2 + NO_2$ (in OFR)	$\sim 7 \times 10^{-12}$ [c]	RO_2NO_2[b]
$RO_2 + OH$	$\sim 1 \times 10^{-10}$ [d]	ROOOH (for $\geq$C4 RO_2), RO (smaller RO_2)[e]
RO_2 isomerization	Autoxidation: $\sim 10^{-3}$–10^{2} [f] Other: up to 10^{6} [g]	Generally another RO_2
RO_2 photolysis	$\sim 10^{-18}$ at 254 nm[h] $\sim 10^{-21}$–10^{-19} in UVA and UVB[h]	Mainly R, other photochemical products possible[i]
$RO_2 + NO_3$	~ 1–3×10^{-12} [b]	RO[b]
$RO_2 + O_3$	$\sim 10^{-17}$ [b]	RO[b]

[a] Ref. 7. [b] Ref. 51. [c] Typical value within the reported range in ref. 51; thermal decomposition rate coefficients of nitrates of acyl and non-acyl RO_2 are assumed to be 0.0004 and 3 s^{-1}, respectively, also typical values within the reported ranges in ref. 51. [d] Value used in the present work based on ref. 120 and 124–127. [e] Ref. 124 and 127–129. [f] Ref. 119. [g] Ref. 132. [h] Ref. 55. [i] Ref. 121.

of RO_2 with O_3 and NO_3 are of minor or negligible importance in OFR chemistry. To limit the complexity in their results and present them in an understandable fashion, Peng *et al.* discussed, by modeling a generic RO_2 in OFR, the RO_2 fates in two steps: (i) RO_2 fates by HO_2, RO_2, NO and NO_2, which have been extensively investigated and reviewed by Orlando and Tyndall,[51] and (ii) RO_2 + OH and isomerization, which have very recently been shown to be major RO_2 fates.[119,122] In this Review, we follow the structure of Peng *et al.*[50] to discuss the complex fates of RO_2 in OFR utilizing a generic RO_2.

3.3.1. RO_2 fates by HO_2, RO_2, NO and NO_2. As discussed in Section 3.2.2, $RO_2 + NO_2 \leftrightarrow RO_2NO_2$ for non-acyl RO_2 can be regarded as an equilibrium and RO_2NO_2 acts as a reservoir of RO_2 to some extent. If its reaction with NO_2 is not considered as a sink of RO_2, the remaining three RO_2 fates taken into account here, *i.e.* reactions of RO_2 with HO_2, NO and another RO_2, can be clearly shown in triangle plots such as Fig. 5.

RO_2 reacts with HO_2 and NO at $\sim 1.5 \times 10^{-11}$ and 9×10^{-12} cm^3 $molecule^{-1}$ s^{-1}, respectively. Rate coefficients of self-/cross-reactions of RO_2 are highly RO_2-structure-dependent,[7,51] with those for common non-acyl RO_2 ranging from $\sim 10^{-17}$ to $\sim 10^{-11}$ cm^3 $molecule^{-1}$ s^{-1}, those for acylperoxy radicals (acyl RO_2; –C(=O)$OO^{\bullet}$) slightly higher than 1×10^{-11} cm^3 $molecule^{-1}$ s^{-1}. Rate coefficients for a few highly specific aromatic-derived RO_2 radicals have been reported to be as high as 10^{-10} cm^3 $molecule^{-1}$ s^{-1},[123] although some debate persists about these values.

The scatter of the OFR185-iN_2O data points for a wide range of conditions in Fig. 5 clearly shows that OFR185(-iN_2O) is able to achieve NO-dominated and HO_2-dominated RO_2 fates, and so is OFR254(-iN_2O).[50] For "medium" $RO_2 + RO_2$ (at 1×10^{-13} cm^3 $molecule^{-1}$ s^{-1}) and many other RO_2 with slower self-/cross-reaction rate coefficients, the contribution of $RO_2 + RO_2$ to RO_2 fate is negligible in OFR185(-iN_2O) (Fig. 5a). For faster RO_2 self-/cross-reactions (*e.g.* "fast" $RO_2 + RO_2$ (at 1×10^{-11} cm^3 $molecule^{-1}$ s^{-1})), $RO_2 + RO_2$ can play a substantial role in RO_2 loss (Fig. 5b).[50] In OFR254(-iN_2O), similar features can be observed in case of significant $RO_2 + NO$ in RO_2 fate (Fig. 5c and d). However, at low (or zero) NO, the relative importance of $RO_2 + RO_2$ can be much higher than in OFR185(-iN_2O) under similar conditions (Fig. 5c and d). Peng *et al.*[50] found that, at high OHR_{VOC} (hundreds of s^{-1}), RO_2 production is very strong in OFR254-iN_2O. High O_3 in OFR254-iN_2O reduces OH suppression by the high OHR_{VOC} and keeps a relatively high OH. Then the product of OH and OHR_{VOC}, *i.e.* P_{RO_2}, is elevated and $RO_2 + RO_2$, whose rate depends quadratically on RO_2, increases even more.

At low NO, acyl RO_2 radicals have similar fates as fast (at 1×10^{-11} cm^3 $molecule^{-1}$ s^{-1}) self-/cross-reacting RO_2, because of their similar $RO_2 + RO_2$ rate coefficients. However, as long as NO_x plays some role in RO_2 loss (*i.e.* NO_y chemistry is significant), $RO_2 + NO_2 \rightarrow RO_2NO_2$ becomes the dominant fate of acyl RO_2.[50] Acylperoxy nitrates are much more stable than non-acyl peroxy nitrates. Their thermal decomposition lifetime is typically ~ 1 h, while that of non-acyl RO_2NO_2 typically ~ 1 s.[51] Thus acylperoxy nitrate should not be regarded as an RO_2 reservoir but a sink in OFR, whose residence times are only minutes.[50] With N_2O at percent-level, other loss pathways than acyl $RO_2 + NO_2$ can still be significant in OFR185-iN_2O as reaction with NO_2 accounts for $\sim$60–80% RO_2 loss, while in OFR254-iN_2O, the relative contribution of $RO_2 + NO_2$ is close to 100%. This difference is also due to higher O_3 in OFR254-iN_2O, which greatly promotes the $NO \rightarrow NO_2$ conversion.

3.3.2. RO_2 + OH. Despite some small disagreements among the measurements of the CH_3O_2 + OH rate coefficient[124–126] and small differences between rate coefficients and CH_3O_2 + OH and larger RO_2[120] (Table 2), the range of rate coefficients of RO_2 + OH can be reasonably narrowed to $\sim 1 \times 10^{-10}$ cm^3 $molecule^{-1}$ s^{-1} or slightly higher. By contrast, the rate coefficient of RO_2 + HO_2 is about an order of magnitude smaller ($\sim 1.5 \times 10^{-11}$ cm^3 $molecule^{-1}$ s^{-1}). Thus, RO_2 + OH may play an important role in RO_2 fate in OH OFR, when $RO_2 + HO_2$ is a major RO_2 loss pathway (*i.e.* at low NO) and the HO_2-to-OH ratio

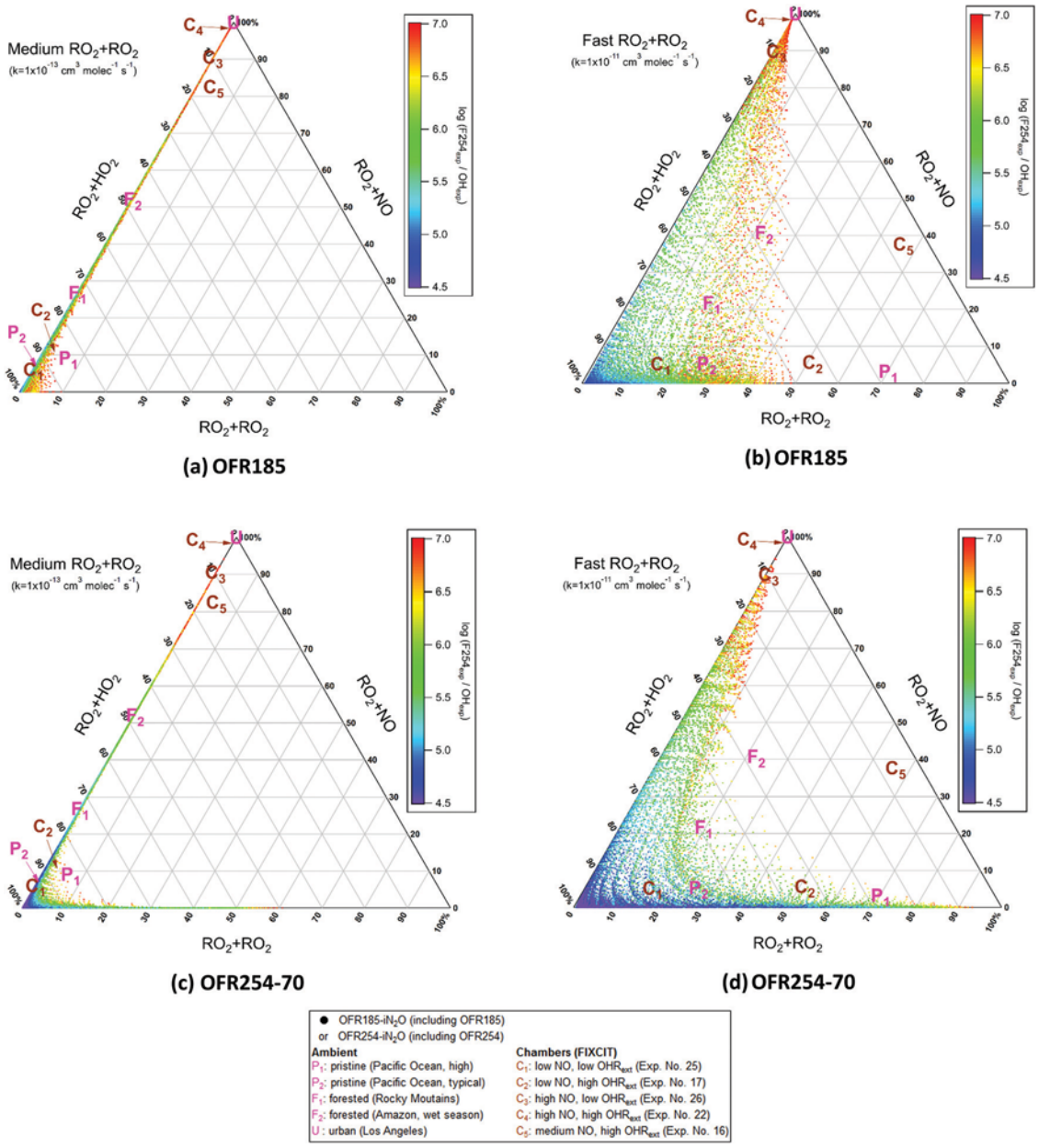

Fig. 5 Triangle plots of RO_2 fate by $RO_2 + HO_2$, $RO_2 + RO_2$ and $RO_2 + NO$ (without $RO_2 + OH$ and RO_2 isomerization considered in the model) for RO_2 with the medium self/cross reaction rate coefficient (1×10^{-13} cm^{-3} molecule^{-1} s^{-1}) in (a) OFR185 (including OFR185-iN_2O) and (c) OFR254-70 (including OFR254-70-iN_2O) and for RO2 with the fast self/cross reaction rate coefficient (1×10^{-11} cm^{-3} molecule^{-1} s^{-1}) in (b) OFR185 (including OFR185-iN_2O) and (d) OFR254-70 (including OFR254-70-iN_2O). Inclined tick values on an axis indicate the grid lines that should be followed (in parallel to the inclination) to read the corresponding values on this axis. The OFR data points are colored by the logarithm of the exposure ratio between 254 nm photon flux and OH, a measure of badness of OFR conditions in terms of 254 nm organic photolysis. Several typical ambient and chamber cases (see Table 2 of ref. 50 for details of these cases) are also shown for comparison.

is close to or lower than 10.[50] At high H_2O and UV in OFR185 and OFR254 (low-NO OFR modes), primary production pathways overwhelmingly dominates OH production, resulting in very low HO_2-to-OH ratio (close to 1), as H_2O photolysis at 185 nm produces OH and HO_2 at 1 : 1 and $H_2O + O(^1D)$ only produces OH.[50] The main organic product of $RO_2 + OH$ is likely to be a carbonyl species: CH_3O has been identified as the main direct organic product of CH_3O_2,[124,127,128] and it very rapidly converts to HCHO through reaction with O_2. The main direct product of reactions of OH with larger RO_2 radicals tend to be trioxides (ROOOH).[129] Nevertheless, Anglada and Solé[130] found *via* quantum chemical calculations that H abstraction from the –OOOH group of ROOOH by OH is very fast (rate coefficient on the order of 10^{-11} cm^3 molecule s^{-1}) and the organic product of this reaction, ROOO, is likely to quickly decompose to RO and O_2, the former of which finally leads to carbonyl production.[7] A significant production of carbonyls from $RO_2 + OH$ at low NO can be an issue (if its relative fraction is larger than for the

atmosphere) because the main organic product of RO_2 + NO, *i.e.* the high-NO pathway, is also RO (and then carbonyl).[7,51]

3.3.3. RO_2 isomerization. RO_2 isomerization rate coefficients are highly RO_2-structure-dependent, spanning from $\sim 10^{-3}$–10^6 s^{-1}.[53,119,131–133] Except for the extremely rapidly isomerizing RO_2 (*e.g.* some substituted acyl RO_2),[132] most RO_2 isomerizations need some time (very roughly 0.1–1000 s) to take place.[119,131] The RO_2 lifetimes (isomerization not taken into account) in OFR185 and OFR254 under a very wide range of conditions explored by Peng *et al.*[50] range from $\sim$0.1 s to a few tens of s. Therefore, the slowest RO_2 isomerizations may not have sufficient time to occur in low-NO OFR. Other RO_2 isomerizations (with lifetimes on the orders of 0.1–10 s) include several common types, *e.g.* some peroxy radicals attached to the C backbone of oxygenated alkanes[119,131] and isoprene-[134,135] and monoterpene-derived[136] RO_2, can occur in low-NO OFR.[50] However, if all these common RO_2 isomerizations need to happen, RO_2 lifetime should be $\sim$10 s and only relatively low H_2O and UV conditions, which limit HO_x production and thereby RO_2 consumption by HO_x, meet this requirement.

Under typical high-NO conditions, RO_2 + NO dominates over RO_2 + HO_2 and RO_2 + OH in RO_2 loss. Also, all bimolecular RO_2 fates make RO_2 lifetime too short to allow most common RO_2 isomerizations.[50] Nevertheless, there do exist some transition regimes (*e.g.* clean urban areas),[131] where reaction of RO_2 with NO still dominates over that with HO_x but RO_2 lifetime is long enough for some isomerizations to occur. These cases will be discussed in Sections 4 and 5.

3.3.4. RO_2 + SO_2. SO_2 is present in ambient air, and it is often used for calibrating OFR OH_{exp}.[30,45,116] The perturbation to RO_2 caused by RO_2 + SO_2 is negligible under most OFR conditions, while that to SO_2 may not be negligible if RO_2 is very high. Richards-Henderson *et al.*[80] found that the multistep adduct formation proposed by Kan *et al.*[137] is a more reasonable description of RO_2 + SO_2 than a one-step bimolecular mechanism. In the multistep mechanism, RO_2 and SO_2 first form an adduct RO_2SO_2, which then combines with O_2 to form the larger adduct $RO_2SO_2O_2$. This adduct can react with another RO_2 radical to yield final products. As a result, the overall rate coefficient of RO_2 + SO_2 depends quadratically on RO_2 concentration. In case of highly elevated RO_2 (*e.g.* when both OHR_{VOC} and OH are high (see Section 3.3.1) or in particles that confine and concentrate RO_2 produced from OA heterogeneous oxidation by OH),[80] RO_2 + SO_2 rate increases quadratically and it may become a significant sink of SO_2. This may have implications for OH calibration experiments, where SO_2 is often used (see Section 3.4).

3.4. Oxidant/reactant quantification and related uncertainties

Many species of interest in OFR are highly reactive and/or radicals, and thus difficult to directly measure. Measurements based on depletion of stable, more easily measured species by these species[116] and model calculations[45,46] are two common ways for their quantification. Nevertheless, both methods have significant uncertainties.

3.4.1. OH. Lambe *et al.*[116] quantified OH_{exp} by measuring SO_2 decay in the PAM and TPOT OFRs due to its OH oxidation. The decays of other injected tracer gases with different OH oxidation lifetimes, such as CO,[36,45] hexane,[76] hexanal[80] and NO,[37] have also been used to cover different ranges of OH_{exp}. However, several issues are related to this method:

– In case of online OH calibration with high OHR_{VOC} and/or high OA concentration in OFR254, RO_2 may be a significant SO_2 consumer in addition to OH (Section 3.3.3), leading to overestimation of OH_{exp}. Further investigation on the reactivity of various RO_2 with SO_2 is needed to fully clarify this issue.

– NO is actually not a good tracer for OH calibration, as its decay due to HO_2 and O_3 oxidation is difficult to disentangle from OH oxidation, potentially leading to OH_{exp} overestimation. Even if this issue is disregarded, NO still can cause OH_{exp} overestimation in offline OH calibrations. NO lifetime is much shorter than some other OH reactants (*e.g.* benzene, short-chain alkanes and CO). Those species effectively suppress OH for a longer period and result in an OH_{exp} lower than in the presence of NO only. This OH_{exp} overestimation by offline calibration has been discussed in detail by Ortega *et al.*[34]

– Due to actual non-plug flow in many commonly used OFR (*e.g.* PAM, TPOT, CPOT and TSAR), the average OH_{exp} that a species sees *via* its oxidation by OH is not identical to an OH_{exp} calculated simply from the integration of OH that is present in each air parcel based on the measured residence time distribution.[46] Peng *et al.*[46] thus has recommended using the species under study as the tracer for OH calibration when possible. However, this is often experimentally demanding. If it is not possible, added tracers are still very valuable for OH calibration. Addition of tracers during (some of) the actual experiments of interest, and with lifetimes similar to the species of interest are recommended. If an OFR with plug flow is used, the OH_{exp} that any tracer sees is the actual OH_{exp} and OH calibration is more straightforward.

Modeling is another common way to estimate OH. Li *et al.*[45] and Peng *et al.*[46] established the most commonly used OFR radical chemistry model.[34,35,45–49,87,138,139] This plug-flow box model has been validated against laboratory and field OFR experiments and is thought to be within a factor of 2–3 of measurements.[45,46] Of this factor of 2–3 (relative uncertainties of $\sim$100–200%), uncertain kinetic parameters only contribute relatively uncertainties up to $\sim$50%.[46,48] Peng *et al.* also examined other approximations in the model as potential uncertainty sources, such as non-plug flow,[46,48] non-uniform UV field[49] and the use simplified VOC oxidation chemistry,[46,48–50] while Palm *et al.*[31] and Brune[32] discussed the impacts of wall losses. Plug flow and uniform UV field have been found to be good approximations under conditions of practical interest (see Sections 4 and 5 for discussions about practical interest). The results of the plug-flow model can deviate significantly from those of a model taking a measured residence time distribution into account when both UV and OH suppression are strong, which lead to different chemical regimes for different air parcels, *i.e.* low OH at short residence times and high OH (due to decrease in OHR_{ext}) at long residence times.[46,48] A realistic UV field leads to significantly different model outputs than a uniform field does when UV is low on average and significant only around the lamps.[49] In this case, photochemistry is inactive in most of the reactor volume, which is

certainly undesirable. Although future research on the wall losses in OFR is warranted,[32] neglecting them in the model is unlikely to account for most model uncertainty.[31] Simplified VOC oxidation chemistry is likely to be the main uncertainty source of the model.

In the model above, OHR_{VOC} variation due to VOC oxidation is surrogated by that due to SO_2 oxidation,[46] which allows for model simplicity and computational efficiency. OHR_{VOC} variation due to VOC oxidation is highly complex, since a plethora of oxidation intermediates that evolve over time also contribute to it.[140–143] This complex variation is not very well captured even by models as explicit as Master Chemical Mechanism.[141,143] Also, SO_2 reacts with OH more slowly than many primary VOCs. Therefore, its relatively slow decay can, at minimal computational expense, very roughly account for OHR_{VOC} due to oxidation intermediates produced, which makes OHR_{VOC} of total VOCs decay substantially more slowly than that for primary VOCs during oxidation.[46,48–50]

This simplification also removes another piece of information of VOC oxidation that is important for modeling the HO_x chemistry in OFR, *i.e.* HO_x recycling ratio from VOC oxidation (β). Peng *et al.*[46] showed that β does not have a strong impact on OH in low-NO OH OFR unless the reactions of HO_2 produced from the oxidation of a large amount of VOC serve as the main source ($HO_2 + O_3 \rightarrow OH + 2O_2$; at low H_2O, low F254 and high OHR_{VOC} in OFR254) or sink of OH ($OH + HO_2 \rightarrow H_2O + O_2$; at high H_2O, UV and OHR_{VOC} in OFR185 and OFR254). Still, this ratio can affect modeled HO_2 and requires a good estimate. Peng *et al.*[50] reported an estimate of $\beta \sim 0.3$ at zero NO, obtained from the fully chemically explicit GECKO-A model.[144] Under typical high-NO conditions, RO_2 produced by VOC + OH dominantly follows $RO_2 + NO \rightarrow RO + NO_2$. Then RO extremely rapidly react with O_2 to produce HO_2, resulting in $\beta \sim 1$.[51] In case of a transition regime between low and high NO, an average recycling ratio can be estimated based on the two extreme values and the local relative fate of RO_2 in the model.

As the full kinetic model can be complex to run and interpret, Peng *et al.*[45,46,49] fitted algebraic equations to a large number of model outputs (covering a very large range of physical conditions) that allow estimating OH more easily. This topic will be discussed in more detail in Section 5.3. The deviations of estimation equation-predicted OH from the modeled values are usually tens of %, still very minor compared to the ×2–3 overall relative uncertainties. Thus the relative uncertainties of estimation equation-predicted OH are also generally ×2–3.

3.4.2. Other oxidants/reactants. Unlike OH, O_3 is much more stable and can be easily measured by multiple optical and commercial instruments. Li *et al.*[45] measured O_3 as a part of their laboratory characterization of OFR chemistry, and used measured O_3 to constrain the OFR chemistry model, in particular parameters related to UV intensity. Utilizing O_3 measurements to determine F185 in OFR185 is very similar to typical chemical actinometry.[145] UV intensity were also directly measured with photodiodes by Li *et al.*[45] to determine the F185/F254 ratio as a function of lamp setting for the BHK lamps in their OFR (other lamps may have different F185/F254). The commercial aerodyne PAM can include a photodiode to measure UV intensity.

O_3, F185 and F254 can also be estimated by the OFR chemistry model and/or estimation equations.[47] The concentrations of other oxidants/reactants, such as HO_2, NO_2 and NO_3, are usually obtained from the model, and have been fitted to additional estimation equations.[47,49,50] Some of these species (*e.g.* NO_2) are stable, but not easy to measure due to frequently strong interferences in OFR experiments.[87] Modeled and equation-predicted O_3 is almost as accurate as measurements, as UV in the model, governing the O_3 production, is constrained by the O_3 measurements.[45] Other quantities obtained from the model and the estimation equations are estimated to be as uncertain as modeled and equation-predicted OH.

4. Atmospheric relevance of organic chemistry in OFR

The validity of OFR experiments that attempt to simulate atmospheric VOC oxidation and SOA formation requires the atmospheric relevance of the chemistry in OFR, at least the parts directly related to the topics of interest (VOC oxidation and SOA formation). If the chemistry in the OFR deviates strongly from the atmosphere, product species may be very different from those formed in the atmosphere. These products formed in atmospherically irrelevant OFR chemistries can have very different properties (SOA formation potential, light absorption, hygroscopicity, toxicity, mutagenicity *etc.*) than species in atmospheric environments of interest, leading to confusion in the literature. The most basic concerns over the atmospheric relevance of OFR chemistry are OH concentrations that are one or several orders of magnitude higher than ambient values, and that the UV wavelengths initiating the OFR chemistry (for OFR185 and OFR254 variants) do not naturally exist in the troposphere. There are also concerns over the atmospheric relevance of the chemistry of RO_2, OA *etc.* We will discuss these concerns in detail in this section.

4.1. General considerations

First of all, we need to address the fundamental concern, *i.e.* the atmospheric relevance of high OH oxidation conditions, which is also the root cause of the specific advantages of OFR compared to chambers. We prove in Appendix A that in a reaction network of VOC oxidation where all VOCs exclusively react with OH to form another VOC, the product distribution (including all VOC products) solely depends on OH_{exp}, but not on OH. If the network includes (pseudo-)unimolecular reactions not involving OH but at a rate coefficient proportional to OH, the abovementioned statement still holds. In other words, in that basic scheme, VOC oxidation at high OH in OFR and at ambient OH will result in the identical product mixture at a given OH_{exp}. This means that high OH itself is not a concern as long as all processes scale with OH simultaneously. In general, what makes high OH seemingly a concern is the processes in OFR that do not scale with OH, *i.e.* VOC photolysis, RO_2 isomerization, condensation of semivolatile and low-volatility VOCs (SVOCs and LVOCs) onto aerosols *etc.* In the following, to discuss the deviation of the chemistry/process of a species from

that in the atmosphere, we will use the ratio of the concentration or exposure of that species to that of OH when appropriate. Ideally, this type of ratios should be as close to the ambient values as possible. In OFR, these ratios can be either too high or too low to be atmospherically-relevant.

4.2. VOC

In addition to OH, VOCs can in theory react with many other species in OFR, such as photons at 185 and 254 nm, UVA and UVB photons, O_3, $O(^1D)$, $O(^3P)$, HO_2, $^1O_2$ and NO_3. We will compare the relative contribution of the reactions of VOCs with these species to the fate of VOCs with that of the reactions with OH.

4.2.1. VOC fate by photolysis. UV at 185 and 254 nm (in the UVC range), emitted by Hg lamps in OFR, does not naturally exist in the troposphere, as it is absorbed in the stratosphere. Photons at these short wavelengths are highly energetic and can induce VOC dissociations and isomerizations that less energetic photons in the UVB, UVA and visible range cannot cause. Although some primary VOCs may undergo similar photolysis pathways at 185 and/or 254 nm as at longer UV wavelengths (*e.g.* ref. 146), this does not quell the concern about the atmospheric relevance of the 185 and/or 254 nm photolysis pathways of the photolysis products and/or oxidation intermediates, which are numerous and whose photolysis mechanisms are extremely difficult to fully clarify.[47,48] Therefore, ideal F185/OH and F254/OH (which are also exposure ratios as photon fluxes and OH do not significantly vary in most cases) in OFR should be 0, as in the troposphere, implying no contribution of UVC photolysis to VOC fate.

In reality, the only OH OFR operation mode that satisfies this condition is OFR369-i(iPrONO) (or similar modes that do not use non-actinic wavelengths), while in all other OH OFR modes, 185 and/or 254 nm UV is indispensable for OH production. Then a more practical criterion for a condition to be atmospherically relevant in terms of VOC photolysis at 185 nm is insignificance of this photolysis for an overwhelming majority (if not all) of VOCs, including their oxidation intermediates (likely oxygenated VOCs, *e.g.* carbonyls), compared to the reactions of those species with OH, which requires an F185/OH $< 3 \times 10^3$ cm s^{-1},[48] as shown in Fig. 6a. At F185/OH $> \sim 1 \times 10^5$ cm s^{-1}, most carbonyls (as common oxidation intermediates) have significant 185 nm photolysis relative to their reactions with OH, which significantly reduces the atmospheric relevance of the oxidation of any VOCs in OFR.[48] Similarly, the two thresholds for VOC photolysis at 254 nm can be found at $\sim 4 \times 10^5$ and $\sim 1 \times 10^7$ cm s^{-1} (Fig. 6b). Peng *et al.*[48] thus defined "good OFR conditions" (in terms of non-tropospheric VOC photolysis) as those meeting the above criteria for lack of photolysis importance for both 185 and 254 nm, and "bad conditions" as those meeting at least one bad criterion for the two wavelengths. The conditions with F185/OH and F254/OH values in between were defined as "risky conditions," which may be atmospherically relevant for some VOCs (*e.g.* alkanes, which do not absorb 185 or 254 nm photons), while not for others (*e.g.* benzene, which is strongly absorbing at 185 and 254 nm and is not highly reactive toward OH).[27,147] Experiments are often run on risky and bad conditions for typical OFR designs and reactor inputs in the literature,[47] so this issue requires careful attention experimental planning (see Section 5).

Peng *et al.*[47] identified H_2O and OHR_{ext} as the most important physical parameters that affect F185/OH and F254/OH in OH OFR. A higher H_2O elevates OH production (and hence OH concentration) in OFR185 and OFR254 (including variants for high NO), but does not impact UV, leading to lower (and more tropospherically relevant) F185/OH and F254/OH. A higher OHR_{ext} causes heavier OH suppression (and hence a lower OH), but does not lower UV, leading to higher (and less tropospherically relevant) F185/OH and F254/OH.[47] The impact of UV on F185/OH and F254/OH is minor, since OH production is roughly proportional to UV. Thus, a combination of high H_2O and low OHR_{ext} tends to be more tropospherically relevant/good condition in terms of non-tropospheric VOC photolysis, while an opposite condition (low H_2O and high OHR_{ext}) is likely to tropospherically irrelevant/bad.[47]

UVA and UVB photons are also non-OH reactants but they are desirable, which is different from UVC, as UVA and UVB are present in the troposphere. Ambient $F_{UVA-UVB}$/OH is on the orders of 10^7–10^8 cm s^{-1},[21,148] while $F_{UVA-UVB}$/OH is much lower than 10^7 cm s^{-1} in OFR185 and OFR254 (equipped with BHK lamps), as the total intensity of the emissions in these ranges are only a few percent of that at 254 nm.[47,149] This indicates that VOC photolysis at ambient wavelengths is almost completely missing in OFR185 and OFR254, which can be an important atmospheric-relevance issue for OFR. Even with VOC photolysis at 185 and 254 nm included, total VOC photolysis under good OFR conditions is much less important than in the atmosphere.[47] However, OFR369-i(iPrONO), whose light source is UVA lamps, have its F369/OH on the order of 10^7 cm s^{-1}, and thus of the order of atmospheric conditions.[87]

4.2.2. VOC fate by O_3, O atoms, HO_2 and $^1O_2$. Other non-OH reactants, *e.g.* O_3, $O(^1D)$ and $O(^3P)$, follow very similar trends as 185 and 254 nm photons in terms of their relative importance in VOC oxidation.[47] OH is lower at low H_2O and/or high OHR_{ext} because of weak production and/or suppression, while those non-OH reactants are not strongly impacted by H_2O and OHR_{ext}. Thus higher H_2O and lower OHR_{ext} also minimize the relative importance of these non-OH reactants. Note that minimization of their relative importance does not necessarily make OFR chemistry more atmospherically-relevant, as at least O_3 often plays a significant role in ambient VOC oxidation. Significant VOC ozonolysis can also be realized under many OFR conditions (Fig. 6c).

In OFR185, O_3, $O(^1D)$ and $O(^3P)$ all increase with UV, which again makes UV a less important physical parameter governing X/OH (X = O_3, $O(^1D)$ and $O(^3P)$). In OFR254, average O_3 is controlled by injection, and $O(^1D)$ and $O(^3P)$ depend on both injected O_3 and UV.[47] Thus, a higher F254 leads to a higher OH, and hence a lower O_3/OH, while F254 does not strongly affect $O(^1D)$/OH and $O(^3P)$/OH. Note that ambient O_3/OH, $O(^1D)$/OH and $O(^3P)$/OH are not 0 as F185/OH and F254/OH. At ambient O_3/OH, a number of biogenic VOCs (with C=C double bond(s)) are significantly or even dominantly consumed by O_3 (Fig. 6c). Under most OFR185 and OFR254 conditions, O_3/OH is actually

lower than the typical ambient range (Fig. 6c). Although ambient $O(^1D)$/OH and $O(^3P)$/OH are also non-zero, they are so low that the role of $O(^1D)$ and $O(^3P)$ in the oxidation of most VOCs is negligible. Under most OH OFR conditions, the reactions of O atoms with most VOCs contribute little to VOC fates. The role of HO_2 and $^1O_2$ were also found to be negligible by Peng *et al.*[47]

4.2.3. VOC fate by NO_3. In the iNO, cNO and iN_2O modes of OH OFR, NO_3 may be formed in significant amounts (Section 3.2.2) and it can become another major non-OH VOC oxidant. If

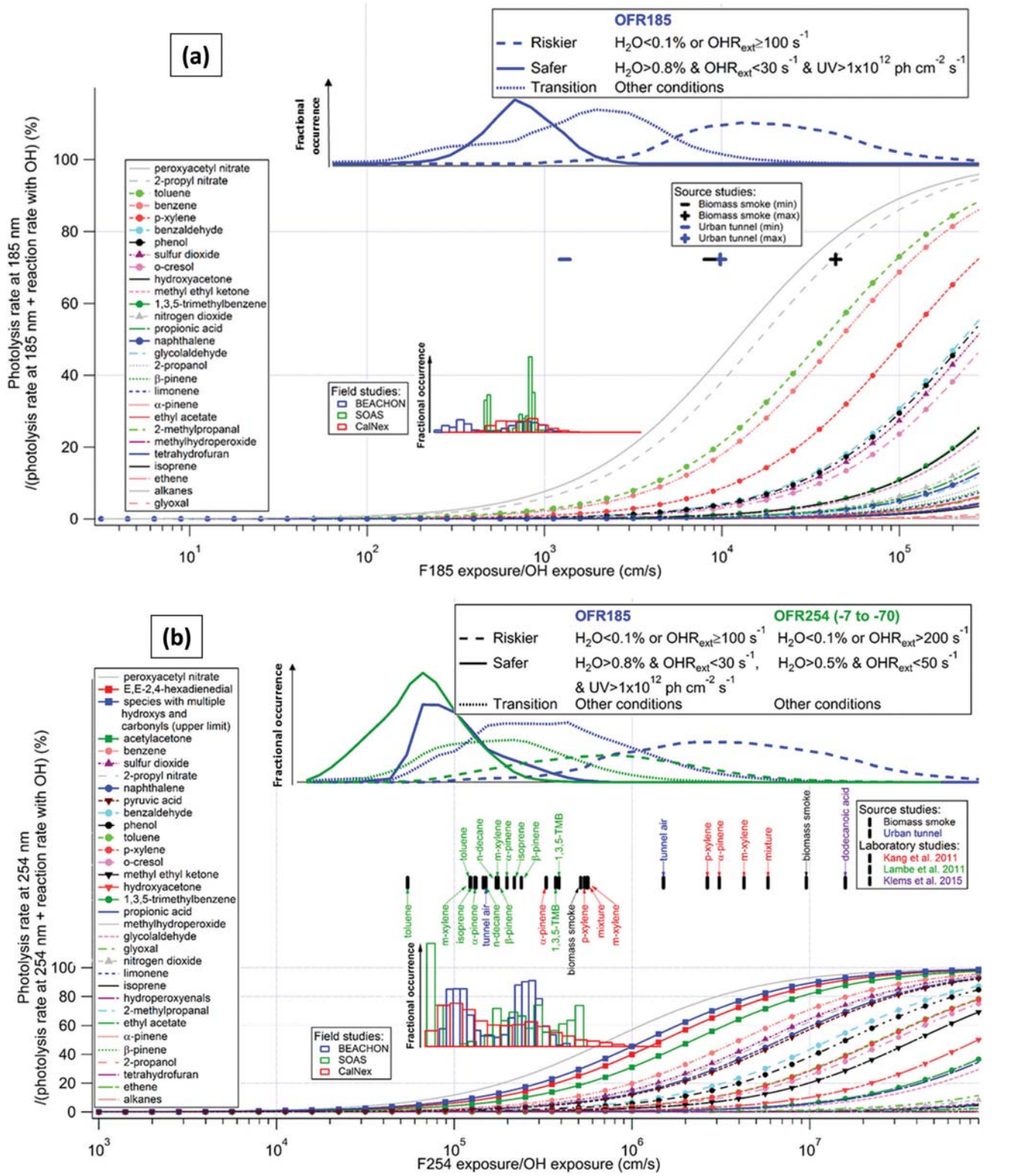

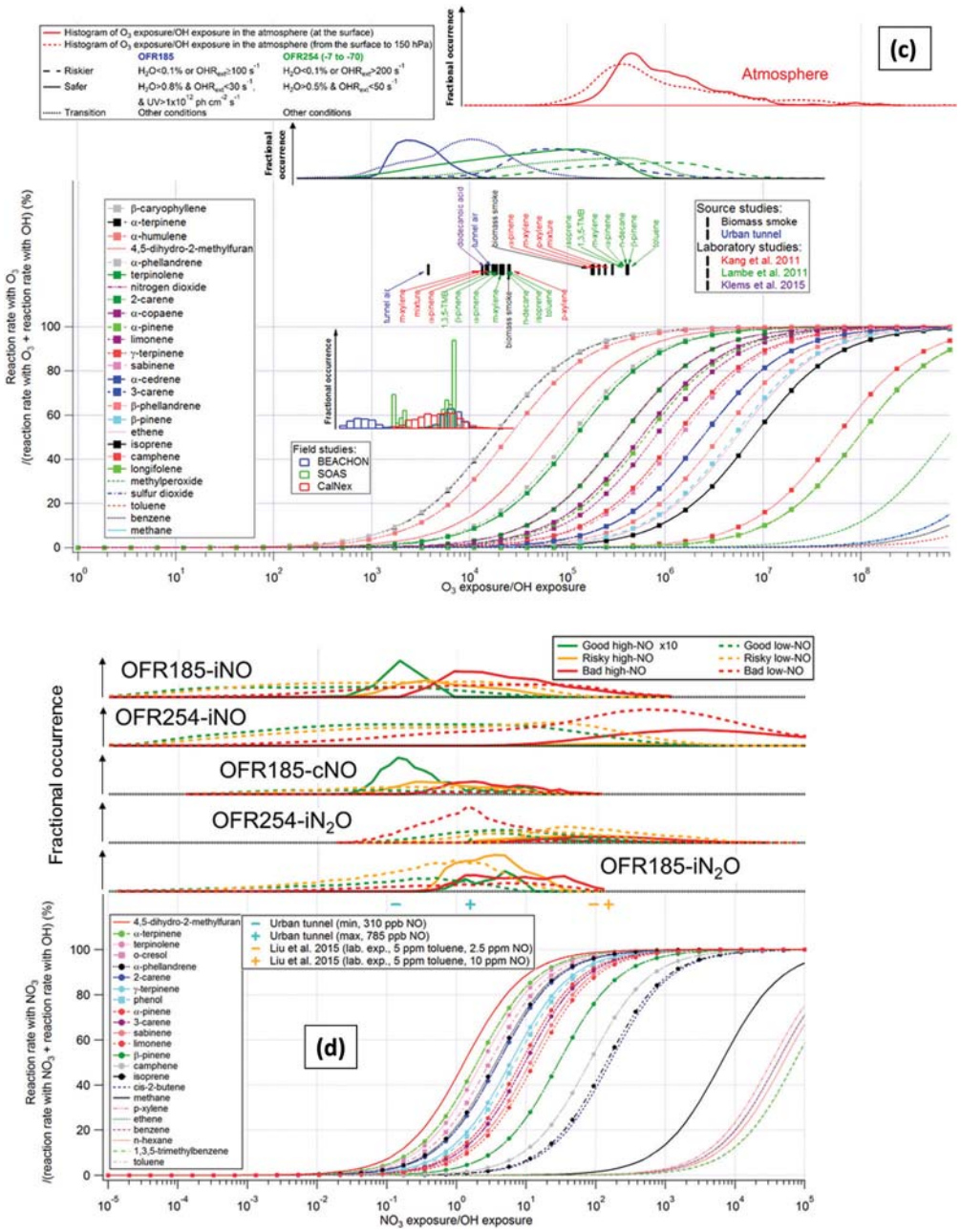

Fig. 6 Fractional importance of the reaction rate of several species of interest with a non-OH reactant ((a) 185 nm photon, (b) 254 nm photon, (c) O_3, and (d) NO_3) *vs.* the reaction rate with OH, as a function of the ratio of exposure to non-OH reactant and OH. The modeled frequency distributions of ratios of non-OH reactant exposure to OH exposure under riskier, safer, and transition conditions for OFR185 and/or OFR254 are also shown in (a–d). In the upper part of (d), also shown are the modeled frequency distributions of ratios of NO_3 exposure to OH exposure under good/risky/bad high/low-NO conditions for OFR185-iNO, OFR254-iNO, OFR185-cNO, OFR254-iN_2O and OFR185-iN_2O. The lower inset in (a–c) shows histograms of model-estimated non-OH reactant-to-OH exposures for three field studies where OFR185 was used to process ambient air. Their ordinate is the fractional occurrence of a given condition (X_{exp}/OH_{exp}). All histograms are normalized to be of identical total area (*i.e.*, total probability of 1). All curves, markers, and histograms in this figure share the same abscissa. (a) The curves of aromatics and inorganic gases are highlighted by solid dots and upward triangles, respectively. The upper inset (black and blue markers) shows similar information for source studies of biomass smoke (FLAME-3)[38] and an urban tunnel.[37] (b) The curves of saturated carbonyl compounds and possible highly absorbing oxidation intermediates are highlighted by downward triangles and squares, respectively. The insets show histograms of model-estimated F254/OH exposures for three field studies where OFR185 was used to process ambient air. In addition to source studies of biomass smoke (FLAME-3)[38] and the urban tunnel,[37] F254 exposure/OH exposure ratios in two laboratory studies[57,59] are shown in the upper inset. Colored tags indicate species used in the laboratory experiments. The lower and upper limits of F254 exposure/OH exposure ratios in the experiments with a certain source in a certain study are denoted by tags below and above the markers, respectively. (c) The curves of biogenics are highlighted by squares. Also shown are modeled distributions of the relative exposure of O_3 and OH at the Earth's surface (solid line) and throughout the column from the surface to a height with a pressure of 150 hPa (dashed line). The distributions were calculated from the mean daily concentrations of O_3 and OH as simulated by the GISS ModelE2. (d) The curves of biogenics and phenols are highlighted by solid dots and squares, respectively. The turquoise and orange markers show the ranges of modeled exposure ratios between NO_3 and OH of a source study in the urban tunnel[37] and a laboratory study[227] using OFR254-iNO, respectively.

the goal of OFR experiments is to simulate daytime atmospheric chemistry, a very low NO_3/OH is preferred. The production and loss of NO_3 both depend on NO_2 (Fig. 3d, f and g). While its main loss pathway is $NO_2 + NO_3 \rightarrow N_2O_5$, its production (*via* $HNO_3 + OH \rightarrow NO_3 + H_2O$ and $NO_2 + O_3 \rightarrow NO_3$) can also be modulated by OH and O_3. As a result, NO_3 generally increases with OH and NO_3/OH does not change substantially.[48,49] However, O_3 may significantly elevate NO_3, and hence NO_3/OH. This explains why OFR185-iN_2O has generally higher NO_3/OH than OFR185-iNO and OFR185-cNO – its O_3 production, from both O_2 and N_2O photolysis, is stronger than OFR185-iNO and OFR185-cNO. Also NO3/OH increases with F185 in OFR185-iN_2O, because of O_3 production increasing with F185.[49] OFR254-iNO and OFR254-iN_2O generally have even higher NO_3/OH because of the injected O_3.[48,49] In contrast, there is no concern about VOC oxidation by NO_3 in OFR369-i(iPrONO), as no O_3 is formed and OH is generally lower in OFR369-i(iPrONO) than in the modes using Hg lamps.[87]

Note that among the iNO, cNO and iN_2O modes, the lowest value of NO_3/OH that that can be reached is around 0.1 (Fig. 6d). At this NO_3/OH, no VOCs are significantly oxidized by NO_3 compared to their reactions with OH. However, in case of a slightly higher NO_3/OH of $\sim$1, dihydrofurans, phenols and a number of terpenes can be significantly consumed by NO_3. This NO_3/OH is not the lower limit of the span of NO_3/OH in these OFR185-based modes. However, even such an NO_3/OH ratio that is sometimes too high (and results in some chemistry irrelevant to a typical daytime atmosphere) cannot be achieved in OFR254-iN_2O (Fig. 6d).[49] For biogenic VOCs (with C=C bond(s)) that are highly reactive toward OH (*e.g.* isoprene), their oxidation by NO_3 may not play a very large role in their fate. However, for aromatic OH oxidation, NO_3 oxidation is still a concern, since the direct products of aromatic oxidation by OH are phenols, which react rapidly with NO_3.[27] For alkanes as precursors, although dihydrofurans can be among their oxidation products under ambient high-NO conditions *via* particle-phase hemiacetal formation and dehydration,[89,150] NO_3 oxidation is still not a concern, since this particle-phase chemistry is usually too slow with respect to OFR residence times.[151] In summary, when simulation of typical daytime chemistry is preferred, VOC oxidation by NO_3 can be an interference in the OH oxidation experiments with aromatic and/or biogenic VOCs as precursors. However, in case of mimicking an early morning chemistry, where both NO_3 and OH may play a major role in VOC fate, conditions leading to significant VOC oxidation by NO_3, as discussed above and also shown in Fig. 6d, may actually be more relevant.

4.2.4. Fate by partitioning. Condensation of SVOCs and LVOCs onto existing aerosols is the key process of SOA growth. This partitioning process is not accelerated at high OH and thus may also be a deviation from atmospherically relevant VOC processing. Similarly, the partitioning of SVOCs and LVOCs to the reactor walls is also a potential deviation. Since these processes are first-order and involve no other reactant/oxidants, we discuss the lifetimes of SVOC and LVOC partitioning *vs.* those of their OH oxidation instead of X/OH (X = other reactant/oxidant). Ambient SVOC and LVOC condensation lifetimes vary with the aerosol condensational sink present in an experiment, but can be as long as several hundreds of s at low aerosol concentrations,[152,153] which is still much shorter than the OH oxidation lifetimes of most VOCs in the atmosphere[27] but can be longer than OFR residence times.[116]

Palm *et al.*[31] established a framework to analyze the fate of LVOCs (also applicable to SVOCs) in OH OFR including OH oxidation and partitioning. In this framework, for a SVOC or LVOC, the lifetime of its condensation onto aerosols is reciprocal of the condensational sink (CS), *i.e.* the integral of the first moment of particle size distribution;[152] the lifetime of SVOC and LVOC wall loss is that of their eddy diffusion to the wall.[26] In their high-CS case (OA concentration >1.5 μg m^{-3}), the condensation lifetime is shorter than 100 s. SVOC and LVOC condensation is thus substantial in OFR. Nevertheless, there can also be significant fractions of SVOC and LVOC lost to the wall or exiting the reactor without undergoing any of these fates, particularly at lower CS and OH (Fig. 7a). As OH increases (so does OH_{exp}), SVOC and LVOC are increasingly likely to react with OH and increasingly unlikely to exit the reactor. At a

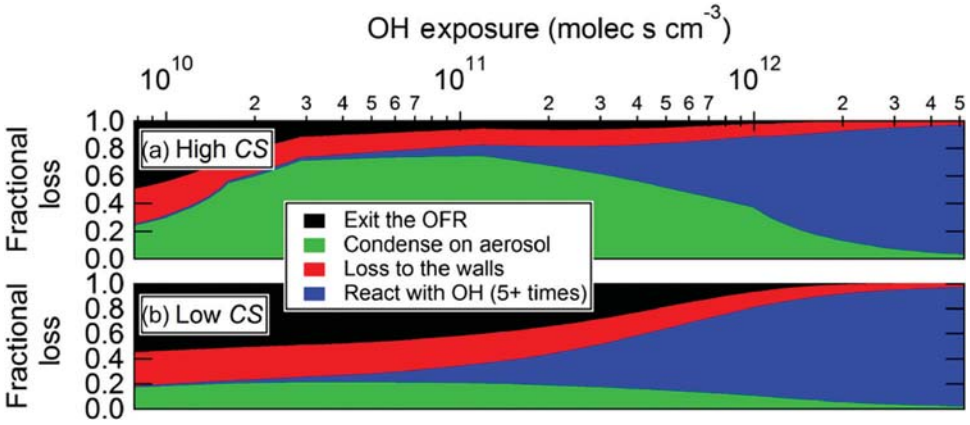

Fig. 7 Fractional fates of loss of LVOCs to OFR walls, condensation to aerosols, reaction with OH to produce volatile products, or exiting the OFR to be lost on sampling line walls as a function of photochemical age for (a) high and (b) low condensational sink (CS) cases; (c) LVOC lifetimes for each of these pathways. Lifetime for condensation to aerosols is shown for all data points (colored by OA enhancement after oxidation) using CS calculated from SMPS measurements.

photochemical eq. age of ~1 d, condensation is the dominant fate of SVOC and LVOC. Repeated reactions with OH become the dominant fate after an eq. age of a few weeks. However, in a low-CS case (OA concentration <0.3 μg m^{-3}), condensation lifetime is longer than 400 s, leading to significantly kinetically limited condensation (Fig. 7b). In this case, exiting the reactor and repeated reactions with OH are the dominant fates at low and high OH, respectively, while condensation is always a minor fate.

Eluri *et al.*[139] systematically modeled this condensation at different levels of aerosol surface area and residence time. Under the assumption of a mass accommodation coefficient of 0.1, they found that SVOC and LVOC condensation can be strongly kinetically limited. At low CS, SOA formed in OFR can be only 0–30% of that formed at equilibrium partitioning, which is often the case in the troposphere as chemical reactions are usually much slower than partitioning processes. If the recently demonstrated near-unity values are adopted for mass accommodation coefficient,[17,154] SOA yields are close to the values at equilibrium under many more conditions while at low CS they may still be as low as ~10% of the values at equilibrium. Therefore, very low CS in OFR can lead to a low bias in SOA yields and somewhat offset OFR's advantage of low wall losses under these conditions. Adding seed particles to increase CS can help overcome this limitation.

4.3. RO_2

In Fig. 5, OFR185(-iN_2O) and OFR254(-iN_2O) are clearly shown to be able to cover much of the area occupied by ambient cases in the $RO_2 + HO_2/RO_2 + RO_2/RO_2 + NO$ triangle plot. The relative importance of $RO_2 + RO_2$ in RO_2 fate is generally smaller than in ambient cases, while in OFR254(-iN_2O), $RO_2 + RO_2$ can dominate RO_2 bimolecular fate at very high OHR_{ext} (>100 s^{-1}).[50] Nevertheless, this is not difficult to explain in terms of RO_2 production and loss: compared to the atmosphere, both P_{RO_2} and L_{RO_2} are enhanced by a similar order of magnitude in those modes, by OH and HO_x, respectively. As a result, steady-state RO_2 concentration is comparable to ambient values, and thus so is the rate of $RO_2 + RO_2$, while $RO_2 + HO_2$ is usually several orders of magnitude faster in OFR than in the atmosphere (Peng *et al.*, 2019).[50] The reason why $RO_2 + RO_2$ can be more important under some OFR254-iN_2O conditions has been explained in Section 3.3.1 – high OHR_{VOC} and OH that is not substantially suppressed.

To simulate atmospheric chemistry relevant to typical urban atmospheres, high NO is an important condition to achieve. If this is the only focus, in the iN_2O modes, N_2O and UV should be as high as possible.[49] The higher N_2O, the higher concentrations of all NO_y species. Although a high UV elevates both NO and HO_x productions, the latter of which is responsible for much of NO loss, a high UV can enhance the dominance of NO over HO_2, as they destroy each other. However, a combination of high N_2O and UV obviously creates problems in other aspects of the atmospheric relevance. First, it produces too much NO_y, which is external OH reactant, suppresses OH and can result in significant non-tropospheric VOC photolysis (Sections 3.1.4 and 4.2.1). Second, this combination also favors an increasing relative importance of NO_3 *vs.* OH in VOC oxidation (Section 4.2.3).[49] In addition, it also produces very large amounts of NO_2. If NO_2 is higher than 1 ppm, it substantially promotes the conversion of RO_2 to RO_2NO_2.[48,49] Even for non-acyl RO_2, whose conversion to RO_2NO_2 is usually considered as reversible, such a high NO_2 can still make RO_2NO_2 a very large RO_2 reservoir and reduce steady-state RO_2 concentration by about an order of magnitude, which substantially slows down the organic radical chemistry in the reactor. Possible photolysis and reactions with OH of non-acyl RO_2NO_2 are unlikely to significantly shift the equilibrium of its reversible formation, since its photolysis and reactions with OH are usually substantially slower than its thermal decomposition.[118,147] We will discuss how to take these different aspects into account in Section 5. OFR369-i(PrONO) does not suffer from either VOC photolysis in the UVC range or VOC oxidation by NO_3, and can well achieve high-NO conditions.[87]

For acyl RO_2 in the iN_2O modes (to achieve high NO), acyl RO_2NO_2 formation has been shown above (Section 3.3.1) to be its dominant fate. However, the degree of this dominance is different in OFR185-iN_2O and OFR254-iN_2O, with the relative contribution of $RO_2 + NO_2$ to RO_2 fate of ~60–80% and ~100% in the former and the latter, respectively. This difference has important implications. Since acyl RO_2NO_2 formation is irreversible in OFR, a ~100% relative contribution of $RO_2 + NO_2$ implies that all other pathways of acyl RO_2 loss are closed and no other products can be formed from acyl RO_2. However, this is not the case in urban atmospheres, where $RO_2 + NO$ is also a significant pathway (Fig. 8).[50] The NO/NO_2 ratio in OFR185-iN_2O is much closer to the ranges for urban atmospheres, indicating that acyl RO_2 chemistry in OFR185-iN_2O is atmospherically relevant.

Under low-NO conditions $RO_2 + HO_2$ and $RO_2 + RO_2$ in OFR are generally atmospherically relevant (Fig. 5). The atmospheric relevance focus is thus on $RO_2 + OH$ and RO_2 isomerization. The atmospheric irrelevance for both types of reactions (too high and too low compared to the atmosphere, respectively) are caused by the same physical conditions, *i.e.* those resulting in high OH (and hence high radical levels). A combination of low OHR_{ext} and high H_2O and UV favors high OH (and generally high radical levels) in both OFR185 and OFR254.[50] Under these

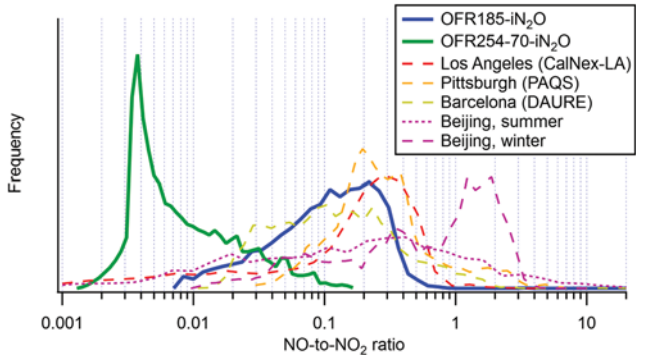

Fig. 8 Frequency occurrence distributions of NO-to-NO_2 ratios for OFR185-iN_2O and OFR254-70-iN_2O model cases and measured at the Los Angeles, Pittsburgh and Barcelona ground sites during the CalNex-LA 2010, PAQS 2002 and DAURE 2009 campaigns, respectively[156,228,229] and at a ground site in Beijing in both summer and winter.[230] OFR cases under bad conditions are filtered out. The total areas of all distributions are identical.

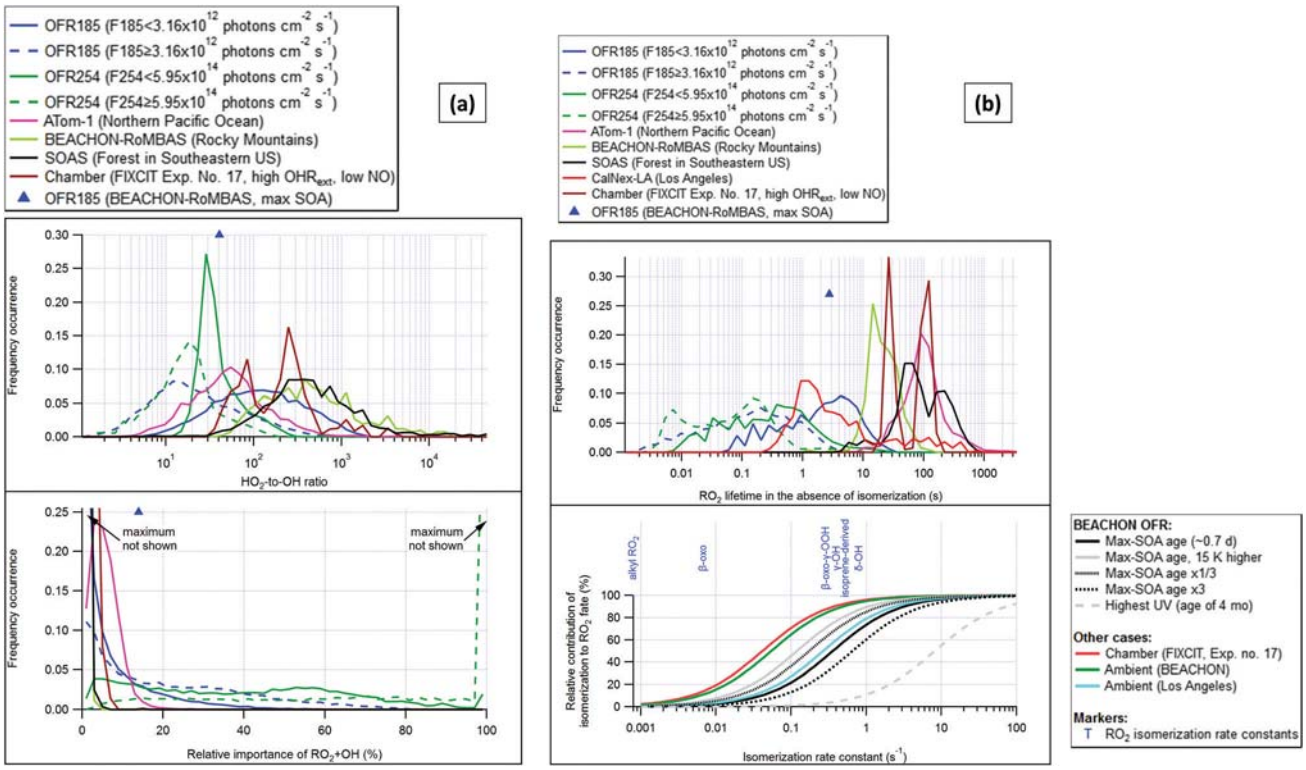

Fig. 9 (a) Frequency distributions of (top) the HO_2-to-OH ratio and (bottom) the relative importance of RO_2 + OH in the fate of RO_2 (with medium self/cross reaction rate coefficient) for OFR185 (including OFR185-iN_2O), OFR254-70 (including OFR254-70-iN_2O) and a chamber experiment and in the atmosphere (a couple of different environments). The OFR distributions for lower (F185 $< 3.16 \times 10^{12}$ photons cm^{-2} s^{-1}; F254 $< 5.95 \times 10^{14}$ photons cm^{-2} s^{-1}) and higher UV (F185 $\geq 3.16 \times 10^{12}$ photons cm^{-2} s^{-1}; F254 $\geq 5.95 \times 10^{14}$ photons cm^{-2} s^{-1}) are shown separately. Only good and risky conditions (in terms of non-tropospheric organic photolysis) are included in the distributions for OFR. Also shown are the HO_2-to-OH and the relative importance of RO_2 + OH for OFR experiments with ambient air input in field studies. (b) The top panel is in the same format as (a), but for RO_2 lifetime (RO_2 isomerization included in the model but excluded from lifetime calculation). The bottom panel shows the relative contribution of isomerization to RO_2 fate as a function of RO_2 isomerization rate coefficient in several model cases for OFR experiments in the BEACHON-RoMBAS campaign,[31] in a chamber experiment and in two ambient cases. Isomerization rate coefficients of several RO_2[119,131] are also shown.

conditions, HO_2/OH can be lowered to ~1, signifying a substantial contribution of RO_2 + OH to RO_2 fate, while ambient HO_2/OH is typically ~100,[21,155] implying the relative contribution of RO_2 + OH of several percent at most (Fig. 9a). On other hand, a lifetime (isomerization excluded) of ~10 s is needed for typical substituted RO_2, many of which isomerize at ~0.1–10 s^{-1} (see discussions in Section 3.3.3),[53,119,131,135] to sufficiently proceed in OFR (Fig. 9b). This is roughly the longest RO_2 lifetime that OFR185 and OFR254 (including variants) are able to achieve. Ambient RO_2 lifetimes are also typically on the order of 10–100 s (Fig. 9b). With the lifetime in this range, very fast-isomerizing RO_2 can always undergo isomerization sufficiently in both OFR and the atmosphere, while hydrocarbyl RO_2 always cannot. Thus, if a 10 s RO_2 lifetime (isomerization excluded) is achieved in OFR, the relative contribution of isomerization to the fate of most RO_2 in OFR is within a factor of 2 of that in the atmosphere (Fig. 9b).[50] To have a such long RO_2 time in OFR, limiting HO_x is needed, which can be achieved under the same conditions avoiding strong RO_2 + OH, *i.e.* lower H_2O, lower UV and/or higher OHR_{ext}.[50] However, low H_2O and/or high OHR_{ext} may cause significant non-tropospheric VOC photolysis. We will discuss in Section 5 how to straddle both sides of this consideration in more detail.

The abovementioned conditions that limit HO_x (lower H_2O, lower UV and/or higher OHR_{ext}) also lead to longer NO lifetime in OFR185-iNO, where O_3 is lower than OFR254-iNO. These OFR185-iNO cases are relevant to relatively clean urban atmospheres, such as Los Angeles during the CalNex-LA campaign.[34,156] Under these conditions, NO is expected to exist for significantly longer than 10 s, as the rate coefficient of NO + HO_2 is slightly smaller than that of RO_2 + HO_2 and that of NO + OH much smaller than that of RO_2 + OH. Also, the relative importance of NO + O_3 is minor at low F185, which does not produce a large amount of O_3. If a significantly higher amount of NO than HO_2 (*e.g.* tens of ppb) is injected in the OFR185-iNO mode, the dominance of RO_2 + NO over RO_2 + HO_2 can be achieved and typical RO_2 isomerizations are still possible. Similar conditions in OFR185-cNO have also been shown to be able to achieve high-NO conditions.[49] However, high NO in OFR254-iNO is impossible because of very short NO lifetime, as discussed in Section 3.2.1.

4.4. OA

Except for heterogeneous oxidation of OA by OH,[28,76,157–159] no processes occurring in the particle phase or on the particle

surface scale with gas-phase OH concentration.[160] The rates of particle-phase reactions,[158,159,161,162] gas-particle partitioning[17] and reactive uptake of gases other than OH[163–165] are all independent of gas-phase OH. Nevertheless, some of these processes can be accelerated so that they do not become minor or too slow compared to enhanced reactions with OH in OFR. What can be done to achieve this will be discussed in Section 5. In this subsection, a few types of possibly atmospherically irrelevant processes are discussed.

4.4.1. OA photolysis. Similar to VOC photolysis, this topic is two-fold, OA photolysis in the UVC range and that in the UVA and UVB range, of which the former is atmospherically irrelevant and the latter relevant. Limited by the lack of quantum yield data of organic photolysis at 185 and 254 nm in the condensed phase, Peng *et al.*[47] found that OA photolysis might be significant during short residence times of OFR if OA photolysis quantum yields are non-negligible. Nevertheless, they also pointed out that condensed-phase photolysis quantum yield may be very low. Malecha *et al.*[166] confirmed by quartz crystal microbalance measurements of OA under 254 nm irradiation that OA photolysis at 254 nm is so slow as to be negligible during short residence times of OFR. Peng *et al.*[47] found OA photolysis at 185 nm to be less important than that at 254 nm because of F185 lower than F254. Nevertheless, this finding was based on the assumption of relatively high quantum yields, which has been found to be not true for 254 nm photolysis. 185 nm photons, $\sim$170 kJ mol^{-1} more energetic than those at 254 nm, may still result in substantially higher quantum yields and be more important for OA photolysis. Besides, if the particles have a significant water content, OH and HO_2 production from its photolysis in the particle phase can be strong and oxidation processes in OA may be further accelerated. Neither of the two types of reactions that 185 nm photons may induce in the particle phase has been investigated experimentally. Future research on them is warranted. As organic photolysis in the UVA and UVB range is much weaker than in the UVC range (Section 4.2.1), OA photolysis at tropospheric wavelengths is negligible, while ambient OA photolysis is an important OA aging process.[167–169] and hence represents a known deviation between atmospheric and OFR conditions.

4.4.2. Heterogeneous and particle-phase processes. Chemistry involving heterogeneous and particle-phase processes is a large field of research itself and not the main focus of this Review. Nevertheless, slow rate constants of heterogeneous oxidation and the need for high OH to accelerate it under laboratory conditions have led to frequent application of OFR in this subfield.[28,71,75–81,109] We thus also discuss some concerns over the atmospheric relevance of timescales of heterogeneous processes and related particle-phase chemistry in OFR, although it has been shown that it is appropriate to consider oxidant concentration and reaction time as interchangeable parameters with oxidant exposure being conserved in many OFR applications in heterogeneous oxidation.[170]

Of the heterogeneous processes that are not as accelerated in OFR as OA heterogeneous oxidation, OA growth, *i.e.* condensable gases partitioning to particle phase, is of most importance. Due to the short residence times of OFR, Palm *et al.*,[31] Ahlberg *et al.*[171] and Eluri *et al.*[139] showed by different experimental and modeling methods that the gas-particle partitioning of SVOCs and LVOCs are often not sufficiently fast to reach equilibrium within OFR residence times, especially at low OA concentrations. A higher condensational sink and/or a longer residence time favor the relative importance of condensation.[31,139,171] Besides, if OH is too high, reactions of SVOCs and LVOCs with OH are more kinetically favorable than their condensations.[31] At low CS, kinetically limited condensation can significantly lower OA yield,[139] which is one of the most important quantities measured in OFR experiments. Hu *et al.*[33] discussed a similar issue, *i.e.* kinetically unfavorable VOC reactive uptake by OA in the OFR. In their OFR experiments, the reactive uptake of isoprene epoxydiols (IEPOX) by acidic aerosols, a major or even dominant fate of IEPOX in the atmosphere, is negligible compared to its reactions with OH. This deviation can be remedied by using an acidic seed.[33] On the other hand, heterogeneous oxidation may also compete with OA evaporation in OFR,[172] while in the atmosphere, the former is orders of magnitude slower than the latter.

Heterogeneous oxidation itself is not simply linearly accelerated by increasing OH concertation. Renbaum and Smith[170] and Slade and Knopf[173] noted that heterogeneous oxidation of OA by OH can be explained by the Langmuir–Hinshelwood mechanism, which means that at high oxidant concentrations, saturation of active adsorption sites on OA surface and competition for these sites between oxidants may occur. Decrease in the reactive uptake coefficient of this type of processes with increasing OH and inhibition of OH heterogeneous reactions by high O_3 were observed in OFR.[170,173] High OH on the OA surface may also cause diffusion limitations for key organic species in OA even with low viscosity, where the species near the surface is more rapidly consumed by OH than replenished by its diffusion from the bulk, and hence depleted.[159,174,175] This phenomenon should be much less important in the atmosphere as heterogeneous oxidation is orders of magnitude slower than in OFR. Particle-phase RO_2 + RO_2 can also be accelerated far more than linearly in OA, especially near the surface, as OH increases, resulting in a large role of this reaction in particle-phase chemistry in this type of OFR applications.[174] NO and SO_2 were found to be able to extend the chain of the radical reactions involving RO_2 in OA by converting RO_2 to RO,[79,80] but such an effect is much smaller in OFR than in the atmosphere as RO_2 lifetime in OFR is much shorter.

A key parameter to gauge the impact of higher-than-ambient OH in OFR on particle-phase chemistry is the reaction-diffusion index (I_{RD}), defined as the ratio of particle-phase diffusion timescale to that of heterogeneous oxidation by OH.[174,175] I_{RD} depends on OH concentration, particle size and diffusion coefficient. Houle *et al.*[175] showed that OFR experiments of alkane OA oxidation yield OA composition predictive of that in the atmosphere at $I_{RD} < \sim 10$, implying that the chemistry is not seriously limited by diffusion. For that particular type of experiments, OH only needs to be $\ll 10^{14}$ molecules cm^{-3} (under the assumption of a particle diameter of 150 nm) for $I_{RD} \ll \sim 10$. This condition can be met in all OFR experiments with alkane OA, which is not viscous. Maximal OH allowed in other experiments to keep the general atmospheric relevance in OA chemistry can be orders of magnitude different depending

on particle size and phase state and the type of specific heterogeneous oxidation.[175]

Another important type of particle-phase reactions are acid-catalyzed reactions (*e.g.* acid-catalyzed oligomerization and cyclic hemiacetal dehydration).[151,176] Substrates in these catalytic reactions are often products of gas-phase chemistry partitioning to the particle-phase. Their supply in the particle phase is thus often controlled by condensation. As a result, at a particle acidity similar to that in ambient particles, these particle-phase reactions are not as much accelerated as heterogeneous oxidation in OFR. Similar to IEPOX reactive uptake, this deviation in particle-phase chemistry can also be remedied by increasing particle acidity.

For particle-phase oligomerizations that are not catalyzed, their own rate constants are the governing factor for their atmospheric relevance. Those with ambient timescales substantially longer than OFR timescales (*e.g.* hours) do not proceed significantly in OFR, but can be significant processes in the atmosphere. Those with ambient timescales shorter than condensation timescales (seconds or shorter) are very fast and limited by condensation in both the atmosphere and OFR. Other particle-phase oligomerizations have ambient timescales comparable to or slightly longer than OFR timescales (minutes). Their atmospheric relevance depends on both gas-phase monomer concentration and condensation rate. The former is not necessarily much higher in OFR than in the atmosphere (see Section 4.1), and thus the latter is likely to be more easily adjusted experimentally (*e.g.* by adding seed aerosol).

4.4.3. Particle charging. As 185 nm photons are highly energetic (6.7 eV), and it was reported that Hg lamp emissions could photoionize ambient aerosols of mainly organic material,[177] there is some speculation that OA may be significantly photoelectrically charged by 185 nm photons in OFR and thus aerosol dynamics and physics may significantly deviate from a mainly neutral growth as in the atmosphere.[152,178] Palm *et al.*[63] compared charged particles detected by a scanning mobility particle sizer with and without using a radioactive neutralizer to charge particles at the exit of their OFR. They found that an overwhelming majority of smaller particles (newly formed in the OFR) were not charged (and thereby not detected) without using the neutralizer, and suggested that OFR does not inherently produce little amount of charged OA particles by its UVC light.

This is consistent with the fact that except organic molecules with a very large conjugation (*e.g.* PAH), all common possible organic components of aerosols have a gas-phase ionization potential higher than 8.7 eV,[179] higher than the 185 nm photon energy (6.7 eV). The impact of the small size and the large surface curvature of nanoparticles on their work function/ionization potential is only of the order of 0.01–0.1 eV.[180,181] OA matrix polarization typically lowers ionization potential by 1–2 eV relative to the gas phase.[182] Therefore, even with all these effects taken into account, most organic aerosol components are not photoionizable at 185 nm. However, large polycyclic aromatic hydrocarbons (PAHs), soot in combustion exhausts and some metal material in aerosols can be ionized by 185 nm (and even 254 nm) photons.[183] These types of material mixed into OA can make OA photoionizable in the UVC range. This is why some ambient aerosols that are mainly organic can be ionized by Hg lamp emissions.[183,184] If OFR is used to process gases containing PAHs, soot or metals (*e.g.* vehicle exhausts), particle charging by Hg lamp emissions can be significant, increasing particle wall losses.[185]

5. Experimental planning considerations

Having discussed the atmospheric relevance of different aspects of VOC oxidation and SOA formation in OFR, we will recommend physical conditions for atmospherically relevant chemistry and provide several practical measures to include this chemistry and/or avoid undesirable chemistry in OFR.

5.1. Conditions and/or measures to deal with specific deviations from tropospheric chemistry

In Section 4, a number of issues concerning the atmospheric relevance of the chemistry in the main OH OFR modes (OFR185 and OFR254 variants) have been raised (Table 3). We list them in roughly decreasing severity as follows: (1) non-tropospheric VOC photolysis, (2) non-acyl RO_2 suppression by high NO_2, (3) insufficient condensational sink or reactive uptake, (4) insufficient RO_2 isomerization at relatively low NO, (5) excessive reaction of RO_2 with OH at low NO, (6) undesired VOC oxidation by NO_3, (7) high NO not achieved (if it is desired), (8) nearly total acyl RO_2 loss through $RO_2 + NO_2$, (9) particle charging by UV, (10) insufficient OA photolysis at tropospheric wavelengths, and (11) VOC ozonolysis (if its exclusion is desired) or insufficient VOC ozonolysis (if its inclusion is needed). Note that the severity of these issues may be different than listed above depending on the specific conditions used and the goal(s) of specific experiments.

We detail our rationales for the abovementioned order of severity as follows: non-tropospheric VOC photolysis is labeled as the most severe issue since it affects most VOCs, both primary and secondary, and it is likely to fundamentally alter VOC oxidation mechanism. The oxidation of an overwhelming majority of primary and secondary VOCs involves non-acyl RO_2. In the presence of very high NO_2, RO_2 suppression by NO_2 causes a substantial delay of the entire reaction network of VOC oxidation. This issue is thus ranked as the second most problematic. Insufficient condensational sink or reactive uptake is ranked next because under some conditions it can substantially affect OA yield, which is an important parameter quantified in many OFR studies (Table 4). Insufficient RO_2 isomerization and significant RO_2 + OH at low NO are roughly at the same severity level, which is below the first three issues, as their atmospheric irrelevance, though obvious, is only for a part of the relevant RO_2 chemistry. VOC oxidation by NO_3 in OH OFR and failure to achieve high NO when it is desired deviate a part of VOC oxidation from pathways occurring in the atmosphere. Nevertheless, in terms of products, these issues have some mitigating factors: the main products of VOC oxidation by

Table 3 Common issues of undesired processes or lack of desired processes in roughly decreasing severity, species directly affected by these issues and physical conditions to avoid and/or other measures to implement to avoid these issues

Number	Issue	Primary VOCs	Gas-phase intermediates and products	RO_2	OA	Corresponding condition(s) to avoid in OFR185 and OFR254 (including variants)	Other mitigation measure(s)
1	Non-tropospheric VOC photolysis	×	×			Low H_2O and/or high OHR_{ext}	Use UVA and/or UVB as light source (*e.g.* OFR369-i(iPrONO))
2	Non-acyl RO_2 suppression by high NO_2			×		Primarily high O_3 (high F185 in OFR185 variants; high injected O_3 in OFR254 variants)	Use OFR369-i(iPrONO) but avoid very high iPrONO and F369
3	Insufficient condensational sink		×		×	High H_2O, high UV and/or very low OHR_{ext}; very short residence time	Add seed aerosol
4	Insufficient RO_2 isomerization at relatively low NO			×		High H_2O, high UV and/or very low OHR_{ext}	Increase temperature
5	Reaction of RO_2 with OH at low NO			×		High H_2O, high UV and/or very low OHR_{ext}	
6	Excessive VOC oxidation by NO_3 in OH reactor	×	×			Primarily high O_3 (high F185 in OFR185 variants; high injected O_3 in OFR254 variants)	Use OFR369-i(iPrONO) if appropriate
7	High NO not achieved (if it is desired)			×		Low NO injection or precursor, high H_2O and/or high UV	Use OFR369-i(iPrONO) if appropriate
8	Nearly total acyl RO_2 loss through $RO_2 + NO_2$			×		OFR254-iNO at very high NO and OFR254-iN_2O at significant N_2O level	
9	Particle charging by UV				×	Source with existing aerosols containing PAHs, soot and/or metals	Use UVA and/or UVB as light source (*e.g.* OFR369-i(iPrONO))
10	Insufficient OA photolysis at tropospheric wavelengths		×		×	(Present under all conditions)	Use modes with UVA/UVB light sources; add strong UVA/UVB lights in OFR185 and OFR254 variants
11	VOC ozonolysis (if its exclusion is desired); Insufficient VOC ozonolysis (if its inclusion is desired)	×	×			Low H_2O and/or high OHR_{ext} (more strictly for OFR254 variants); high H_2O and/or low OHR_{ext} in OFR185 variants	Use lower O_2 in OFR185 variants; inject additional O_3 in OFR185 variants

Table 4 Studies using PAM (listed in PAM Wiki)[66] for different experimental purposes in roughly increasing difficulty in experimental planning

Experimental application		Ref.	Number
Mainly OA heterogeneous oxidation		33, 57, 116, 205, 226 and 231	6
Inorganic gas processing/aerosol formation		45, 64 and 232	3
Organic VOC oxidation/aerosol formation	OA carbon oxidation state/O:C	34, 36–38, 56, 57, 59, 62–64, 101, 116, 171, 200, 203, 204, 208, 226 and 233–246	32
	SOA formation/yield/enhancement	31, 34, 36–38, 59, 63, 64, 101, 116, 171, 203, 204, 226, 234, 237, 240, 243 and 247–252	24
	OA hygroscopicity/cloud condensation nucleus activity/viscosity/phase state/ice nucleation activity/volatility	56, 57, 63, 116, 208, 233, 239, 242, 246 and 252–256	14
	Positive matrix factorization/source apportionment of OA	63 and 242	2
	Aerosol size distribution/dynamics	31, 64, 171, 250, 252 and 256	6
	OA optical property	227, 235, 241, 244, 245 and 247	6
	OA health effects	200	1
	Specific gas-phase organic product(s)	31, 86, 87, 236, 240 and 257	6
	Chemical speciation of organic gas/aerosol product(s)	201, 242 and 258	3

NO_3, organic nitrates, are also produced by RO_2 + NO, the key reaction of high-NO chemistry, although the structures of the nitrates formed can be different. Failure to reach high NO is somewhat coupled with high H_2O and/or UV, which produces large amounts of oxidants and simultaneously elevates the relative importance of RO_2 + OH, which then generates the main high-NO pathway organic product, *i.e.* RO. While nearly total inhibition of acyl RO_2 chemistry by acyl RO_2 + NO_2 is a serious problem for acyl RO_2, acylperoxy radicals only form after several (at least 2) steps of oxidation[51] and are not the main type of RO_2 even at relatively high photochemical ages.[50] We thus would rank this issue the 8th. Particle charging by UV is considered as the 9th because it can be an issue only in the presence of PAHs, soot and/or metals in the sources injected into the reactor, only affecting certain types of experiments (mainly those with combustion exhaust, which however are very common OFR applications). We believe that insufficient OA photolysis at tropospheric wavelengths has a similar severity as it also has a negligible impact on the gas-phase chemistry (through releasing a very small amount of volatile photo-products). VOC ozonolysis is ranked as the last as this process is significant in the atmosphere as well as under many OFR conditions (Fig. 6c) and its exclusion is desired only for specific experimental purposes (*e.g.* study of VOC oxidation by OH only for experimental simplicity).

In the following, we will discuss the physical conditions that need to be avoided in the OFR185 and OFR254 operation mode variants and additional measures that may be adopted in these or other modes to avoid each of these issues.

5.1.1. Non-tropospheric VOC photolysis. As discussed in Section 4.2.1, low H_2O and/or high OHR_{ext} should be avoided to keep non-tropospheric VOC photolysis minor or negligible. Peng *et al.*[47] recommended the criteria of $H_2O > 0.8\%$, $OHR_{ext} < 30\ s^{-1}$ and $F185 > 1 \times 10^{12}$ photons $cm^{-2}\ s^{-1}$ and of $H_2O > 0.5\%$ and $OHR_{ext} < 50\ s^{-1}$ for "safer" conditions in OFR185 and OFR254, respectively. These criteria are mainly for operational purposes, *i.e.* ensuring minor or negligible non-tropospheric VOC photolysis, and thus largely sufficient (but not necessary) conditions for good conditions as later defined by Peng and Jimenez[48] (see Section 4.2.1) (Fig. 6a, b and 10c). The additional requirement for "safer" conditions in OFR185, *i.e.* $F185 > 1 \times 10^{12}$ photons $cm^{-2}\ s^{-1}$, was added for a simple and practical recommendation, as at low UV in OFR185, OHR_{int} is low and the system is more susceptible to OH suppression (Section 3.1.4) and the thresholds of H_2O and OHR_{ext} need to be adjusted according to each other, which is more complex than an easy-to-use criterion for "safer" conditions. Similarly, Peng *et al.*[47] recommended avoiding "riskier" conditions that reach $H_2O < 0.1\%$ or $OHR_{ext} \geq 100\ s^{-1}$ in OFR185 and $H_2O < 0.1\%$ or $OHR_{ext} > 200\ s^{-1}$ in OFR254 and called other conditions "transition" conditions (Fig. 6a, b and 10a, b). Again, these criteria were made for simple and practical use. Under "riskier" conditions, a non-good (risky or bad) condition is almost guaranteed. "Riskier" conditions cover almost all bad conditions and a part of risky conditions (Fig. 6a, b and 10c). "Transition" conditions may actually lead to both good and risky conditions (Fig. 6a, b and 10c). Also, as more and more aspects of atmospheric relevance in addition to non-tropospheric VOC photolysis are taken into account, the abovementioned criteria are no longer practical for a simple use in experimental planning. Therefore, recent classifications of conditions (also in this Review) have been mainly based on the good/risky/bad one[48–50] (see Section 4.2.1).

Many past OFR laboratory and source studies failed to meet the requirements for "safer" conditions (Fig. 10a and b) and likely there were indeed non-tropospheric VOC photolysis problems in many experiments in those studies (Fig. 6a and b). Some were due to very high OHR_{ext}, which can be avoided by diluting sources or injecting a smaller amount of sources/precursors, and others due to very low H_2O (Fig. 10a and b), which can be avoided by humidifying sources. The recommended dilution factor for vehicle exhausts to be processed in OFR185 without major non-tropospheric VOC photolysis is >100.[48] Interestingly, past OFR field experiments were generally conducted under "safer" (Fig. 10a and b) and hence good conditions (Fig. 10c) and they were mainly good when F185/OH and F254/OH are examined (Fig. 6a and b). This is because in ambient air, relatively humidity is rarely very low ($< \sim 3\%$) and OHR_{ext} does not often substantially exceed $30\ s^{-1}$.

OFR369-i(iPrONO) inherently does not have non-tropospheric VOC photolysis as its light source wavelength, 369 nm, is tropospheric. However, it is only for high-NO experiments and can only reach an equivalent photochemical age of $\sim$1 d.

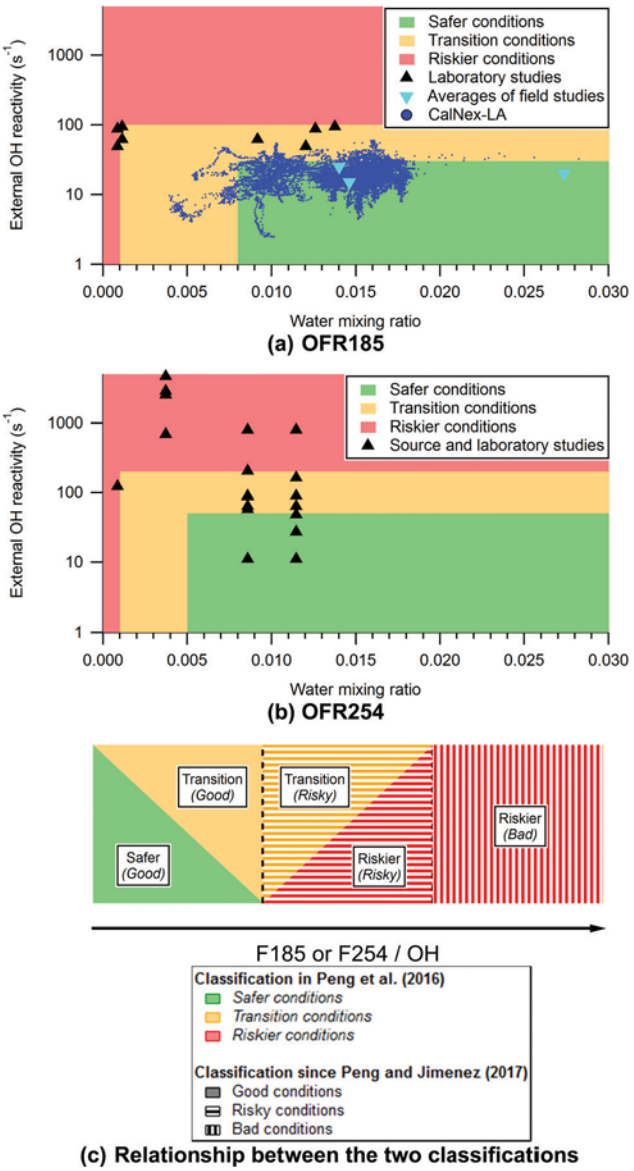

Fig. 10 (a) "Safer", "transition" and "riskier" conditions in OFR185; (b) same plot for OFR254; (c) schematic illustrating an approximate relationship between the safer/transition/riskier and good/risky/bad classifications of conditions. Also shown are data points for several field, laboratory and source studies using OFR.[31,33,34,57,59,227] The scatter is for a time series of an OFR study in the CalNex-LA campaign.[34] The data points of the averages of the OFR experiments in field studies correspond to (from left to right) the CalNex-LA, BEACHON-RoMBAS[31] and SOAS[33] campaigns.

5.1.2. Non-acyl RO_2 suppression by high NO_2. As discussed in Sections 3.2, 3.3 and 4.3, a very large amount of NO_2 produced *via* $NO + O_3 \rightarrow NO_2 + O_2$ is the main reaction causing this issue. Thus, there are two ways that effectively avoid it, *i.e.* limiting NO and limiting O_3. The former way simply means injecting less NO or its precursor in OFR185 and OFR254 variants; the latter translates into avoiding high F185 in OFR185 variants and into injecting less O_3 in OFR254 variants.

OFR369-i(iPrONO) can also avoid a ppm-level NO_2 under most conditions because of no O3 and relatively low HO_x and NO_x production (compared to the iN_2O modes). Nevertheless, a combination of very high iPrONO and F369 should be avoided, as when they are both very high, NO_2 can exceed 1 ppm, leading to significant non-acyl RO_2 sequestration.[87]

5.1.3. Insufficient condensational sink or reactive uptake. According to the discussions in Sections 4.2.4 and 4.4.2, kinetically limited OA growth/gas condensation can be mitigated either at longer residence times, which allows relatively slow condensations to sufficiently proceed, or with a higher condensational sink, which can be realized by using seed aerosols. Note that residence time for typical OFR cannot be easily prolonged to $> \sim$10 min, at which condensable gas wall loss will be significant.[31,32]

Insufficient reactive uptake of VOCs by OA is conceptually similar to insufficient condensational sink. Enhancing the particle-phase reactant(s) involved in the reactive uptake can accelerate the reactive uptake. For instance, Hu *et al.*[33] proposed to use strongly acidified seeds to promote IEPOX reactive uptake by acidic OA.

5.1.4. Insufficient RO_2 isomerization at relatively low NO. As shown in Section 4.3, it is difficult to attain RO_2 lifetimes in OFR (without isomerization) of $\sim$10 s at low NO, and to achieve it, relatively low UV and H_2O and a significant OHR_{ext} are preferred. Peng *et al.*[50] also proposed increasing temperature by $\sim$15 K, which may lead to an $x \sim 3$ increase in typical RO_2 isomerization rate coefficients (because of their relatively high activation energies) and minor or negligible changes to most rate coefficients, which have little temperature-dependence (Fig. 9b). Some change in aerosol partitioning is expected as saturation concentrations are expected to change by $\sim$x10 for this temperature change.[186]

5.1.5. Reaction of RO_2 with OH at low NO. As for the RO_2 isomerization issue, a combination of relatively low UV and H_2O and relatively high OHR_{ext} is preferred for a minor relative contribution of $RO_2 + OH$ to RO_2 fate at low NO. Nevertheless, its restrictions are not as tight as for RO_2 isomerization, *i.e.* a larger volume in the physical condition space resulting in minor $RO_2 + OH$ than in significant typical RO_2 isomerization.

5.1.6. Excessive VOC oxidation by NO_3. As discussed in Section 4.2.3, high NO_3/OH is mainly promoted by high O_3. Similar measures as those to avoid RO_2 suppression by high NO_2 can be adopted to avoid high NO_3/OH ratios. Also, OFR369-i(iPrONO) has no NO_3 oxidation issue and is suitable for experiments requiring $< \sim$1 d of aging.

5.1.7. High NO not achieved (if it is desired). To ensure high NO, its sufficient production should be guaranteed and its loss limited. Therefore, at minimum an injection of tens of ppb of NO is needed in the iNO modes, $\sim$1 ppb s^{-1} for OFR185-cNO and $\sim$2–3% N_2O in the iN_2O modes. On the other hand, high H_2O and UV, which create high HO_x (and O_3 in OFR185 variants), should be avoided. Similarly, high O_3 injection should also be avoided in OFR254 variants.

Again, OFR369-i(iPrONO), with a different NO and HO_x production mechanism, always ensures high NO (dominating over HO_2) and is applicable in lower-aging experiments. High-NO aging with age >1 d (*e.g.* similar to eastern China under some conditions) can be better simulated in the iN_2O and cNO modes.

The transition regime, where both high- and low-NO pathways play a major role in RO_2 loss, is a typical chemical regime

in many rural and forest areas (Fig. 6). It can be achieved by the iN_2O and cNO modes if the amount of NO (precursor) injected is well tuned. OFR369-i(iPrONO) cannot simulate transition regime as its chemistry is always dominantly high-NO.

5.1.8. Nearly total acyl RO_2 loss through RO_2 + NO_2. As discussed in Section 4.3, this is an issue solely for OFR254-iNO and OFR254-iN_2O. Also, as long as there is a high NO injection or production, NO_2 should be high enough to dominate acyl RO_2 fate because of fast NO + O_3 → NO_2 + O_2 in OFR254 variants. Thus, hundreds of ppb of injected NO in OFR254-iNO and roughly 1% or more of N_2O should be avoided in these modes.

5.1.9. Particle charging by UV. As discussed in Section 4.4.3, this is an issue in OFR185 and OFR254 (including variants) experiments with sources containing PAHs, soot and metals. Thus, these sources should be avoided, or the issue should be quantified experimentally. Particle charging by UV is no longer an issue if only UVA and UVB light sources are employed in the reactor.

5.1.10. Insufficient OA photolysis at tropospheric wavelengths. This issue is present in all OFR185 and OFR254 variants. To avoid it, operation modes with lamps emitting at tropospheric wavelengths (*e.g.* CPOT with blacklights[61] and OFR369-i(iPrONO)) can be employed. Nevertheless, those less energetic lamps result in lower equivalent photochemical ages than in OFR185 and OFR254 variants. Adding strong UVA and UVB lamps in OFR185 and OFR254 variants could also mitigate this problem.

5.1.11. VOC ozonolysis (if its exclusion is desired). VOC ozonolysis is just another non-OH VOC loss process, in addition to non-tropospheric VOC photolysis. In principle, similar condition as those needed to achieve minor non-tropospheric VOC photolysis should be used to minimize the relative contribution of O_3 to VOC loss if it is desired (*e.g.* ref. 187). In OFR254 variants, a lower O_3 injection can obviously make its reactions with VOCs less important. Peng *et al.*[47] also suggested that lowering O_2 in the source air can reduce O_3 production in OFR185, and thereby the relative importance of VOC ozonolysis. When an atmospherically-relevant contribution of VOC ozonolysis is desired, O_3/OH close to ambient values is needed. If O_3 presence is not sufficient as under some good OFR185 conditions (Fig. 6c), additional O_3 may be injected.

5.2. Comprehensive planning

In many OFR experiments, multiple atmospheric relevance issues should be simultaneously considered in experimental planning. A subspace of physical conditions that satisfy multiple requirements is the intersection of the subspaces that meet the individual requirements. As the number of experimental goals increases, the subspace of conditions that achieve all goals shrinks. Sometimes the subspace of the ideal conditions can be so small that the design of ideal experiments becomes very difficult or even impossible. In this case, it is necessary to tailor the experimental planning requirements based on the main purpose(s) of the experiments and loosen or drop some requirements that are not critical to the main purpose(s). In this subsection, we will first show the ideal conditions for typical low- and high-NO experiments in OFR185 and OFR254 variants, and then discuss the trade-off between the difficulty in finding satisfactory conditions and the quality of the outcome of designed experiments in OFR experimental planning. As insufficient OA photolysis at tropospheric wavelengths and particle charging by UV cannot be avoided by a careful selection of suitable conditions in the OFR185 or OFR254 (including variants) physical condition space spanning over the H_2O, UV, OHR_{ext}, O_3 (in OFR254 variants only) and NO precursor (or NO) dimensions, but can be avoided or mitigated by other measures, we will not consider these two issues in the discussions of ideal physical conditions.

5.2.1. Ideal conditions for low NO. At a minimum, (i) non-tropospheric VOC photolysis, (ii) RO_2 + OH and (iii) RO_2 isomerization should be taken into account in order to find the ideal conditions for low-NO experiments in OFR185 and OFR254. To avoid the first and the latter two issues, the requirements for physical conditions are contradictory: high H_2O and low OHR_{ext} are favored to avoid the first issue, while to avoid the others, high H_2O and UV and low OHR_{ext} are not preferable. Therefore, some compromise has to be made during the selection of the best conditions.

The key to keeping RO_2 + OH and RO_2 isomerization atmospherically relevant is a limited level of OH and HO_2. Decreasing H_2O and decreasing UV have almost equal effects on limiting OH and HO_2 (see Section 3.1.1). However, in terms of non-tropospheric VOC photolysis, decreasing UV is certainly preferred to decreasing H_2O.[50] Fig. 9 clearly shows that a lower UV reduces the relative importance of RO_2 + OH in RO_2 fate and prolongs RO_2 lifetime (without isomerization) in both OFR185 and OFR254.

Nevertheless, if bad conditions (in terms of non-tropospheric VOC photolysis) are excluded, although RO_2 lifetime is shown to be longer at lower UV, OFR254 can hardly reach an RO_2 lifetime of ~10 s (Fig. 9b). This is because the high O_3 in OFR254 promotes the interconversion between OH and HO_2 maintain a relatively high OH even at low H_2O and F254 (see Section 3.1.2). High O_3 is also the origin of the resilience of OFR254 to OH suppression. As a consequence, OH cannot be sufficiently low to allow typical RO_2 isomerization unless a substantial OHR_{ext} (relative to OHR_{int}) heavily suppresses OH and causes non-tropospheric VOC photolysis. Therefore, no OFR254 condition is ideal for low-NO OFR experiments.

In contrast to OFR254, a sufficiently long RO_2 lifetime can be reached at low F185 in OFR185, while high H_2O and low OHR_{ext} are maintained to avoid non-tropospheric VOC photolysis. Fig. 11 maps a range of F185 and OHR_{ext} (at H_2O of 2.3%) that satisfy all the three conditions mentioned at the beginning of this subsection. A combination of high H_2O (~2%), moderate or low F185 ($< \sim 1 \times 10^{12}$ photon cm^{-2} s^{-1}) and low (~10 s^{-1}) OHR_{ext} is preferred. OHR_{VOC} (the main component of OHR_{ext} in this case) cannot be too low (close to 0) to ensure a significant RO_2 and OA production.

Under these preferred conditions, OH is relatively low (around 10^9 molecules cm^{-3}) and hence cannot cause overoxidation of SVOCs and LVOCs (as discussed in Sections 4.2.4 and 4.4.2). If gas-particle partitioning is still kinetically limited, seed aerosols and/or a longer residence time can be applied. Then all low-NO atmospheric relevance issues (except insufficient OA photolysis

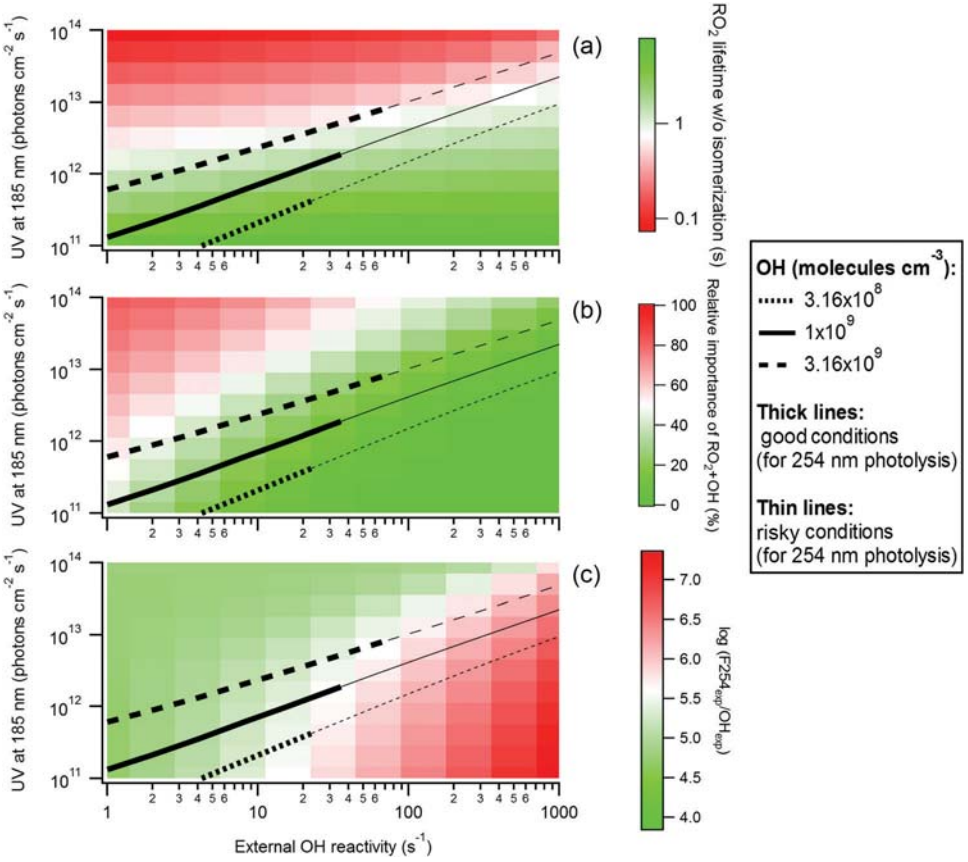

Fig. 11 (a) RO_2 lifetime in the absence of isomerization, (b) relative importance of RO_2 + OH in RO_2 fate and (c) logarithm of the exposure ratio between 254 nm photon flux and OH as a function of 185 nm photon flux and external OH reactivity for OFR185 at N_2O = 0 and H_2O = 2.3%. Three lines denoting conditions leading to OH of 3.16×10^8, 1×10^9 and 3.16×10^9 molecules cm^{-3}, respectively, are added in each panel. The thick and thin parts of these lines correspond to good and risky conditions in terms of 254 nm organic photolysis (which is usually worse than 185 nm organic photolysis)[47] respectively.

at tropospheric wavelengths and particle charging by UV) are addressed. In Fig. 9 and 10a, an OFR field study in the BEACHON-RoMBAS campaign is shown as an example that all these requirements except at low CS causing kinetic limitation in condensation.

On the other hand, also because of the low OH under these conditions, the equivalent photochemical age that these conditions are able to reach is a few days. This age is long enough for the photochemistry to achieve the maximal SOA formation in case of ambient air processing (Fig. 9).[31,34] If both SOA formation at lower photochemical ages (up to a few days) and fragmentation at higher ages (days to weeks)[28,34] need to be studied under atmospherically relevant conditions in OFR185, a two-stage solution was proposed by Peng *et al.*[50] In the first stage, the reactor should be operated as discussed above to achieve the maximal SOA formation; in the second stage, a much higher F185 can be used, often in another reactor in series, to realize heterogeneous oxidation of OA by OH at high photochemical ages. The second stage is viable since past the maximal SOA formation age, gas-phase organic radical chemistry becomes less important for SOA formation, and, at very high OH, particle-phase/heterogeneous and gas-phase chemistries are relatively decoupled.[33,48,79]

5.2.2. Ideal conditions for high NO. If only a lower photochemical age (<1 d) is required, the simplest way to perform a high-NO OFR experiment that meets all the atmospheric relevance requirements discussed above is to just use OFR369-(iPrONO) while avoiding very high iPrONO ($\gg$1 ppm) and F369 ($\gg 1 \times 10^{16}$ photons cm^{-2} s^{-1}) that produce too much NO_2.

Similar to OFR185 and OFR254, there is also somewhat of a dilemma in the selection of the ideal high-NO conditions in OFR185-iNO (OFR254-iNO does not lead to any meaningful high-NO conditions; see Section 3.2.1). For minor or negligible non-tropospheric VOC photolysis, high H_2O and low OHR_{ext} are desired, while high H_2O and UV and low OHR_{ext} elevate HO_x and O_3 levels, which shortens NO lifetime. For similar reasons discussed in Section 5.2.1, a low UV is much preferred to a low H_2O. In addition, NO, necessary for high-NO conditions, is also an external OH reactant, which tends to make conditions worse. Thus, another compromise for NO needs to be made. Fig. 12a maps good/risky/bad high-/low-NO conditions for OFR185-iNO in detail and clearly identifies good high-NO conditions at high H_2O, low F185, low OHR_{ext} and initial NO between $\sim$10 and a few hundreds of ppb. Obviously, such a range of conditions also lead to relatively low OH (equivalent photochemical age up to a few days). Also, low F185 limits O_3, and thereby NO_2 and NO_3 production. Thus, good high-NO conditions in OFR185-iNO have no issues of RO_2 suppression by high NO_2 and VOC oxidation by NO_3 (Fig. 6d).[48] Note that, because of the low

oxidant levels under OFR185-iNO good high-NO conditions, RO_2 + NO only dominates over RO_2 + HO_2 and RO_2 lifetime is still sufficient for active typical RO_2 isomerization, which is analogue of less-polluted urban atmospheres.[50] Besides, even under OFR185-iNO good high-NO conditions, NO level is not stable during the residence time as it is always being consumed by oxidants. This is another point that may need to be considered in the experimental planning. Overall the iNO mode is not

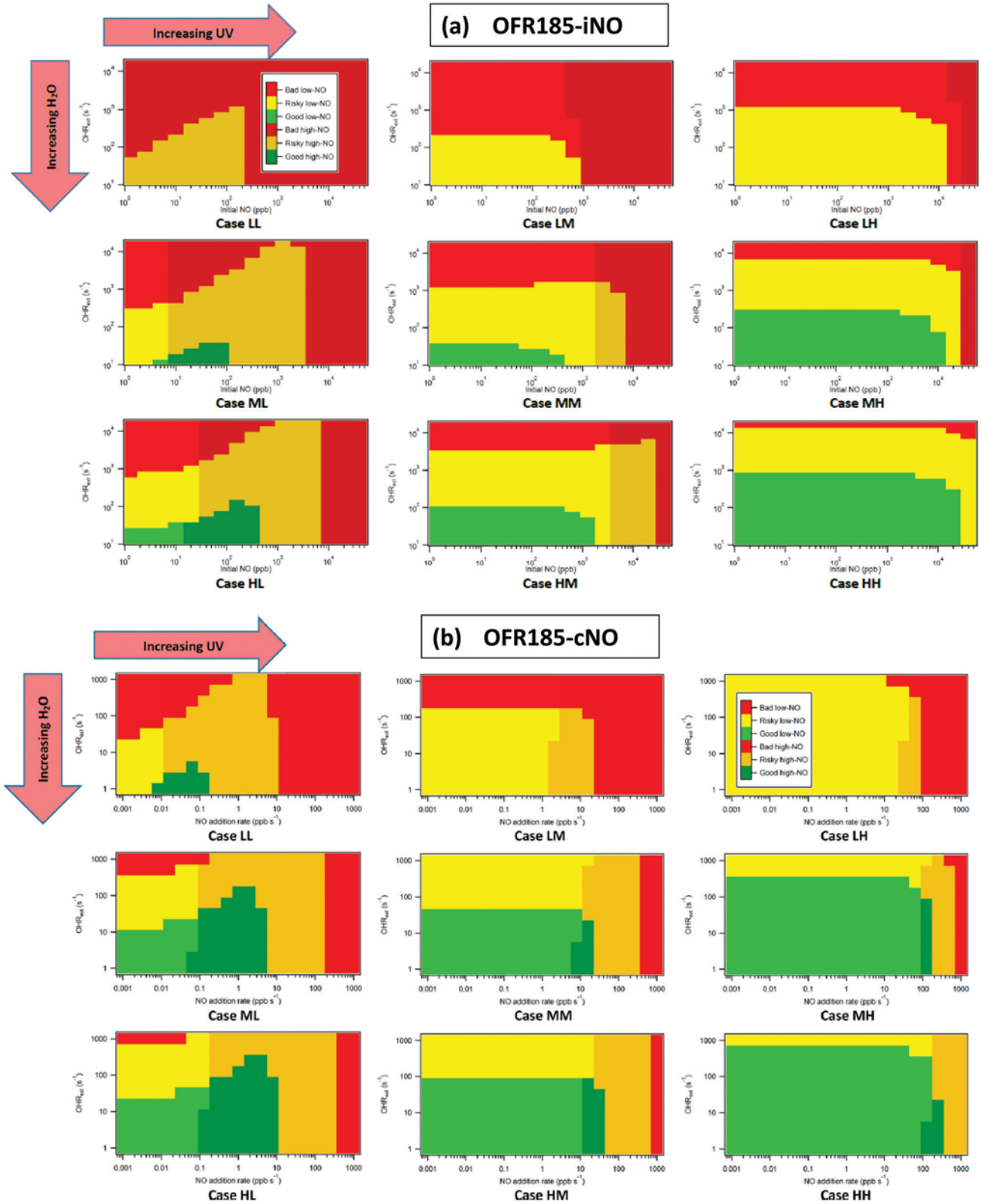

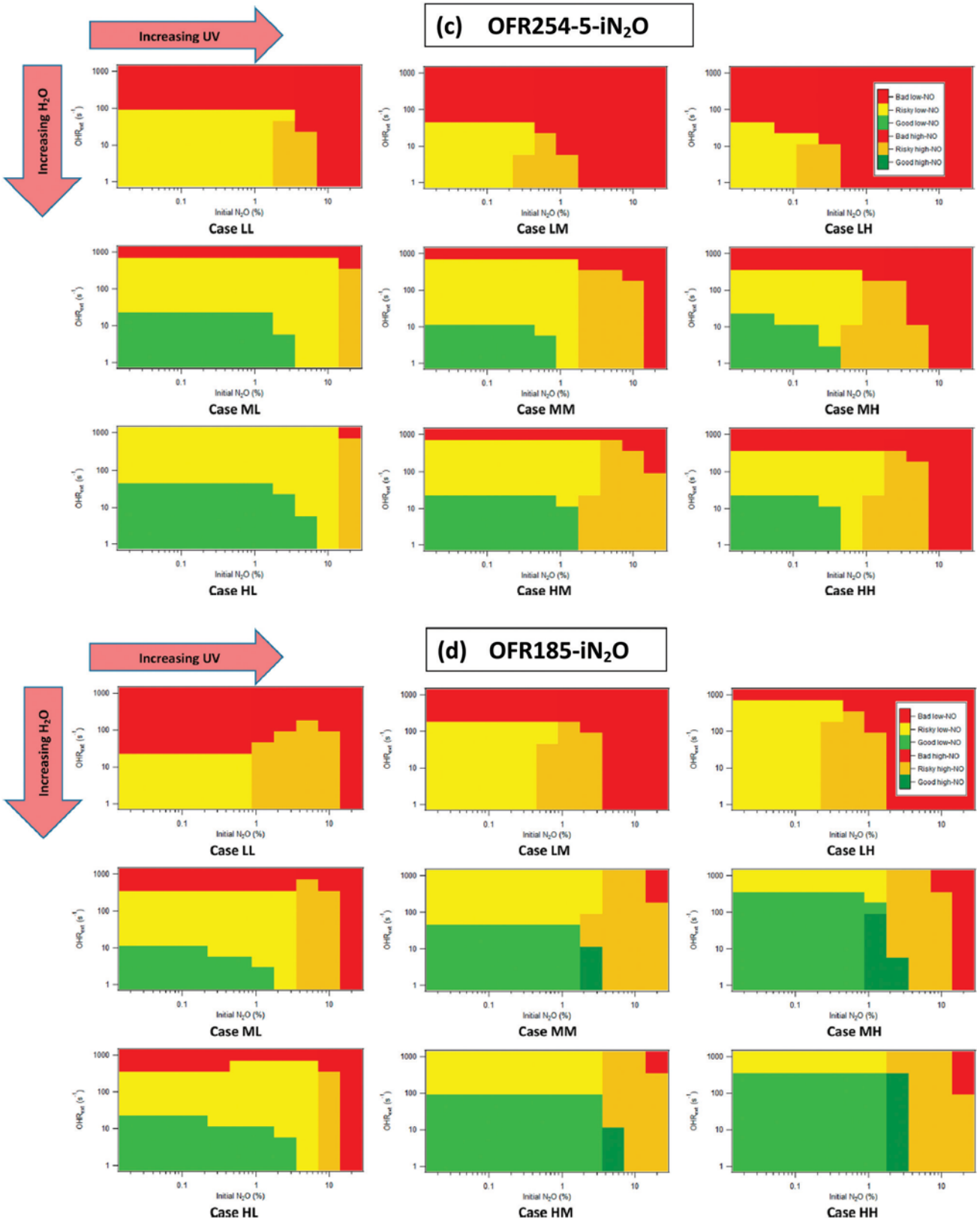

Fig. 12 Image plots of the condition types (good/risky/bad high-/low-NO) *vs.* external OH reactivity (excluding N-containing species) and NO (precursor) injection amount/rate for several typical cases in (a) OFR185-iNO, (b) OFR185-cNO, (c) OFR254-5-iN_2O and (d) OFR185-iN_2O. The first and second letters in case labels denote water mixing ratio (L: 0.07%; M: 1%; H: 2.3%) and UV intensity (L: F185 = 10^{11} photons cm^{-2} s^{-1}, F254 = 4.2×10^{13} photons cm^{-2} s^{-1}; M: F185 = 10^{13} photons cm^{-2} s^{-1}, F254 = 1.4×10^{15} photons cm^{-2} s^{-1}; H: F185 = 10^{14} photons cm^{-2} s^{-1}, F254 = 8.5×10^{15} photons cm^{-2} s^{-1}), respectively. Brighter colors indicate low-NO conditions; shading indicates high-NO conditions. (b–d) Reprinted with permission from ref. 49. Copyright 2018 American Chemical Society.

recommended, but has been discussed in some detail here since it is inherent to some experiments (*e.g.* when oxidizing exhaust from combustion sources).

For OFR185-cNO, the rationale to find the ideal conditions is similar to that for OFR185-iNO. Again, higher H_2O, lower F185, lower OHR_{ext} and significant (but not too high) NO injection rate are preferred. The map in Fig. 12b shows that the subspace of good high-NO conditions in OFR185-cNO is larger than in OFR185-iNO, demonstrating the promise of OFR185-cNO. Also, NO_2 and NO_3 are both relatively low and do not cause problems under good high-NO conditions in OFR185-cNO (Fig. 6d). Another advantage of OFR185-cNO with respect to OFR185-iNO is the higher photochemical age that OFR185-cNO can reach under good high-NO conditions (weeks *vs.* days).

The map of OFR254-5-iN_2O (as in ref. 49) contains no good high-NO conditions. A closer examination by Peng *et al.*[49] found that a higher O_3 favors good high-NO conditions in OFR254-iN_2O because the resilience to OH suppression originates from O_3 while both NO production and loss are roughly proportional to O_3. O_3, along with a significantly high N_2O to ensure high NO, leads to high NO_3/OH ($> \sim 5$; Fig. 6d), which is obviously not ideal.

For OFR185-iN_2O, a combination of high H_2O and low OHR_{ext} can ensure good conditions. A high F185 is found to favor both good conditions and high NO (Fig. 12d) and also lead to high photochemical ages (days to weeks). In addition, good high-NO conditions are most likely to be at $N_2O \sim$ 2–3%. A lower N_2O cannot guarantee a sufficient NO production, while a high N_2O tends to produce too much NO_y, which can suppress OH and make conditions worse. However, the mapping in Fig. 12d only concerns two atmospheric relevance issues, *i.e.* non-tropospheric VOC photolysis and high NO. While the good high-NO conditions in OFR185-iN_2O were also found to not result in ppm-level NO_2,[49] high F185 for those conditions leads to high NO_3/OH. To attain an ideal NO_3/OH (<1), F185 has to be on the order of 10^{12} photon cm^{-2} s^{-1} at most, which is undesirable in terms of creating good high-NO conditions. With all these requirements taken into account, $<0.1\%$ of the physical condition space explored by Peng *et al.*[49] can be deemed ideal.

If only ideal conditions are pursued, such a small (zero) volume in the condition space for OFR185-iN_2O (OFR254-iN_2O) is of little interest for experimental planning. Nevertheless, many OFR-iN_2O experiments do not have to be conducted under ideal conditions to avoid all major atmospheric relevance issues and the fraction of practically viable conditions can be much larger. More details are given below.

5.2.3. Practical considerations. As shown above, the ideal conditions, if possible to find, are highly specific. It is almost impossible to demonstrate that these highly specific conditions are ideal by *a priori* qualitative analysis only. Even if the ideal condition range has been identified by an OFR user, it is difficult to explore experimental outputs as a function of physical conditions within the ideal condition range, as it is often small. Thus, there is indeed a need to operate OFR under sub-optimal conditions. There are at least two ways to realize this without substantially degrading the quality of OFR experiment results.

The first way concerns the precursor. If the composition of the precursor(s) is known, it is possible to predict at least some major intermediates in its oxidation process according to the existing knowledge of VOC oxidation chemistry.[7,27,51] If the primary VOCs and anticipated oxidation intermediates are not highly susceptible to some atmospherically irrelevant processes, the constraints on the experimental conditions due to those processes can be loosened or dropped. For instance, if particle-phase formation of unsaturated (with C=C bond(s)) VOCs (*e.g.* dihydrofurans), which is very slow and may be a problem in OFR (see Section 4.4.2), is not a major focus, alkane oxidation at high NO can be carried out in OFR185-N_2O under many more conditions than the "ideal" ones discussed in Section 5.2.2 and even in OFR254-iN_2O without significant non-tropospheric VOC photolysis or VOC oxidation by NO_3. In the absence of added acidic seeds, the precursors (alkanes) and the likely intermediates (saturated hydroperoxides, carbonyls *etc.*) react with NO_3 very slowly compared to their reactions with OH (Fig. 6d). Therefore, the requirement for avoiding VOC oxidation by NO_3 can be ignored and OFR254-iN_2O also becomes applicable. In addition, for non-tropospheric VOC photolysis, only the abovementioned oxidation intermediates need to be considered, as alkanes do not absorb at 185 or 254 nm. And F185/OH and F254/OH that peroxides and carbonyls tolerate are much higher than conjugated unsaturated organic compounds, such as aromatics (Fig. 6a and b). For alkane oxidation, although high H_2O and low OHR_{ext} are still preferred, moderate H_2O and OHR_{ext} also become acceptable.

Another way concerns the experimental output. OFR are very often used to produce SOA for various analyses (Table 4), but for most of them to yield useful results compared to the corresponding analysis results for ambient OA, an identical chemical composition of OFR-produced SOA to ambient OA down to the molecular level is not necessary. Considering both the experimental purpose (Table 4) and the severity of different atmospheric relevance issues (Table 3), an OFR user may find a best compromise between the experimental result quality and the difficulty in planning experiments, exploring conditions *etc.* by loosening and/or dropping some atmospheric relevance requirements.

PAM, by far the most popular OFR, is commonly employed for the following purposes (Table 4):[66] (i) OA heterogeneous oxidation,[33] (ii) inorganic gas oxidation and related aerosol formation, (iii) investigation of OA O:C elemental ratio[188] or carbon oxidation state,[189] (iv) SOA formation, yield or enhancement,[62] (v) investigation of a range of OA physical properties (hygroscopicity[190] or cloud condensation nucleus (CCN) activity,[28] viscosity or phase state,[191,192] ice nucleation activity[193] and volatility),[194,195] (vi) positive matrix factorization[196] or source apportionment of OA,[197] (vii) analysis of aerosol size distribution or dynamics,[198] (viii) investigation of OA optical properties,[199] (ix) investigation of OA health effects,[200] (x) formation of specific gas-phase organic product(s)[86] and (xi) chemical speciation of organic gas and/or aerosol product(s).[201] These applications as listed are roughly increasingly demanding to have SOA produced in an atmospherically relevant manner in OFR.

As gas-phase VOC oxidation and heterogeneous OA oxidation are relatively decoupled, the concerns over the atmospheric

relevance of gas-phase chemistry generally do not also apply to heterogeneous oxidation. If heterogeneous oxidation of OA is the only main focus of an OFR experiment, OH concentration is often the only parameter that needs to be taken into account in experimental planning (see Section 4.4.2 for more details). In this case, OH cannot be too high, but in many applications even the highest OH that a specific OFR can reach is still acceptable. In addition, the oxidation of inorganic gases (*e.g.* SO_2 and CO) and related possible inorganic aerosol formation (*e.g.* sulfate aerosol) are relatively simple in terms of chemistry. The considerations for complex organic compound oxidation are generally not relevant. Even if the photolysis of some inorganic gases (*e.g.* SO_2 and NO_2) at 185 and 254 can be significant with their reactions with OH under some conditions, the main photolysis products either are the same as that of ambient photolysis (*e.g.* $NO_2 + h\nu \rightarrow NO + O$),[55] or can very rapidly convert back to the original species (*e.g.* $SO_2 + h\nu(185\ nm) \rightarrow SO + O$; $SO + O_2 \rightarrow SO_2 + O$).[202]

Both Lambe *et al.*[203] and Bruns *et al.*[204] showed that PAM and chambers produced similar SOA in terms of yields and elemental ratios (H : C and O : C). The chamber results are believed to be generally atmospherically relevant because of the light source wavelengths and the OH level similar to the atmosphere, although chamber wall issues[24] were not well understood for the chamber studies used for comparison. In summary, there is some evidence that PAM can produce SOA in similar yields to ambient ones with similar elemental ratios as ambient SOA. The studies of Lambe *et al.*[205] and Bruns *et al.*[204] covered a range of experimental conditions, but most of them were not in the ideal range as discussed in Section 5.2.2. This implies that failure to meet some requirements for atmospheric relevance does not have a strong negative impact on the elemental ratios and yields of OFR-produced SOA, both of which are bulk quantities and only reflect limited information at molecular level. As long as the VOC oxidation is mainly undertaken by OH, OH_{exp} is a good measure of photochemical aging and of the degree of oxidation of the products (O : C ratio and carbon oxidation state).[28,189] As discussed in Section 5.1, the difference between the effects of high and low NO may not be salient in OFR185 and OFR254 (including variants), since $RO_2 + OH \rightarrow \cdots \rightarrow RO$ also produces the main high-NO product and a high NO_3 (not necessarily high-NO) leads to the formation of organic nitrates, which are also formed by RO_2 + NO. We speculate that loosening or disregarding the requirements 4–7 in Table 3 would result in SOA yields and degrees of oxidation between those obtained under typical high- and low-NO conditions, which then may compare well with those under both high- and low-NO conditions at a certain equivalent ages. We thus believe that only the first three requirements are critical to be satisfied (for the reasons discussed in Section 5.1) to have generally satisfactory SOA yields and degrees of oxidation in OFR185 and OFR254 (including variants).

Note that these two have also been the most common applications of PAM so far (Table 4), although we expect more applications involving the molecular identity or structure of products to come in the future. The degree of oxidation of OA is also very often related to its hygroscopicity,[190] CCN activity,[28] viscosity[206] and phase state[206,207] (thereby to ice nucleation activity)[208] and volatility.[194] OA source apportionment is also linked to OA elemental ratios.[196,197] Therefore, meeting the requirements 1–3 in Table 3 is likely to yield OA in OFR with similar properties as ambient OA for similar conditions. However, even with the same degree of oxidation, composition of OA produced in OFR may still be significantly different from those of chamber and ambient OA. It is possible that this leads to deviations from previously established relationships between degree of oxidation of chamber and ambient OA and their abovementioned photochemical properties. More research on these topics is needed to further clarify this issue.

For the other types of OFR applications in Table 4, experimental planning is more demanding:

– Because of the impact of gas-phase chemistry (in particular fragmentation) on aerosol size-distribution dynamics in OFR,[209] for aerosol size-distribution dynamics to be more atmospherically relevant, SVOC and LVOC overoxidation and kinetically limited growth created by high OH needs to be avoided, for the reasons discussed in Sections 4.2.4, 4.4.2 and 5.1.

– Optical properties are also physical properties. Cappa *et al.*[210] showed OA light extinction cross section to increase with photochemical age/O : C ratio for two model OA, while another key optical property, *i.e.* light absorption, is not as correlated with the degree of oxidation as some physical properties discussed above. Ambient OA mass absorption efficiency does not vary monotonically with equivalent age.[211] Instead, it is more dictated by the type and abundance of chromophores.[211–213] It is well known that $RO_2 + HO_2$[51] and RO_2 autoxidation (*i.e.* the most common RO_2 isomerization pathway)[119] generate more –OOH groups, while RO_2 + NO generates more carbonyls *via* RO and more nitrates *via* recombination[51] (Table 2). The photoabsorptions of –OOH and –C(=O)– groups significantly differ. In addition, oxidized nitrogen-containing organic compounds are generally strong absorbers. Therefore, the requirements 4–8 in Table 3 also need to be considered in experimental planning, although they may not need to be as strictly implemented as under the ideal conditions discussed in Sections 5.2.1 and 5.2.2.

– High/low NO and RO_2 chemistry have been shown to affect the health effects of SOA.[214,215] For studies of on this topic, similar requirements as for optical properties are needed, as these effects also depend more on OA functional groups (*e.g.* peroxy and hydroperoxy groups[215,216] and PAH structures)[217] than on degree of oxidation.

– The remaining two categories of applications in Table 4 have the highest requirements for experimental planning, as they concern the chemical speciation of products. The yield, age, degree of oxidation, functional group(s) and molecular identity of product(s) of interest should be achieved in as atmospherically relevant chemistry as possible. In case of only several products of interest, a similar way as from the precursor angle to expand the acceptable physical condition range as discussed above can be adopted. For studies aiming to largely chemically speciate the products of VOC oxidation/SOA formation, all aspects of the experiments should be made as atmospherically relevant as possible. In this case, the ideal conditions discussed in Sections 5.2.1 and 5.2.2 can serve as references.

Table 5 Estimation equations for the experimental planning in different OFR operation modes compiled from the previous studies.[45,46,49,87] UV in the equations for OFR185 (including variants) and OFR254 (variants) are the photon fluxes at 185 and 254 nm, respectively. $O_{3,in}$ and $O_{3,out}$ are O_3 mixing ratios (in ppm) at the entrance and exit of the reactor, respectively. The ratio of the latter to the former is rO_3. rNO^{in} is the OFR185-cNO continuous NO injection rate (in ppb s^{-1}). $r(RO_2 + NO)/r(RO_2 + HO_2)$ is the average ratio of the reactive fluxes of RO_2 + NO and RO_2 + HO_2. Exposures of molecular species are in molecules cm^{-3} s, those of photon in photons cm^{-2}, H_2O unitless, UV in photons cm^{-2} s^{-1}, OHR_{ext} in s^{-1}, N_2O unitless and residence time t in s. Also shown are the relative average deviations (RAD) of the equation-estimated quantities to the corresponding model outputs over the explored physical condition ranges

OFR mode	Estimation equation	RAD (%)
OFR185	$\log OH_{exp} = 26.89 + (-1.7629 - 1.2947OHR_{ext}^{0.076549} + 0.14469\log(O_{3,out}\cdot 180/t)\cdot OHR^{0.046})\cdot\log(O_{3,out}\cdot 180/t) + \log H_2O + \log(t/180)$	10
	$\log O_{3exp} = 3.1825 + 0.98741\log UV + 40.352H_2O - 3.8184H_2O\cdot\log UV$	6
	$\log O(^3P)_{exp} = 313.61 - 558.66\log(\log O_{3exp}) - 171.59H_2O + 254.33(\log(\log O_{3exp}))^2 + 147.27H_2O\cdot\log(\log O_{3exp})$	6
	$\log O(^1D)_{exp} = 90.595 - 208.28\log(\log O_{3exp}) - 155.9H_2O + 114.15(\log(\log O_{3exp}))^2 + 134.4H_2O\cdot\log(\log O_{3exp})$	4
	$\log(F185_{exp}/OH_{exp}) = -2.7477 - 0.79645\log H_2O + 0.25018\log O_{3exp} + 3.8051\log OHR_{ext} - 0.22685\log OHR_{ext}\cdot\log O_{3exp} + 0.0086381(\log OHR_{ext})^2\cdot\log O_{3exp}$	14
	$\log(F254_{exp}/OH_{exp}) = 3.325 - 0.8268\log H_2O + 3.7467\log OHR_{ext} - 0.22294\log OHR_{ext}\cdot\log O_{3exp} + 0.0086345(\log OHR_{ext})^2\cdot\log O_{3exp}$	14
OFR254	$\log OH_{exp} = 15.514 + 0.79292\log H_2O + 0.023076(\log H_2O)^2 - 1.0238\log UV + 0.060786(\log UV)^2 - \log\left(1+\exp\left(\frac{-0.42602-\log(O_{3,in}/OHR_{ext})}{0.39479}\right)\right) + \log(t/180)$	15
	$\log OH_{exp} = 13.322 + \log(-\log rO_3) - 0.22101(OHR_{ext}/O_{3,in})^{0.43529} + \log(t/180)$	9
	$\log O_{3exp} = 15.559 + \log O_{3,in} + 0.42073\log rO_3$	1
	$\log O(^3P)_{exp} = 7.6621 + 0.16135\log(-\log rO_3) - 1.1342\log H_2O + 0.59182\log O_{3,in} - 0.17007\log H_2O\cdot\log(-\log rO_3) - 0.3797(\log(-\log rO_3))^2 + 0.099902\log OHR_{ext}$	12
	$\log O(^1D)_{exp} = 3.7371 + 0.1608\log(-\log rO_3) - 1.1344\log H_2O + 0.59179\log O_{3,in} - 0.17019\log H_2O\cdot\log(-\log rO_3) - 0.37983(\log(-\log rO_3))^2 + 0.099941\log OHR_{ext}$	12
	$\log(F254_{exp}/OH_{exp}) = 2.8045 - 0.888519\log H_2O - 0.015648\log(-\log rO_3) - 0.2607\log OHR_{ext} - 0.1641(\log(-\log rO_3))^2 + (OHR_{ext}/O_{3,in})^{0.25142}$	14
OFR185-cNO	$\log OH_{exp} = 1.4925 + 0.84112\log H_2O + 0.93605\log UV - 0.40821\log(0.053029\cdot OHR_{ext}) - 0.13011\log rNO^{in} - 0.12465(\log rNO^{in})^2 + 0.13817\log(0.053029\cdot OHR_{ext})\cdot\log rNO_{in} - 0.024808(\log rNO^{in})^3 + \log(t/180)$	41
	$\log(r(RO_2 + NO)/r(RO_2 + HO_2)) = -7.0532 - 0.77641\log H_2O + 2.176\log UV - 0.2457\log(0.053029\cdot OHR_{ext}) + 1.3428\log rNO^{in} + 0.16559(\log rNO^{in})^2 + 0.029843(\log rNO^{in})^3 - 0.14042(\log UV)^2$	55
	$\log NO_{2exp} = -12.836 + 1.8654\log H_2O + 4.6604\log UV - 0.16471\log H_2O\cdot\log UV - 1.8623\log rNO^{in} + 0.22523\log UV\cdot\log rNO^{in} - 0.068328(\log rNO^{in})^2 - 0.20312(\log UV)^2 - 0.018197(\log rNO^{in})^3 + \log(t/180)$	55
	$\log NO_{3exp} = 0.53522 - 0.018119\log H_2O + 0.85631\log UV - 0.090146\log(0.053029\cdot OHR_{ext}) - 2.7659\log rNO^{in} + 0.23337\log rNO^{in}\cdot\log UV - 0.47692\lvert\log rNO^{in}\rvert^{1.3339} + \log(t/180)$	68
OFR185-iN_2O	$\log OH_{exp} = 4.5729 + 0.77767\log H_2O + 0.46802\log UV - 1.9026\log(0.053029\cdot OHR_{ext}) - 1.6968\log N_2O - 0.18407\log N_2O\cdot\log UV + 0.18535\log N_2O\cdot\log(0.053029\cdot OHR_{ext}) + 0.14406\log UV\cdot\log(0.053029\cdot OHR_{ext}) - 2.3556\lvert\log N_2O\rvert^{1.2694} + \log(t/180)$	38
	$\log(r(RO_2 + NO)/r(RO_2 + HO_2)) = -3.3568 + 0.12188\log UV\cdot\lvert\log N_2O\rvert^{0.38477} - \log H_2O + 0.23345\log UV - 0.38953(\log N_2O)^2 + 1.6815\log N_2O - 0.089369(\log N_2O)^3 - 0.089447\log(0.053029\cdot OHR_{ext})$	34
	$\log NO_{2exp} = -4.0392 - 0.33444\log H_2O + 1.1288\log UV - 14.386\lvert\log N_2O\rvert^{1.5} - 14.734\log N_2O + 3.55(\log N_2O)^2 + \log(t/180)$	33
	$\log NO_{3exp} = -2.8709 - 0.3351(\log N_2O)^3 + 0.80081\log UV - 0.088975\log(0.053029\cdot OHR_{ext}) - 0.084044\log N_2O - 2.8001(\log N_2O)^2 - 0.48384\log N_2O\cdot\log UV - 2.0429\log H_2O + 0.17734\log H_2O\cdot\log UV + 0.14604\log N_2O\cdot\log H_2O + \log(t/180)$	35
OFR254-iN_2O	$\log OH_{exp} = 4.8743 + 0.83757\log H_2O + 0.41214\log UV - 0.082962\log(0.053029\cdot OHR_{ext}) + 3.8224\log O_{3,in} + 1.6179\log N_2O - 0.23589((2.5\cdot N_2O))^2 - 0.17025(\log(0.053029\cdot OHR_{ext}))^2 + 0.12603\log(2.5\cdot N_2O)\cdot\log(0.053029\cdot OHR_{ext}) - 0.19932\log(2.5\cdot N_2O)\cdot\log UV - 0.21057\log UV\cdot\log O_{3,in} + \log(t/180)$	31
	$\log(r(RO_2 + NO)/r(RO_2 + HO_2)) = -2.5169 - 1.0663\log H_2O - 0.7398\log UV + 0.060477(\log UV)^2 - 0.32204\log O_{3,in} - 1.3207\log(2.5\cdot N_2O) + 0.033(\log(2.5\cdot N_2O))^2 - 0.016813(\log(2.5\cdot N_2O))^3 + 0.046499\log(2.5\cdot N_2O)\cdot\log(0.053029\cdot OHR_{ext}) + 0.16192\log(2.5\cdot N_2O)\cdot\log UV - 0.22746\log(2.5\cdot N_2O)\cdot\log H_2O$	23
	$\log NO_{2exp} = 12.005 + 2.944\log H_2O + 0.17631\log UV - 0.21949\log UV\cdot\log H_2O + 0.51464\log O_{3,in} + 0.89696\log(2.5\cdot N_2O) - 0.0229(\log(2.5\cdot N_2O))^2 + \log(t/180)$	28
	$\log NO_{3exp} = 0.27517 - 3.3766\log H_2O + 0.71155\log UV + 0.21731\log UV\cdot\log H_2O + 1.1035\log O_{3,in} - 29.058\log(250\cdot N_2O) - 0.25958(\log(250\cdot N_2O))^2 - 0.1581\log(250\cdot N_2O)\cdot(\log UV)^2 - 0.0049287\log(0.053029\cdot OHR_{ext})\cdot\log UV + 4.3563\log(250\cdot N_2O)\cdot\log UV + 0.13338\log(250\cdot N_2O)\cdot\log H_2O + \log(t/180)$	27
OFR369-i(iPrONO)	$\log OH_{exp} = \log UV - 0.0026728\cdot OHR_{ext} + 0.46017\log RONO + 1.1928\log t + 0.35317\log RONO\cdot\log OHR_{ext} - 0.11109\log OHR_{ext}\cdot\log t - 0.015606\log UV\cdot\log RONO\cdot\log t - 7.6164$	29
	$\log NO_2 = \log UV + \log RONO + \log t - 6.2198$	19
OFR369-i(iPrONO-d_7)	$\log OH_{exp} = 0.85558\log UV - 0.0029546\cdot OHR_{ext} + 0.61837\log RONO + 1.2115\log t + 0.36081\log RONO\cdot\log OHR_{ext} - 0.15501\cdot\log OHR_{ext}\cdot\log t - 0.017061\log UV\cdot\log RONO\cdot\log t - 5.1541$	29
	$\log NO_2 = \log UV + \log RONO + \log t - 6.2607$	19

5.3. Experimental planning tools

As shown above, OFR experimental planning can be challenging in some cases, especially when multiple issues need to be taken into account simultaneously. To address this difficulty and enable faster and semi-quantitative experimental planning, Peng *et al.* have fitted equations that are able to estimate various quantities of interest (*e.g.* exposures of OH, O_3, NO_2 and NO_3, F185 and F254, ratios between HO_2 and OH and between NO and HO_2) from the modeling results in their series of OFR chemistry studies.[45–47,49,50,87] All these estimation equations are compiled in Table 5. They use physical condition parameters (H_2O, F185, F254, OHR_{ext}, N_2O *etc.*) and easily measurable quantities (*e.g.* O_3 at the reactor exit, $O_{3,out}$) as variables. Uncertainties of the equation estimates are thought to be similar to the model uncertainties (*i.e.* a factor of 2–3; see discussions in Section 3.4). When OH calibration is possible, we recommended using a single tuning factor for OH estimated by the equations based on equation-predicted OH_{exp} *vs.* that measured in the actual reactor for a tracer, as Palm *et al.*[31,63] did in their experiments. Also note that the currently available equations for OFR185 (including variants) are only compatible with OFR equipped with BHK low-pressure Hg lamps with its specific F185/F254, as Peng *et al.*'s[45–47,49,50] model cases were based on this type of OFR. The derivation of similar equations for the OFR185 variants in the commercialized Aerodyne PAM reactor[49,86,87] with a different F185/F254 is ongoing. In contrast, the equations for the OFR254 and OFR369 modes (including variants) are applicable to all PAM-type reactors. As the NO_y chemistry in the iNO modes is highly temporally heterogeneous (see Section 3.2.1), the equations for these modes are too difficult to derive. Instead, Peng and Jimenez[48] provided highly detailed modeling results for the iNO modes in a visual form in Fig. S3 of their paper.

Peng *et al.* also developed the OFR Exposure Estimator[47,49,50] (the latest version of which also contains the OFR RO_2 Fate Estimator)[50] with all estimation equations for OFR185 and OFR254 variants incorporated. The software in the formats of Igor experiment (full version) and Excel spreadsheet (some functionalities unavailable) calculates, according to estimations equations, the key quantities for experimental planning upon variable inputs by users, and outputs those quantities in an informative and interactive fashion. It can also provide some simple guidance on experimental planning in the format of Fig. 6 and 10. Palm *et al.*[31] developed an estimator for LVOC condensation losses in OFR. Both estimators by Peng *et al.* and Palm *et al.* are freely available on the site of PAM Wiki, including their source code.[218]

In addition, as part of this Review, we also release the model used in and developed in the course of Peng *et al.*'s series of OFR chemistry studies.[45–50] In these studies, the model was run in KinSim,[219] an Igor Pro (WaveMetrics, Inc., Lake Oswego, Oregon, USA)-based free, user-friendly, visual chemical-kinetics simulator developed by us. We provide an ITX (Igor Text) file (including mechanism, initial conditions and key parameter for model setup) in ESI.† It can be directly loaded into KinSim for more advanced OFR experimental planning.

6. Summary and outlook

After a decade of developments, characterizations and applications, OFR are a promising alternative to environmental chambers, and have become a mainstream atmospheric chemistry research tool for the investigations of VOC oxidation, SOA formation and aging and other topics. In this Review, we focused on the radical chemistry in OFR, for which a relatively comprehensive picture (including the chemistries of HO_x and O_3, NO_y, VOCs and RO_2) was not established until very recently. We tried to summarize the recent advancements in this field in a systematic and synthetic manner by relating knowledge on chemistry, concerns over atmospheric relevance and implications for experimental planning together. This synthesis, we believe, will help address many of the concerns over the atmospheric relevance of the OFR chemistry stemming from the high oxidant levels and/or oxidant production mechanisms that do not exist in the troposphere, as it clarifies under what conditions the OFR chemistry is atmospherically relevant and under what conditions it is not, explaining the underlying reasons. Both types of conditions do exist. Therefore, OFR is a useful tool as some OFR conditions lead to atmospherically relevant chemistry. On other hand, it is far from a foolproof tool and requires careful experimental planning to avoid the conditions resulting in chemistry irrelevant to the atmosphere.

The core concept to understand the variations of this chemistry under different conditions is OH suppression, the reduction of OH concentration by external OH reactants. This concept can be well understood in terms of OH production and loss at steady state. Based on this, the resilience of OFR254 (including variants) to OH suppression can be explained by the large fraction of OHR_{int} in total OHR. OH suppression is also one of the two key causes of an increase in the relative importance of reactions with non-OH reactants in VOC fate in OFR185 and OFR254 (including variants), since non-OH reactants usually are not suppressed significantly by external OH reactants. The other cause is low H_2O, which limits OH production but not that of non-OH reactants. The most problematic pathways in non-OH VOC oxidation are VOC photolysis at 185 and/or 254 nm, which are sufficiently short wavelengths to lead to possibly very different photolysis products than in the troposphere, and which can quickly become major under typical OFR conditions for many experimental conditions.

Due to its short lifetime under high OH, NO was long thought to be very rapidly oxidized in OFR. However, its significant presence has recently been shown to be possible in OFR185-iNO, but not in OFR254-iNO, due to the high O_3 oxidizing NO in the latter. Several new operation modes, *i.e.* OFR185-cNO, OFR254-iN_2O, OFR185-iN_2O and OFR369-i(iPrONO) (see Table 1), have very recently been proposed and shown to be able to maintain a high-NO environment in OH OFR. In general, high O_3 in OFR254 variants and high F185 (and thereby relatively high O_3) in OFR185 variants are likely to produce a significant amount of NO_3 and enable NO_3 to compete with OH in the oxidation of some VOCs. In these modes, it is also possible that a very large amount of NO_2 is generated as a byproduct (from NO oxidation) while high NO is maintained. This very high NO_2 may suppress RO_2 by

converting it into a reservoir or sink species RO_2NO_2, and delay the entire organic radical chemistry in OFR.

In addition to the common low-NO fates by HO_2 and RO_2 and common high-NO fates by NO and NO_2, RO_2 + OH and RO_2 isomerization also need to be considered at relatively low NO in OFR. The former is generally minor and typical pathways of the latter can be significant in the atmosphere. Under the conditions leading to high HO_x production (also HO_2-to-OH ratio close to 1), RO_2 + OH is significant and RO_2 has too short a lifetime to isomerize. A relatively low F185 is necessary for the atmospheric relevance of these two pathways in OFR185, while in OFR254, HO_x recycling promoted by high O_3 sustains a relatively high HO_x level even at low H_2O and F254, which makes it difficult to find appropriate conditions for atmospherically relevant RO_2 + OH and RO_2 isomerization.

Along with the abovementioned aspects, other atmospheric relevance issues, such as gas-particle partitioning and OA photolysis at tropospheric wavelengths, also need attention depending on conditions and the purposes of OFR experiments. For an ideal experimental planning, multiple issues often need to be taken into account simultaneously, resulting in a very small range of viable physical conditions. Thus, some trade-offs between the quality of planned experiments and the difficulty in experimental planning should be made in practical OFR experimental planning. For the most common OFR applications concerning OA properties (generally average bulk properties) less relevant to molecular identities of the components, *e.g.* production of SOA at atmospherically relevant degrees of oxidation with atmospherically relevant yields, most atmospheric relevance issues discussed in this Review may not be critical. Only non-tropospheric VOC photolysis and strong RO_2 suppression by high NO_2, which need attention in all OFR experimental planning, certainly should be largely avoided. For other applications that require significantly closer simulation of the molecular identity of the products, such as OA optical property and health effects and chemical speciation of gas- and particle-phase products, more atmospheric relevance issues need to be considered at the same time, implementing them more strictly as well. Experiments for the last of the abovementioned applications, *i.e.* chemical speciation of products, should be carried out under the ideal conditions or as close to them as possible. OFR369-i(PrONO) does not cause most of the atmospheric relevance problems discussed in this Review *per se*, thanks to its atmospherically relevant light source. However, due to the same light source, OH production is much weaker than the modes using Hg lamps and only an equivalent age of $\sim$1 d can be achieved in OFR369-i(iPrONO).

It is also of interest to discuss the role of OFR in the bigger picture of research tools for VOC oxidation and SOA formation. Compared to chambers, the cost of OFR is much lower and its operation much easier, and OFR are suitable on many experiments that are difficult or impossible for chambers, *e.g.* mobile laboratory[83] and aircraft[36] applications (Table 6). Due to the long residence times, wall losses of gases and particles are significant in chambers, although they are now better understood and potentially partially correctable.[24,220] OFR residence times are much shorter, relative to wall contact timescales, and hence lead to less wall losses,[32] although quantitative experimental investigations are still needed. On the other hand, the long residence times in chambers also ensure sufficient equilibration for gas-particle partitioning (Table 6), while partitioning can be seriously kinetically limited in OFR under low aerosol conditions, which can be a major issue for OFR as OA yield is a quantity of key interest in many OFR studies. With regard to the chemistry, that in chambers can in principle be relatively easily kept in very similar regimes with the atmosphere, although in practice some chamber studies did not achieve it due to lack of detailed knowledge of the chemistry and/or experimental/instrumental requirements in experimental planning (*e.g.* high precursor concentrations for sufficient signals in instruments). Chemistry in chambers are atmospherically relevant as long as concentrations of reactants such as VOCs, O_3, NO_x *etc.* are comparable to ambient levels, since the light sources in chambers usually emit photons that also exist in the troposphere and OH level in chambers is also comparable to that in the troposphere. Therefore, chemistry in chambers is still atmospherically relevant when UV lights are turned up/down or on/off to simulate diurnal cycles and when different amounts of NO are injected to simulate transition of the chemical regime regarding NO (*i.e.* low-NO, transition and high-NO). By contrast, it is more difficult to perform such complex operations in OFR due to its short residence time and small volume.

In addition, OFR can result in deviations from the chemistry in the atmosphere, as discussed throughout this Review, but the performance of different OFR operation modes also differ in terms of the aspects listed in Table 6. In OFR185 and its variants, all these atmospherically irrelevant chemistry issues (non-tropospheric VOC photolysis, VOC ozonolysis, VOC oxidation by NO_3, fate of RO_2 (both non-acyl and acyl)) can be avoided or largely mitigated at least under certain conditions. However, OFR254 (including variants) shows difficulty in attaining atmospheric relevance in several aspects of the radical chemistry, *e.g.* VOC oxidation by NO_3, non-acyl RO_2 fate at low NO and acyl RO_2 fate at high NO, all of which are due to the high O_3 in OFR254 variants. Although the chemistry in OFR185 variants is more susceptible to external perturbations (*e.g.* OH suppression) than OFR254 variants, this can also be regarded as a flexibility when it is desired to realize different chemical regimes to address various issues and/or achieve different experimental goals. Therefore, for highly demanding experimental planning, OFR185 variants are preferred to OFR254 variants, and show, to some extent, its versatility even compared to chambers. Even so, ideal OFR experiments where all aspects in consideration are as atmospherically relevant as in chambers are, if any, rare. In OFR experimental planning, compromises almost always have to be made for specific goals. For simple experimental planning with non-tropospheric VOC photolysis being the only concern (at low NO), the reaction system in OFR254 is more stable and may be easier to control because of its high O_3. When high-NO conditions with relatively low ages ($<\sim$1 d) are needed, OFR369-i(PrONO) is certainly the preferred mode, since its radical generation method is similar to chambers and naturally

Table 6 Advantages and disadvantages of OFR185 (including variants), OFR254 (including variants), OFR369-i(iPrONO) and chambers for simulating the chemistry of the atmosphere. Properties of OFR and chamber are colored in green, light green, yellow, light red and red, representing positive, slightly positive, relatively neutral, slightly negative and negative properties, respectively. The importance of different aspects will vary with the experimental goals

		Atmosphere	Chambers	OFR185 (including variants)	OFR254 (including variants)	OFR369-i(iPrONO)
Operation	Experimental timescale	Hours–days	Hours-days	~5 min		~2 min
	Concentrations similar to ambient values	Always ambient values	Possible	Possible for precursors Impossible for oxidants		
	Inlet needed	No	Yes	No (ring inlet)		
	Application to source in the field	N/A	Possible but not easy	Possible		
	Aging of ambient air	Occurring in the atmosphere	Possible but not easy	Possible		
	Application in mobile laboratories	N/A	Possible but not easy	Possible		
	Application in aircraft	N/A	Very difficult	Possible		
Physics	Time for condensation and partitioning	High	High	Moderate		
	Wall loss of semi-volatile gases	No	Significant (correctable)	Moderate		
	Wall loss of particles	No	Significant (correctable)	Minor		
Chemistry	Maximum age	Days–weeks	~1 d	Weeks		~1 d
	VOC photolysis at non-tropospheric wavelengths	No	No	185 and 254 nm Not significant compared to reactions with OH, except for in low-H_2O or high-OHR_{ext} cases	254 nm Not significant compared to reactions with OH, except for in low-H_2O or high-OHR_{ext} cases	No
	O_{3exp}/OH_{exp}	~10^5–10^7 during daytime	Photooxidation: <~$1x10^6$ Ozonolysis: >~$1x10^8$	~$3x10^2$–$2x10^6$	~$1x10^3$–$1x10^7$	<~$1x10^4$
	Fate of RO_2 at low NO	Most pathways may be dominant depending on conditions	Most pathways may be dominant depending on conditions	Atmospheric relevance achievable at high H_2O, low–moderate UV, and low–moderate OHR_{ext}	Difficult to ensure the significance of common RO_2 isomerization	Low NO impossible
	High-NO conditions	Common in urban areas	Realizable	Maintainable in cNO and iN_2O modes, also realizable in iNO mode	More difficult to achieve than in OFR185 because of high O_3	Always at high NO
	NO_{3exp}/OH_{exp}	<~1 during daytime on average	<~1 realizable	~0.03–1000 at high NO	~1–10^6 at high NO	<~1
	NO/NO_2	Up to ~1 in urban areas	~1 realizable	Up to ~1 at high NO	<<0.1 at high NO	~0.07–7
	Day-night and high-to-low NO transitions with the same air	Occurring in the atmosphere	Possible	Very difficult		Impossible
	Heterogeneous OA oxidation	Occurring in the atmosphere	OH_{exp} insufficient	Atmospherically relevant if OH is not too high		OH_{exp} insufficient
	Particle-phase reactions	Occurring in the atmosphere	Similar rates as the atmosphere	Timescales in s or shorter: significant as in the atmosphere Timescales in min: need acceleration by more catalyst and/or stronger condensation Timescales in hr or longer: not as significant as in the atmosphere		

Positive | Slightly positive | Relatively neutral | Slightly negative | Negative

avoids the problems associated with the radical generation by Hg-lamp emissions (*e.g.* non-tropospheric VOC photolysis).

Although we believe that the recent studies of OFR chemistry are able to form a comprehensive picture of it, this picture is not complete. The most needed future development to advance our understanding of this chemistry by modeling is the inclusion of explicit chemical mechanisms to describe VOC oxidation, which is also a great challenge. As discussed in Section 3.4, the largest uncertainty source in Peng *et al.*'s[45–50] OFR chemistry model is VOCs being surrogated by SO_2, using MCM may lead to a limited improvement of model accuracy. GECKO-A[144] may be able to generate mechanisms that can better capture the evolutions of OHR_{VOC} and of HO_x recycling ratio in the course of VOC oxidation, both of which are critical parameters in Peng *et al.*'s box model. Incorporation of GECKO-A mechanisms can also provide more information about the fates (including photolysis) of specific VOCs (including oxidation intermediates). The need for more accurate evolutions of OHR_{VOC} and of HO_x recycling ratio can also be addressed by experiments. Such measurements have been carried out in chambers,[140–143] but those under OFR conditions are also needed.

In addition to OFR chemistry, more attention also needs to be paid to other characteristics of OFR. Most OFR have non-plug-flow RTDs. Although RTD-averaged OH_{exp} has been shown to be close to that in the plug-flow model under conditions of practical interest,[46,48] a distribution of OH_{exp} resulting from RTD leads to various degrees of aging of organic gases and OA in each air parcel. Different degrees of oxidation in air parcels would result in a distribution of properties of OA and gas mixture. This has never been previously explored and will require both experimental and modeling efforts. Besides, smaller wall losses have been thought to be an advantage of OFR compared to chambers. However, experimental studies of vapor wall losses in OFR have not yet been carried out in as detailed and quantitative a

way as for chambers.[22,24,221] Moreover, OFR walls might even play a role in its chemistry. Metal reactors may catalyze reactions by their walls;[25,222] even quartz and Teflon OFR may have a water film developed on their walls,[221,223,224] which may allow OH to be directly produced on the wall through the photolysis of adsorbed water and react with adsorbed VOCs. These potential wall effects can all be future research topics for OFR.

As discussed in Section 5.2, it is often impossible to plan "perfect" OFR experiments. Compromises in experimental planning can often be made according to the type of OFR application, in other words, the type of measurement(s) of the properties of gas- and particle-phase products formed in OFR. As for planned experiments to achieve atmospheric relevance in this sense, they only need to yield products whose measurement(s) have the same or similar signals in the instruments as ambient gases and SOA have. Up to date, there have been only three studies of this type[203,204,225] and two of them concern only SOA yield and elemental ratios the other also included analyses by other techniques (*e.g.* infrared and nuclear magnetic resonance spectroscopies). Also needed are studies relating OFR physical conditions to the atmospheric relevance of other properties of products, such as OA viscosity, optical properties in UV-visible range and toxicity. This type of studies would greatly inform the planning of future OFR experiments focused on specific properties of products instead of their chemical speciation. They may also expand the range of practically viable conditions for experiments aimed at studying certain product properties: for instance, studies might show that some OFR conditions lead to optical properties of OA produced in the reactor similar to those of ambient OA, even if they are significantly different in terms of molecular identity.

Finally, we also call for new OFR operation modes and/or designs. Recently developed modes to achieve high NO[49,86,87] are examples. Directions of future OFR design and/or operation mode development may include, but not be limited to, further reduction of wall losses[32] and proper incorporation of atmospherically relevant photolytic aging of gases and OA. As understanding of OFR is advancing in various aspects, we believe that new OFR operation modes and/or designs should be and can be made possible to address the existing and emerging needs of OFR user community.

Conflicts of interest

There are no conflicts to declare.

Appendix A: proof of the exclusive dependence on OH_{exp} of species concentrations in a reaction scheme of VOCs bimolecularly reacting with OH

We consider a reaction scheme exclusively composed of (pseudo-) bimolecular reactions of VOCs (A_1, A_2,..., A_n) with OH with the following form

$$A_i + OH \rightarrow A_j,\ k_{ij}, \quad i, j = 1, 2, \ldots, n,$$

where k_{ij} is the rate coefficient of the reaction. If A_i cannot be converted into A_j, $k_{ij} = 0$. The rate equation of the reaction above is

$$r_{ij} = k_{ij}[OH][A_i], \quad i, j = 1, 2, \ldots, n,$$

where square bracket denotes species concentration. And the rate equation of a species A_i is

$$r_i = \frac{d[A_i]}{dt} = \sum_{j=1}^{n} r_{ji} - \sum_{j=1}^{n} r_{ij} = \sum_{j=1}^{n} \left(k_{ji}[OH]\left[A_j\right] - k_{ij}[OH][A_i]\right), \quad i = 1, 2, \ldots, n,$$

where t is reaction time. Therefore, the concentration of A_i at the time t, $[A_i]_t$, is expressed as follows

$$[A_i]_t = \int_0^t r_i dt = \int_0^t \sum_{j=1}^{n} \left(k_{ji}\left[A_j\right] - k_{ij}[A_i]\right)[OH]dt, \quad i = 1, 2, \ldots, n.$$

Note that by definition, the OH exposure at the time t, $OH_{exp,t} = \int_0^t [OH]dt$, and $OH_{exp,0} = 0$. The integration variable t can be substituted by OH_{exp}, then

$$[A_i]_t = \int_0^{OH_{exp,t}} \sum_{j=1}^{n} \left(k_{ji}\left[A_j\right] - k_{ij}[A_i]\right) dOH_{exp}, \quad i = 1, 2, \ldots, n.$$

Thus, the vector $([A_1]_t, [A_2]_t, \ldots, [A_n]_t)$ can be expressed as a function of $OH_{exp,t}$, the vector $([A_1]_0, [A_2]_0, \ldots, [A_n]_0)$, and the matrix (k_{ij}), $i, j = 1, 2, \ldots, n$, and does not depend on [OH].

Note that $([A_1]_t, [A_2]_t, \ldots, [A_n]_t)$ is also a function of t, but t and $OH_{exp,t}$ are bijective as long as $[OH] > 0$, implying that if $OH_{exp,t}$ is given, it is unnecessary to know t to determine $([A_1]_t, [A_2]_t, \ldots, [A_n]_t)$. If the vector $([A_1]_0, [A_2]_0, \ldots, [A_n]_0)$, and the matrix (k_{ij}), $i, j = 1, 2, \ldots, n$, are given, $([A_1]_t, [A_2]_t, \ldots, [A_n]_t)$ depends exclusively on $OH_{exp,t}$.

Acknowledgements

This work was partially supported by grants EPA STAR 83587701-0 and NSF AGS-1822664. We are grateful to William Brune, Andrew Lambe, Jonathan Abbatt, Jay Slowik and other pioneers in the OFR field for their trailblazing work and many discussions. We also thank Brett Palm, Weiwei Hu, Julia Lee-Taylor, Pedro Campuzano-Jost, Benjamin Nault, Amber Ortega, John Orlando, Geoffrey Tyndall, Joel Thornton, Paul Wennberg, Andrew Grieshop, Yuanlong Huang and many others in the OFR user community for their useful discussions and suggestions. The EPA has not reviewed this manuscript and thus no endorsement should be inferred.

References

1 H. Levy II, Normal atmosphere: large radical and formaldehyde concentrations predicted, *Science*, 1971, **173**, 141–143.
2 A. J. Haagen-Smit, Chemistry and Physiology of Los Angeles Smog, *Ind. Eng. Chem.*, 1952, **44**, 1342–1346.
3 W. Chameides, R. Lindsay, J. Richardson and C. Kiang, The role of biogenic hydrocarbons in urban photochemical smog: Atlanta as a case study, *Science*, 1988, **241**, 1473–1475.

4 M. Hallquist, J. C. Wenger, U. Baltensperger, Y. Rudich, D. Simpson, M. Claeys, J. Dommen, N. M. Donahue, C. George, A. H. Goldstein, J. F. Hamilton, H. Herrmann, T. Hoffmann, Y. Iinuma, M. Jang, M. E. Jenkin, J. L. Jimenez, A. Kiendler-Scharr, W. Maenhaut, G. McFiggans, T. F. Mentel, A. Monod, A. S. H. Prevot, J. H. Seinfeld, J. D. Surratt, R. Szmigielski and J. Wildt, The formation, properties and impact of secondary organic aerosol: current and emerging issues, *Atmos. Chem. Phys.*, 2009, **9**, 5155–5236.

5 T. Hoffmann, J. R. Odum, F. Bowman, D. Collins, D. Klockow, R. C. Flagan and J. H. Seinfeld, Formation of Organic Aerosols from the Oxidation of Biogenic Hydrocarbons, *J. Atmos. Chem.*, 1997, **26**, 189–222.

6 J. R. Odum, T. Hoffmann, F. Bowman, D. Collins, C. Flagan Richard and H. Seinfeld John, Gas particle partitioning and secondary organic aerosol yields, *Environ. Sci. Technol.*, 1996, **30**, 2580–2585.

7 P. J. Ziemann and R. Atkinson, Kinetics, products, and mechanisms of secondary organic aerosol formation, *Chem. Soc. Rev.*, 2012, **41**, 6582–6605.

8 M. Kampa and E. Castanas, Human health effects of air pollution, *Environ. Pollut.*, 2008, **151**, 362–367.

9 A. J. Cohen, M. Brauer, R. Burnett, H. R. Anderson, J. Frostad, K. Estep, K. Balakrishnan, B. Brunekreef, L. Dandona, R. Dandona, V. Feigin, G. Freedman, B. Hubbell, A. Jobling, H. Kan, L. Knibbs, Y. Liu, R. Martin, L. Morawska, C. A. Pope, H. Shin, K. Straif, G. Shaddick, M. Thomas, R. van Dingenen, A. van Donkelaar, T. Vos, C. J. L. Murray and M. H. Forouzanfar, Estimates and 25-year trends of the global burden of disease attributable to ambient air pollution: an analysis of data from the Global Burden of Diseases Study 2015, *Lancet*, 2017, **389**, 1907–1918.

10 A. Nel, Air Pollution-Related Illness: Effects of Particles, *Science*, 2005, **308**, 804–806.

11 T. F. Stocker, D. Qin, G.-K. Plattner, M. Tignor, S. K. Allen, J. Boschung, A. Nauels, Y. Xia, V. Bex and P. M. Midgley, *Climate Change 2013 - The Physical Science Basis*, Cambridge University Press, Cambridge, 2014.

12 J. Abbatt, C. George, M. Melamed, P. Monks, S. Pandis and Y. Rudich, New Directions: Fundamentals of atmospheric chemistry: Keeping a three-legged stool balanced, *Atmos. Environ.*, 2014, **84**, 390–391.

13 J. B. Burkholder, J. P. D. Abbatt, I. Barnes, J. M. Roberts, M. L. Melamed, M. Ammann, A. K. Bertram, C. D. Cappa, A. G. Carlton, L. J. Carpenter, J. N. Crowley, Y. Dubowski, C. George, D. E. Heard, H. Herrmann, F. N. Keutsch, J. H. Kroll, V. F. McNeill, N. L. Ng, S. A. Nizkorodov, J. J. Orlando, C. J. Percival, B. Picquet-Varrault, Y. Rudich, P. W. Seakins, J. D. Surratt, H. Tanimoto, J. A. Thornton, Z. Tong, G. S. Tyndall, A. Wahner, C. J. Weschler, K. R. Wilson and P. J. Ziemann, The Essential Role for Laboratory Studies in Atmospheric Chemistry, *Environ. Sci. Technol.*, 2017, **51**, 2519–2528.

14 R. Atkinson, Kinetics and mechanisms of the gas-phase reactions of the hydroxyl radical with organic compounds under atmospheric conditions, *Chem. Rev.*, 1986, **86**, 69–201.

15 D. R. Cocker, R. C. Flagan and J. H. Seinfeld, State-of-the-Art Chamber Facility for Studying Atmospheric Aerosol Chemistry, *Environ. Sci. Technol.*, 2001, **35**, 2594–2601.

16 W. P. L. Carter, D. R. Cocker, D. R. Fitz, I. L. Malkina, K. Bumiller, C. G. Sauer, J. T. Pisano, C. Bufalino and C. Song, A new environmental chamber for evaluation of gas-phase chemical mechanisms and secondary aerosol formation, *Atmos. Environ.*, 2005, **39**, 7768–7788.

17 X. Liu, D. A. Day, J. E. Krechmer, W. Brown, Z. Peng, P. J. Ziemann and J. L. Jimenez, Direct measurements of semi-volatile organic compound dynamics show near-unity mass accommodation coefficients for diverse aerosols, *Commun. Chem.*, 2019, **2**, 98.

18 J. Kirkby, J. Curtius, J. Almeida, E. Dunne, J. Duplissy, S. Ehrhart, A. Franchin, S. Gagné, L. Ickes, A. Kürten, A. Kupc, A. Metzger, F. Riccobono, L. Rondo, S. Schobesberger, G. Tsagkogeorgas, D. Wimmer, A. Amorim, F. Bianchi, M. Breitenlechner, A. David, J. Dommen, A. Downard, M. Ehn, R. C. Flagan, S. Haider, A. Hansel, D. Hauser, W. Jud, H. Junninen, F. Kreissl, A. Kvashin, A. Laaksonen, K. Lehtipalo, J. Lima, E. R. Lovejoy, V. Makhmutov, S. Mathot, J. Mikkilä, P. Minginette, S. Mogo, T. Nieminen, A. Onnela, P. Pereira, T. Petäjä, R. Schnitzhofer, J. H. Seinfeld, M. Sipilä, Y. Stozhkov, F. Stratmann, A. Tomé, J. Vanhanen, Y. Viisanen, A. Vrtala, P. E. Wagner, H. Walther, E. Weingartner, H. Wex, P. M. Winkler, K. S. Carslaw, D. R. Worsnop, U. Baltensperger and M. Kulmala, Role of sulphuric acid, ammonia and galactic cosmic rays in atmospheric aerosol nucleation, *Nature*, 2011, **476**, 429–433.

19 J. Wang, J. F. Doussin, S. Perrier, E. Perraudin, Y. Katrib, E. Pangui and B. Picquet-Varrault, Design of a new multi-phase experimental simulation chamber for atmospheric photosmog, aerosol and cloud chemistry research, *Atmos. Meas. Tech.*, 2011, **4**, 2465–2494.

20 O. Möhler, O. Stetzer, S. Schaefers, C. Linke, M. Schnaiter, R. Tiede, H. Saathoff, M. Krämer, A. Mangold, P. Budz, P. Zink, J. Schreiner, K. Mauersberger, W. Haag, B. Kärcher and U. Schurath, Experimental investigation of homogeneous freezing of sulphuric acid particles in the aerosol chamber AIDA, *Atmos. Chem. Phys.*, 2003, **3**, 211–223.

21 J. Mao, X. Ren, W. H. Brune, J. R. Olson, J. H. Crawford, A. Fried, L. G. Huey, R. C. Cohen, B. Heikes, H. B. Singh, D. R. Blake, G. W. Sachse, G. S. Diskin, S. R. Hall and R. E. Shetter, Airborne measurement of OH reactivity during INTEX-B, *Atmos. Chem. Phys.*, 2009, **9**, 163–173.

22 A. Matsunaga and P. J. Ziemann, Gas-Wall Partitioning of Organic Compounds in a Teflon Film Chamber and Potential Effects on Reaction Product and Aerosol Yield Measurements, *Aerosol Sci. Technol.*, 2010, **44**, 881–892.

23 X. Zhang, R. C. McVay, D. D. Huang, N. F. Dalleska, B. Aumont, R. C. Flagan and J. H. Seinfeld, Formation and evolution of molecular products in α-pinene secondary organic aerosol, *Proc. Natl. Acad. Sci. U. S. A.*, 2015, **112**, 14168–14173.

24 J. E. Krechmer, D. Pagonis, P. J. Ziemann and J. L. Jimenez, Quantification of Gas-Wall Partitioning in Teflon Environmental Chambers Using Rapid Bursts of Low-Volatility

Oxidized Species Generated in Situ, *Environ. Sci. Technol.*, 2016, **50**, 5757–5765.
25 J. M. St. Clair, J. C. Rivera-Rios, J. D. Crounse, E. Praske, M. J. Kim, G. M. Wolfe, F. N. Keutsch, P. O. Wennberg and T. F. Hanisco, Investigation of a potential HCHO measurement artifact from ISOPOOH, *Atmos. Meas. Tech.*, 2016, **9**, 4561–4568.
26 P. H. McMurry and D. Grosjean, Gas and aerosol wall losses in Teflon film smog chambers, *Environ. Sci. Technol.*, 1985, **19**, 1176–1182.
27 R. Atkinson and J. Arey, Atmospheric Degradation of Volatile Organic Compounds, *Chem. Rev.*, 2003, **103**, 4605–4638.
28 I. J. George and J. P. D. Abbatt, Heterogeneous oxidation of atmospheric aerosol particles by gas-phase radicals, *Nat. Chem.*, 2010, **2**, 713–722.
29 I. J. George, A. Vlasenko, J. G. Slowik, K. Broekhuizen and J. P. D. Abbatt, Heterogeneous oxidation of saturated organic aerosols by hydroxyl radicals: uptake kinetics, condensed-phase products, and particle size change, *Atmos. Chem. Phys.*, 2007, **7**, 4187–4201.
30 E. Kang, M. J. Root, D. W. Toohey and W. H. Brune, Introducing the concept of Potential Aerosol Mass (PAM), *Atmos. Chem. Phys.*, 2007, **7**, 5727–5744.
31 B. B. Palm, P. Campuzano-Jost, A. M. Ortega, D. A. Day, L. Kaser, W. Jud, T. Karl, A. Hansel, J. F. Hunter, E. S. Cross, J. H. Kroll, Z. Peng, W. H. Brune and J. L. Jimenez, *In situ* secondary organic aerosol formation from ambient pine forest air using an oxidation flow reactor, *Atmos. Chem. Phys.*, 2016, **16**, 2943–2970.
32 W. H. Brune, The Chamber Wall Index for Gas–Wall Interactions in Atmospheric Environmental Enclosures, *Environ. Sci. Technol.*, 2019, **53**, 3645–3652.
33 W. Hu, B. B. Palm, D. A. Day, P. Campuzano-Jost, J. E. Krechmer, Z. Peng, S. S. de Sá, S. T. Martin, M. L. Alexander, K. Baumann, L. Hacker, A. Kiendler-Scharr, A. R. Koss, J. A. de Gouw, A. H. Goldstein, R. Seco, S. J. Sjostedt, J.-H. Park, A. B. Guenther, S. Kim, F. Canonaco, A. S. H. Prévôt, W. H. Brune and J. L. Jimenez, Volatility and lifetime against OH heterogeneous reaction of ambient isoprene-epoxydiols-derived secondary organic aerosol (IEPOX-SOA), *Atmos. Chem. Phys.*, 2016, **16**, 11563–11580.
34 A. M. Ortega, P. L. Hayes, Z. Peng, B. B. Palm, W. Hu, D. A. Day, R. Li, M. J. Cubison, W. H. Brune, M. Graus, C. Warneke, J. B. Gilman, W. C. Kuster, J. de Gouw, C. Gutiérrez-Montes and J. L. Jimenez, Real-time measurements of secondary organic aerosol formation and aging from ambient air in an oxidation flow reactor in the Los Angeles area, *Atmos. Chem. Phys.*, 2016, **16**, 7411–7433.
35 T. Liu, L. Zhou, Q. Liu, B. P. Lee, D. Yao, H. Lu, X. Lyu, H. Guo and C. K. Chan, Secondary Organic Aerosol Formation from Urban Roadside Air in Hong Kong, *Environ. Sci. Technol.*, 2019, **53**, 3001–3009.
36 B. A. Nault, P. Campuzano-Jost, D. A. Day, J. C. Schroder, B. Anderson, A. J. Beyersdorf, D. R. Blake, W. H. Brune, Y. Choi, C. A. Corr, J. A. de Gouw, J. Dibb, J. P. DiGangi, G. S. Diskin, A. Fried, L. G. Huey, M. J. Kim, C. J. Knote, K. D. Lamb, T. Lee, T. Park, S. E. Pusede, E. Scheuer, K. L. Thornhill, J.-H. Woo and J. L. Jimenez, Secondary organic aerosol production from local emissions dominates the organic aerosol budget over Seoul, South Korea, during KORUS-AQ, *Atmos. Chem. Phys.*, 2018, **18**, 17769–17800.
37 D. S. Tkacik, A. T. Lambe, S. Jathar, X. Li, A. A. Presto, Y. Zhao, D. Blake, S. Meinardi, J. T. Jayne, P. L. Croteau and A. L. Robinson, Secondary Organic Aerosol Formation from in-Use Motor Vehicle Emissions Using a Potential Aerosol Mass Reactor, *Environ. Sci. Technol.*, 2014, **48**, 11235–11242.
38 A. M. Ortega, D. A. Day, M. J. Cubison, W. H. Brune, D. Bon, J. A. de Gouw and J. L. Jimenez, Secondary organic aerosol formation and primary organic aerosol oxidation from biomass-burning smoke in a flow reactor during FLAME-3, *Atmos. Chem. Phys.*, 2013, **13**, 11551–11571.
39 Å. K. Watne, M. Psichoudaki, E. Ljungström, M. Le Breton, M. Hallquist, M. Jerksjö, H. Fallgren, S. Jutterström and Å. M. Hallquist, Fresh and Oxidized Emissions from In-Use Transit Buses Running on Diesel, Biodiesel, and CNG, *Environ. Sci. Technol.*, 2018, **52**, 7720–7728.
40 N. Yamamoto, D. Hospodsky, K. C. Dannemiller, W. W. Nazaroff and J. Peccia, Indoor Emissions as a Primary Source of Airborne Allergenic Fungal Particles in Classrooms, *Environ. Sci. Technol.*, 2015, **49**, 5098–5106.
41 Z. J. Wu, J. Zheng, D. J. Shang, Z. F. Du, Y. S. Wu, L. M. Zeng, A. Wiedensohler and M. Hu, Particle hygroscopicity and its link to chemical composition in the urban atmosphere of Beijing, China, during summertime, *Atmos. Chem. Phys.*, 2016, **16**, 1123–1138.
42 Interactive comment on ''Time-resolved characterization of primary and secondary particle emissions of a modern gasoline passenger car'' by P. Karjalainen *et al.*, *Atmos. Chem. Phys. Discuss*, 2016, **15**, C11859–C11866.
43 Interactive comment on ''Controlled nitric oxide production *via* O (1D) + N_2O reactions for use in oxidation flow reactor studies'' by Andrew Lambe, *Atmos. Meas. Tech. Discuss.*, DOI: 10.5194/amt-2016-394-RC2.
44 Interactive comment on '' Time-resolved characterization of primary and secondary particle emissions of a modern gasoline passenger car'' by P. Karjalainen *et al.*, *Atmos. Chem. Phys. Discuss*, 2016, **15**, C12039–C12042.
45 R. Li, B. B. Palm, A. M. Ortega, W. Hu, Z. Peng, D. A. Day, C. Knote, W. H. Brune, J. de Gouw and J. L. Jimenez, Modeling the radical chemistry in an Oxidation Flow Reactor (OFR): radical formation and recycling, sensitivities, and OH exposure estimation equation, *J. Phys. Chem. A*, 2015, **119**, 4418–4432.
46 Z. Peng, D. A. Day, H. Stark, R. Li, J. Lee-Taylor, B. B. Palm, W. H. Brune and J. L. Jimenez, HOx radical chemistry in oxidation flow reactors with low-pressure mercury lamps systematically examined by modeling, *Atmos. Meas. Tech.*, 2015, **8**, 4863–4890.
47 Z. Peng, D. A. Day, A. M. Ortega, B. B. Palm, W. Hu, H. Stark, R. Li, K. Tsigaridis, W. H. Brune and J. L. Jimenez, Non-OH chemistry in oxidation flow reactors for the study of atmospheric chemistry systematically examined by modeling, *Atmos. Chem. Phys.*, 2016, **16**, 4283–4305.

48 Z. Peng and J. L. Jimenez, Modeling of the chemistry in oxidation flow reactors with high initial NO, *Atmos. Chem. Phys.*, 2017, **17**, 11991–12010.
49 Z. Peng, B. B. Palm, D. A. Day, R. K. Talukdar, W. Hu, A. T. Lambe, W. H. Brune and J. L. Jimenez, Model Evaluation of New Techniques for Maintaining High-NO Conditions in Oxidation Flow Reactors for the Study of OH-Initiated Atmospheric Chemistry, *ACS Earth Space Chem.*, 2018, **2**, 72–86.
50 Z. Peng, J. Lee-Taylor, J. J. Orlando, G. S. Tyndall and J. L. Jimenez, Organic peroxy radical chemistry in oxidation flow reactors and environmental chambers and their atmospheric relevance, *Atmos. Chem. Phys.*, 2019, **19**, 813–834.
51 J. J. Orlando and G. S. Tyndall, Laboratory studies of organic peroxy radical chemistry: an overview with emphasis on recent issues of atmospheric significance, *Chem. Soc. Rev.*, 2012, **41**, 6294–6317.
52 P. O. Wennberg, Let's abandon the ''high NOx'' and ''low NOx'' terminology, *IGAC News*, 2013, **50**, 3–4.
53 F. Bianchi, T. Kurtén, M. Riva, C. Mohr, M. P. Rissanen, P. Roldin, T. Berndt, J. D. Crounse, P. O. Wennberg, T. F. Mentel, J. Wildt, H. Junninen, T. Jokinen, M. Kulmala, D. R. Worsnop, J. A. Thornton, N. Donahue, H. G. Kjaergaard and M. Ehn, Highly Oxygenated Organic Molecules (HOM) from Gas-Phase Autoxidation Involving Peroxy Radicals: A Key Contributor to Atmospheric Aerosol, *Chem. Rev.*, 2019, **119**, 3472–3509.
54 D. D. Parrish, H. B. Singh, L. Molina and S. Madronich, Air quality progress in North American megacities: A review, *Atmos. Environ.*, 2011, **45**, 7015–7025.
55 J. B. Burkholder, S. P. Sander, J. Abbatt, J. R. Barker, R. E. Huie, C. E. Kolb, M. J. Kurylo, V. L. Orkin, D. M. Wilmouth and P. H. Wine, *Chemical Kinetics and Photochemical Data for Use in Atmospheric Studies: Evaluation Number 18*, Pasadena, CA, USA, 2015.
56 P. Massoli, A. T. Lambe, A. T. Ahern, L. R. Williams, M. Ehn, J. Mikkilä, M. R. Canagaratna, W. H. Brune, T. B. Onasch, J. T. Jayne, T. Petäjä, M. Kulmala, A. Laaksonen, C. E. Kolb, P. Davidovits and D. R. Worsnop, Relationship between aerosol oxidation level and hygroscopic properties of laboratory generated secondary organic aerosol (SOA) particles, *Geophys. Res. Lett.*, 2010, **37**, L24801.
57 A. T. Lambe, T. B. Onasch, P. Massoli, D. R. Croasdale, J. P. Wright, A. T. Ahern, L. R. Williams, D. R. Worsnop, W. H. Brune and P. Davidovits, Laboratory studies of the chemical composition and cloud condensation nuclei (CCN) activity of secondary organic aerosol (SOA) and oxidized primary organic aerosol (OPOA), *Atmos. Chem. Phys.*, 2011, **11**, 8913–8928.
58 Y. Kang, M. Liu, Y. Song, X. Huang, H. Yao, X. Cai, H. Zhang, L. Kang, X. Liu, X. Yan, H. He, Q. Zhang, M. Shao and T. Zhu, High-resolution ammonia emissions inventories in China from 1980 to 2012, *Atmos. Chem. Phys.*, 2016, **16**, 2043–2058.
59 E. Kang, D. W. Toohey and W. H. Brune, Dependence of SOA oxidation on organic aerosol mass concentration and OH exposure: experimental PAM chamber studies, *Atmos. Chem. Phys.*, 2011, **11**, 1837–1852.
60 A. Keller and H. Burtscher, A continuous photo-oxidation flow reactor for a defined measurement of the SOA formation potential of wood burning emissions, *J. Aerosol Sci.*, 2012, **49**, 9–20.
61 Y. Huang, M. M. Coggon, R. Zhao, H. Lignell, M. U. Bauer, R. C. Flagan and J. H. Seinfeld, The Caltech Photooxidation Flow Tube reactor: design, fluid dynamics and characterization, *Atmos. Meas. Tech.*, 2017, **10**, 839–867.
62 M. J. Cubison, A. M. Ortega, P. L. Hayes, D. K. Farmer, D. Day, M. J. Lechner, W. H. Brune, E. Apel, G. S. Diskin, J. A. Fisher, H. E. Fuelberg, A. Hecobian, D. J. Knapp, T. Mikoviny, D. Riemer, G. W. Sachse, W. Sessions, R. J. Weber, A. J. Weinheimer, A. Wisthaler and J. L. Jimenez, Effects of aging on organic aerosol from open biomass burning smoke in aircraft and laboratory studies, *Atmos. Chem. Phys.*, 2011, **11**, 12049–12064.
63 B. B. Palm, S. S. de Sá, D. A. Day, P. Campuzano-Jost, W. Hu, R. Seco, S. J. Sjostedt, J.-H. Park, A. B. Guenther, S. Kim, J. Brito, F. Wurm, P. Artaxo, R. Thalman, J. Wang, L. D. Yee, R. Wernis, G. Isaacman-VanWertz, A. H. Goldstein, Y. Liu, S. R. Springston, R. Souza, M. K. Newburn, M. L. Alexander, S. T. Martin and J. L. Jimenez, Secondary organic aerosol formation from ambient air in an oxidation flow reactor in central Amazonia, *Atmos. Chem. Phys.*, 2018, **18**, 467–493.
64 E. Kang, M. Lee, W. H. Brune, T. Lee, T. Park, J. Ahn and X. Shang, Photochemical aging of aerosol particles in different air masses arriving at Baengnyeong Island, Korea, *Atmos. Chem. Phys.*, 2018, **18**, 6661–6677.
65 P. K. Saha, S. M. Reece and A. P. Grieshop, Seasonally Varying Secondary Organic Aerosol Formation From In-Situ Oxidation of Near-Highway Air, *Environ. Sci. Technol.*, 2018, **52**, 7192–7202.
66 A. T. Lambe and J. L. Jimenez, PAM Wiki: Publications Using the PAM Oxidation Flow Reactor, https://sites.google.com/site/pamwiki/publications, accessed 8 March 2019.
67 J. Li, Q. Liu, Y. Li, T. Liu, D. Huang, J. Zheng, W. Zhu, M. Hu, Y. Wu, S. Lou, Å. M. Hallquist, M. Hallquist, C. K. Chan, F. Canonaco, A. S. H. Prévôt, J. C. H. Fung, A. K. H. Lau and J. Z. Yu, Characterization of Aerosol Aging Potentials at Suburban Sites in Northern and Southern China Utilizing a Potential Aerosol Mass (Go:PAM) Reactor and an Aerosol Mass Spectrometer, *J. Geophys. Res.: Atmos.*, 2019, **124**, 5629–5649.
68 S. M. Reece, A. Sinha and A. P. Grieshop, Primary and Photochemically Aged Aerosol Emissions from Biomass Cookstoves: Chemical and Physical Characterization, *Environ. Sci. Technol.*, 2017, **51**, 9379–9390.
69 W. M. Champion, N. E. Rothfuss, M. D. Petters and A. P. Grieshop, Volatility and Viscosity Are Correlated in Terpene Secondary Organic Aerosol Formed in a Flow Reactor, *Environ. Sci. Technol. Lett.*, 2019, **6**, 513–519.
70 N. E. Rothfuss, S. S. Petters, W. M. Champion, A. P. Grieshop and M. D. Petters, Characterization of a dimer

preparation method for nanoscale organic aerosol, *Aerosol Sci. Technol.*, 2019, **53**, 998–1011.
71 I. J. George, J. Slowik and J. P. D. Abbatt, Chemical aging of ambient organic aerosol from heterogeneous reaction with hydroxyl radicals, *Geophys. Res. Lett.*, 2008, **35**, L13811.
72 A. Vlasenko, I. J. George and J. P. D. Abbatt, Formation of Volatile Organic Compounds in the Heterogeneous Oxidation of Condensed-Phase Organic Films by Gas-Phase OH, *J. Phys. Chem. A*, 2008, **112**, 1552–1560.
73 J. P. S. Wong, A. K. Y. Lee, J. G. Slowik, D. J. Cziczo, W. R. Leaitch, A. Macdonald and J. P. D. Abbatt, Oxidation of ambient biogenic secondary organic aerosol by hydroxyl radicals: Effects on cloud condensation nuclei activity, *Geophys. Res. Lett.*, 2011, **38**, L22805.
74 J. G. Slowik, J. P. S. Wong and J. P. D. Abbatt, Real-time, controlled OH-initiated oxidation of biogenic secondary organic aerosol, *Atmos. Chem. Phys.*, 2012, **12**, 9775–9790.
75 J. H. Kroll, J. D. Smith, D. L. Che, S. H. Kessler, D. R. Worsnop and K. R. Wilson, Measurement of fragmentation and functionalization pathways in the heterogeneous oxidation of oxidized organic aerosol, *Phys. Chem. Chem. Phys.*, 2009, **11**, 8005–8014.
76 J. D. Smith, J. H. Kroll, C. D. Cappa, D. L. Che, C. L. Liu, M. Ahmed, S. R. Leone, D. R. Worsnop and K. R. Wilson, The heterogeneous reaction of hydroxyl radicals with sub-micron squalane particles: a model system for understanding the oxidative aging of ambient aerosols, *Atmos. Chem. Phys.*, 2009, **9**, 3209–3222.
77 S. H. Kessler, J. D. Smith, D. L. Che, D. R. Worsnop, K. R. Wilson and J. H. Kroll, Chemical Sinks of Organic Aerosol: Kinetics and Products of the Heterogeneous Oxidation of Erythritol and Levoglucosan, *Environ. Sci. Technol.*, 2010, **44**, 7005–7010.
78 S. H. Kessler, T. Nah, K. E. Daumit, J. D. Smith, S. R. Leone, C. E. Kolb, D. R. Worsnop, K. R. Wilson and J. H. Kroll, OH-Initiated Heterogeneous Aging of Highly Oxidized Organic Aerosol, *J. Phys. Chem. A*, 2012, **116**, 6358–6365.
79 N. K. Richards-Henderson, A. H. Goldstein and K. R. Wilson, Large Enhancement in the Heterogeneous Oxidation Rate of Organic Aerosols by Hydroxyl Radicals in the Presence of Nitric Oxide, *J. Phys. Chem. Lett.*, 2015, **6**, 4451–4455.
80 N. K. Richards-Henderson, A. H. Goldstein and K. R. Wilson, Sulfur Dioxide Accelerates the Heterogeneous Oxidation Rate of Organic Aerosol by Hydroxyl Radicals, *Environ. Sci. Technol.*, 2016, **50**, 3554–3561.
81 C. Y. Lim, E. C. Browne, R. A. Sugrue and J. H. Kroll, Rapid heterogeneous oxidation of organic coatings on submicron aerosols, *Geophys. Res. Lett.*, 2017, **44**, 2949–2957.
82 J. D. Hearn and G. D. Smith, A mixed-phase relative rates technique for measuring aerosol reaction kinetics, *Geophys. Res. Lett.*, 2006, **33**, L17805.
83 P. Simonen, E. Saukko, P. Karjalainen, H. Timonen, M. Bloss, P. Aakko-Saksa, T. Rönkkö and J. Keskinen, and M. Dal Maso, A new oxidation flow reactor for measuring secondary aerosol formation of rapidly changing emission sources, *Atmos. Meas. Tech.*, 2017, **10**, 1519–1537.
84 M. Ihalainen, P. Tiitta, H. Czech, P. Yli-Pirilä, A. Hartikainen, M. Kortelainen, J. Tissari, B. Stengel, M. Sklorz, H. Suhonen, H. Lamberg, A. Leskinen, A. Kiendler-Scharr, H. Harndorf, R. Zimmermann, J. Jokiniemi and O. Sippula, A novel high-volume Photochemical Emission Aging flow tube Reactor (PEAR), *Aerosol Sci. Technol.*, 2019, **53**, 276–294.
85 D. L. Che, J. D. Smith, S. R. Leone, M. Ahmed and K. R. Wilson, Quantifying the reactive uptake of OH by organic aerosols in a continuous flow stirred tank reactor, *Phys. Chem. Chem. Phys.*, 2009, **11**, 7885–7895.
86 A. Lambe, P. Massoli, X. Zhang, M. Canagaratna, J. Nowak, C. Daube, C. Yan, W. Nie, T. Onasch, J. Jayne, C. Kolb, P. Davidovits, D. Worsnop and W. Brune, Controlled nitric oxide production *via* O(1D) + N2O reactions for use in oxidation flow reactor studies, *Atmos. Meas. Tech.*, 2017, **10**, 2283–2298.
87 A. T. Lambe, J. E. Krechmer, Z. Peng, J. R. Casar, A. J. Carrasquillo, J. D. Raff, J. L. Jimenez and D. R. Worsnop, HOx and NOx production in oxidation flow reactors *via* photolysis of isopropyl nitrite, isopropyl nitrite-d7, and 1,3-propyl dinitrite at λ = 254, 350, and 369 nm, *Atmos. Meas. Tech.*, 2019, **12**, 299–311.
88 R. Atkinson, D. L. Baulch, R. A. Cox, R. F. Hampson, J. A. Kerr, M. J. Rossi and J. Troe, Evaluated Kinetic and Photochemical Data for Atmospheric Chemistry: Supplement VI. IUPAC Subcommittee on Gas Kinetic Data Evaluation for Atmospheric Chemistry, *J. Phys. Chem. Ref. Data*, 1997, **26**, 1329–1499.
89 C. M. Strollo and P. J. Ziemann, Products and mechanism of secondary organic aerosol formation from the reaction of 3-methylfuran with OH radicals in the presence of NOx, *Atmos. Environ.*, 2013, **77**, 534–543.
90 R. Atkinson, W. P. L. Carter, A. M. Winer and J. N. Pitts, An Experimental Protocol for the Determination of OH Radical Rate Constants with Organics Using Methyl Nitrite Photolysis as an OH Radical Source, *J. Air Pollut. Control Assoc.*, 1981, **31**, 1090–1092.
91 J. D. Raff and B. J. Finlayson-Pitts, Hydroxyl radical quantum yields from isopropyl nitrite photolysis in air, *Environ. Sci. Technol.*, 2010, **44**, 8150–8155.
92 L. Renbaum-Wolff and G. D. Smith, 'Virtual injector' flow tube method for measuring relative rates kinetics of gas-phase and aerosol species, *J. Phys. Chem. A*, 2012, **116**, 6664–6674.
93 D. Hanson, H. Abdullahi, S. Menheer, J. Vences, M. Alves and J. Kunz, H_2SO_4 and particle production in a photolytic flow reactor: Chemical modeling, cluster thermodynamics and contamination issues, *Atmos. Chem. Phys.*, 2019, **19**, 8999–9015.
94 J. P. D. Abbatt, K. L. Demerjian and J. G. Anderson, A new approach to free-radical kinetics: radially and axially resolved high-pressure discharge flow with results for hydroxyl + (ethane, propane, n-butane, n-pentane) products at 297 K, *J. Phys. Chem.*, 1990, **94**, 4566–4575.
95 R. Zhang, I. Suh, W. Lei, A. D. Clinkenbeard and S. W. North, Kinetic studies of OH-initiated reactions of isoprene, *J. Geophys. Res.: Atmos.*, 2000, **105**, 24627–24635.

96 M. Sprengnether, K. L. Demerjian, N. M. Donahue and J. G. Anderson, Product analysis of the OH oxidation of isoprene and 1,3-butadiene in the presence of NO, *J. Geophys. Res.: Atmos.*, 2002, **107**, 4268.
97 C. Li, Q. He, J. Schade, J. Passig, R. Zimmermann, D. Meidan, A. Laskin and Y. Rudich, Dynamic changes in optical and chemical properties of tar ball aerosols by atmospheric photochemical aging, *Atmos. Chem. Phys.*, 2019, **19**, 139–163.
98 D. Zhang, R. Zhang, C. Church and S. W. North, Experimental study of hydroxyalkyl peroxy radicals from OH-initiated reactions of isoprene, *Chem. Phys. Lett.*, 2001, **343**, 49–54.
99 D. Zhang, R. Zhang and S. W. North, Experimental Study of NO Reaction with Isoprene Hydroxyalkyl Peroxy Radicals, *J. Phys. Chem. A*, 2003, **107**, 11013–11019.
100 J. Zhao, R. Zhang, E. C. Fortner and S. W. North, Quantification of Hydroxycarbonyls from OH-Isoprene Reactions, *J. Am. Chem. Soc.*, 2004, **126**, 2686–2687.
101 B. B. Palm, P. Campuzano-Jost, D. A. Day, A. M. Ortega, J. L. Fry, S. S. Brown, K. J. Zarzana, W. Dube, N. L. Wagner, D. C. Draper, L. Kaser, W. Jud, T. Karl, A. Hansel, C. Gutiérrez-Montes and J. L. Jimenez, Secondary organic aerosol formation from in situ OH, O3, and NO3 oxidation of ambient forest air in an oxidation flow reactor, *Atmos. Chem. Phys.*, 2017, **17**, 5331–5354.
102 M. J. Ezell, S. N. Johnson, Y. Yu, V. Perraud, E. A. Bruns, M. L. Alexander, A. Zelenyuk, D. Dabdub and B. J. Finlayson-Pitts, A New Aerosol Flow System for Photochemical and Thermal Studies of Tropospheric Aerosols, *Aerosol Sci. Technol.*, 2010, **44**, 329–338.
103 J. W. Morris, P. Davidovits, J. T. Jayne, J. L. Jimenez, Q. Shi, C. E. Kolb, D. R. Worsnop, W. S. Barney and G. Cass, Kinetics of submicron oleic acid aerosols with ozone: A novel aerosol mass spectrometric technique, *Geophys. Res. Lett.*, 2002, **29**, 1357.
104 G. D. Smith, E. Woods, C. L. DeForest, T. Baer and R. E. Miller, Reactive uptake of ozone by oleic acid aerosol particles: Application of single-particle mass spectrometry to heterogeneous reaction kinetics, *J. Phys. Chem. A*, 2002, **106**, 8085–8095.
105 X. Cai and R. J. Griffin, Secondary aerosol formation from the oxidation of biogenic hydrocarbons by chlorine atoms, *J. Geophys. Res.*, 2006, **111**, D14206.
106 J. D. Hearn and G. D. Smith, Kinetics and Product Studies for Ozonolysis Reactions of Organic Particles Using Aerosol CIMS, *J. Phys. Chem. A*, 2004, **108**, 10019–10029.
107 J. D. Hearn and G. D. Smith, Measuring rates of reaction in supercooled organic particles with implications for atmospheric aerosol, *Phys. Chem. Chem. Phys.*, 2005, **7**, 2549–2551.
108 J. D. Hearn, A. J. Lovett and G. D. Smith, Ozonolysis of oleic acid particles: evidence for a surface reaction and secondary reactions involving Criegee intermediates, *Phys. Chem. Chem. Phys.*, 2005, **7**, 501–511.
109 E. C. Browne, J. P. Franklin, M. R. Canagaratna, P. Massoli, T. W. Kirchstetter, D. R. Worsnop, K. R. Wilson and J. H. Kroll, Changes to the Chemical Composition of Soot from Heterogeneous Oxidation Reactions, *J. Phys. Chem. A*, 2015, **119**, 1154–1163.
110 M. I. Jacobs, B. Xu, O. Kostko, N. Heine, M. Ahmed and K. R. Wilson, Probing the Heterogeneous Ozonolysis of Squalene Nanoparticles by Photoemission, *J. Phys. Chem. A*, 2016, **120**, 8645–8656.
111 N. Heine, F. A. Houle and K. R. Wilson, Connecting the Elementary Reaction Pathways of Criegee Intermediates to the Chemical Erosion of Squalene Interfaces during Ozonolysis, *Environ. Sci. Technol.*, 2017, **51**, 13740–13748.
112 S. S. Petters, S. M. Kreidenweis, A. P. Grieshop, P. J. Ziemann and M. D. Petters, Temperature- and Humidity-Dependent Phase States of Secondary Organic Aerosols, *Geophys. Res. Lett.*, 2019, **46**, 1005–1013.
113 S. C. Wofsy, E. Apel, D. R. Blake, C. A. Brock, W. H. Brune, T. P. Bui, B. C. Daube, J. E. Dibb, G. S. Diskin, J. W. Elkiins, K. Froyd, S. R. Hall, T. F. Hanisco, L. G. Huey, J. L. Jimenez, K. McKain, S. A. Montzka, T. B. Ryerson, J. P. Schwarz, B. B. Stephens, B. Weinzierl and P. Wennberg, *ATom: Merged Atmospheric Chemistry, Trace Gases, and Aerosols*, Oak Ridge, Tennessee, USA, 2018.
114 Y. J. Liu, I. Herdlinger-Blatt, K. A. McKinney and S. T. Martin, Production of methyl vinyl ketone and methacrolein *via* the hydroperoxyl pathway of isoprene oxidation, *Atmos. Chem. Phys.*, 2013, **13**, 5715–5730.
115 H. Fuchs, A. Hofzumahaus, F. Rohrer, B. Bohn, T. Brauers, H.-P. Dorn, R. Häseler, F. Holland, M. Kaminski, X. Li, K. Lu, S. Nehr, R. Tillmann, R. Wegener and A. Wahner, Experimental evidence for efficient hydroxyl radical regeneration in isoprene oxidation, *Nat. Geosci.*, 2013, **6**, 1023–1026.
116 A. T. Lambe, A. T. Ahern, L. R. Williams, J. G. Slowik, J. P. S. Wong, J. P. D. Abbatt, W. H. Brune, N. L. Ng, J. P. Wright, D. R. Croasdale, D. R. Worsnop, P. Davidovits and T. B. Onasch, Characterization of aerosol photooxidation flow reactors: heterogeneous oxidation, secondary organic aerosol formation and cloud condensation nuclei activity measurements, *Atmos. Meas. Tech.*, 2011, **4**, 445–461.
117 N. A. Krotkov, C. A. McLinden, C. Li, L. N. Lamsal, E. A. Celarier, S. V. Marchenko, W. H. Swartz, E. J. Bucsela, J. Joiner, B. N. Duncan, K. F. Boersma, J. P. Veefkind, P. F. Levelt, V. E. Fioletov, R. R. Dickerson, H. He, Z. Lu and D. G. Streets, Aura OMI observations of regional SO_2 and NO_2 pollution changes from 2005 to 2015, *Atmos. Chem. Phys.*, 2016, **16**, 4605–4629.
118 M. Ammann, R. A. Cox, J. N. Crowley, M. E. Jenkin, A. Mellouki, M. J. Rossi, J. Troe, T. J. Wallington, B. Cox, R. Atkinson, D. L. Baulch and J. A. Kerr, IUPAC Task Group on Atmospheric Chemical Kinetic Data Evaluation, http://iupac.pole-ether.fr/#.
119 J. D. Crounse, L. B. Nielsen, S. Jørgensen, H. G. Kjaergaard and P. O. Wennberg, Autoxidation of organic compounds in the atmosphere, *J. Phys. Chem. Lett.*, 2013, **4**, 3513–3520.
120 E. Assaf, S. Tanaka, Y. Kajii, C. Schoemaecker and C. Fittschen, Rate constants of the reaction of C2–C4 peroxy radicals with OH radicals, *Chem. Phys. Lett.*, 2017, **684**, 245–249.

121 J. P. Klems, K. A. Lippa and W. S. McGivern, Quantitative Evidence for Organic Peroxy Radical Photochemistry at 254 nm, *J. Phys. Chem. A*, 2015, **119**, 344–351.
122 C. Fittschen, L. K. Whalley and D. E. Heard, The reaction of CH3O2 radicals with OH radicals: a neglected sink for CH3O2 in the remote atmosphere, *Environ. Sci. Technol.*, 2014, **48**, 7700–7701.
123 T. Berndt, W. Scholz, B. Mentler, L. Fischer, H. Herrmann, M. Kulmala and A. Hansel, Accretion Product Formation from Self- and Cross-Reactions of RO2 Radicals in the Atmosphere, *Angew. Chem., Int. Ed.*, 2018, **57**, 3820–3824.
124 C. Yan, S. Kocevska and L. N. Krasnoperov, Kinetics of the Reaction of CH3O2 Radicals with OH Studied over the 292–526 K Temperature Range, *J. Phys. Chem. A*, 2016, **120**, 6111–6121.
125 E. Assaf, B. Song, A. Tomas, C. Schoemaecker and C. Fittschen, Rate Constant of the Reaction between CH3O2 Radicals and OH Radicals Revisited, *J. Phys. Chem. A*, 2016, **120**, 8923–8932.
126 A. Bossolasco, E. P. Faragó, C. Schoemaecker and C. Fittschen, Rate constant of the reaction between CH3O2 and OH radicals, *Chem. Phys. Lett.*, 2014, **593**, 7–13.
127 J.-F. Müller, Z. Liu, V. S. Nguyen, T. Stavrakou, J. N. Harvey and J. Peeters, The reaction of methyl peroxy and hydroxyl radicals as a major source of atmospheric methanol, *Nat. Commun.*, 2016, **7**, 13213.
128 E. Assaf, L. Sheps, L. Whalley, D. Heard, A. Tomas, C. Schoemaecker and C. Fittschen, The Reaction between CH3O2 and OH Radicals: Product Yields and Atmospheric Implications, *Environ. Sci. Technol.*, 2017, **51**, 2170–2177.
129 E. Assaf, C. Schoemaecker, L. Vereecken and C. Fittschen, Experimental and theoretical investigation of the reaction of RO2 radicals with OH radicals: Dependence of the HO2 yield on the size of the alkyl group, *Int. J. Chem. Kinet.*, 2018, **50**, 670–680.
130 J. M. Anglada and A. Solé, Tropospheric oxidation of methyl hydrotrioxide (CH3OOOH) by hydroxyl radical, *Phys. Chem. Chem. Phys.*, 2018, **20**, 27406–27417.
131 E. Praske, R. V. Otkjær, J. D. Crounse, J. C. Hethcox, B. M. Stoltz, H. G. Kjaergaard and P. O. Wennberg, Atmospheric autoxidation is increasingly important in urban and suburban North America, *Proc. Natl. Acad. Sci. U. S. A.*, 2018, **115**, 64–69.
132 H. C. Knap and S. Jørgensen, Rapid Hydrogen Shift Reactions in Acyl Peroxy Radicals, *J. Phys. Chem. A*, 2017, **121**, 1470–1479.
133 S. Jørgensen, H. C. Knap, R. V. Otkjær, A. M. Jensen, M. L. H. Kjeldsen, P. O. Wennberg and H. G. Kjaergaard, Rapid Hydrogen Shift Scrambling in Hydroperoxy-Substituted Organic Peroxy Radicals, *J. Phys. Chem. A*, 2016, **120**, 266–275.
134 A. P. Teng, J. D. Crounse and P. O. Wennberg, Isoprene Peroxy Radical Dynamics, *J. Am. Chem. Soc.*, 2017, **139**, 5367–5377.
135 P. O. Wennberg, K. H. Bates, J. D. Crounse, L. G. Dodson, R. C. McVay, L. A. Mertens, T. B. Nguyen, E. Praske, R. H. Schwantes, M. D. Smarte, J. M. St Clair, A. P. Teng, X. Zhang and J. H. Seinfeld, Gas-Phase Reactions of Isoprene and Its Major Oxidation Products, *Chem. Rev.*, 2018, **118**, 3337–3390.
136 L. Xu, K. H. Møller, J. D. Crounse, R. V. Otkjær, H. G. Kjaergaard and P. O. Wennberg, Unimolecular Reactions of Peroxy Radicals Formed in the Oxidation of α-Pinene and β-Pinene by Hydroxyl Radicals, *J. Phys. Chem. A*, 2019, **123**, 1661–1674.
137 C. S. Kan, J. G. Calvert and J. H. Shaw, Oxidation of sulfur dioxide by methylperoxy radicals, *J. Phys. Chem.*, 1981, **85**, 1126–1132.
138 C. Liu, J. Liu, Y. Liu, T. Chen and H. He, Secondary organic aerosol formation from the OH-initiated oxidation of guaiacol under different experimental conditions, *Atmos. Environ.*, 2019, **207**, 30–37.
139 S. Eluri, C. D. Cappa, B. Friedman, D. K. Farmer and S. H. Jathar, Modeling the formation and composition of secondary organic aerosol from diesel exhaust using parameterized and semi-explicit chemistry and thermodynamic models, *Atmos. Chem. Phys.*, 2018, **18**, 13813–13838.
140 S. Nehr, B. Bohn, H. Fuchs, R. Häseler, A. Hofzumahaus, X. Li, F. Rohrer, R. Tillmann and A. Wahner, Atmospheric photochemistry of aromatic hydrocarbons: OH budgets during SAPHIR chamber experiments, *Atmos. Chem. Phys.*, 2014, **14**, 6941–6952.
141 R. H. Schwantes, K. A. Schilling, R. C. McVay, H. Lignell, M. M. Coggon, X. Zhang, P. O. Wennberg and J. H. Seinfeld, Formation of highly oxygenated low-volatility products from cresol oxidation, *Atmos. Chem. Phys.*, 2017, **17**, 3453–3474.
142 H. Fuchs, A. Novelli, M. Rolletter, A. Hofzumahaus, E. Y. Pfannerstill, S. Kessel, A. Edtbauer, J. Williams, V. Michoud, S. Dusanter, N. Locoge, N. Zannoni, V. Gros, F. Truong, R. Sarda-Esteve, D. R. Cryer, C. A. Brumby, L. K. Whalley, D. Stone, P. W. Seakins, D. E. Heard, C. Schoemaecker, M. Blocquet, S. Coudert, S. Batut, C. Fittschen, A. B. Thames, W. H. Brune, C. Ernest, H. Harder, J. B. A. Muller, T. Elste, D. Kubistin, S. Andres, B. Bohn, T. Hohaus, F. Holland, X. Li, F. Rohrer, A. Kiendler-Scharr, R. Tillmann, R. Wegener, Z. Yu, Q. Zou and A. Wahner, Comparison of OH reactivity measurements in the atmospheric simulation chamber SAPHIR, *Atmos. Meas. Tech.*, 2017, **10**, 4023–4053.
143 K. Sato, Y. Nakashima, Y. Morino, T. Imamura, J. Kurokawa and Y. Kajii, Total OH reactivity measurements for the OH-initiated oxidation of aromatic hydrocarbons in the presence of NOx, *Atmos. Environ.*, 2017, **171**, 272–278.
144 B. Aumont, S. Szopa and S. Madronich, Modelling the evolution of organic carbon during its gas-phase tropospheric oxidation: development of an explicit model based on a self generating approach, *Atmos. Chem. Phys.*, 2005, **5**, 2497–2517.
145 J. G. Calvert and J. N. Pitts Jr., *Photochemistry*, John Wiley & Sons, New York, 1st edn, 1966.
146 J. M. Roberts and R. W. Fajer, UV absorption cross sections of organic nitrates of potential atmospheric importance and estimation of atmospheric lifetimes, *Environ. Sci. Technol.*, 1989, **23**, 945–951.
147 H. Keller-Rudek, G. K. Moortgat, R. Sander and R. Sörensen, The MPI-Mainz UV/VIS Spectral Atlas of Gaseous Molecules of Atmospheric Interest, www.uv-vis-spectral-atlas-mainz.org, accessed 26 March 2019.

148 Tropospheric Ultraviolet and Visible (TUV) Radiation Model, https://www2.acom.ucar.edu/modeling/tropospheric-ultraviolet-and-visible-tuv-radiation-model, accessed 26 March 2019.
149 Mercury Analamp Emission Graph, http://www.bhkinc.com/index.cfm?action=products, accessed 26 March 2019.
150 S. Aimanant and P. J. Ziemann, Chemical Mechanisms of Aging of Aerosol Formed from the Reaction of n-Pentadecane with OH Radicals in the Presence of NOx, *Aerosol Sci. Technol.*, 2013, **47**, 979–990.
151 A. P. Ranney and P. J. Ziemann, Kinetics of Acid-Catalyzed Dehydration of Cyclic Hemiacetals in Organic Aerosol Particles in Equilibrium with Nitric Acid Vapor, *J. Phys. Chem. A*, 2016, **120**, 2561–2568.
152 J. H. Seinfeld and S. N. Pandis, *Atmospheric Chemistry and Physics: From Air Pollution to Climate Change*, John Wiley & Sons, Inc., Hoboken, NJ, USA, 2006.
153 N. M. Donahue, L. N. Posner, D. M. Westervelt, Z. Li, M. Shrivastava, A. A. Presto, R. C. Sullivan, P. J. Adams, S. N. Pandis and A. L. Robinson, in *Airborne Particulate Matter: Sources, Atmospheric Processes and Health*, ed. R. M. Harrison, R. E. Hester and X. Querol, Royal Society of Chemistry, 2016, pp. 35–71.
154 J. E. Krechmer, D. A. Day, P. J. Ziemann and J. L. Jimenez, Direct Measurements of Gas/Particle Partitioning and Mass Accommodation Coefficients in Environmental Chambers, *Environ. Sci. Technol.*, 2017, **51**, 11867–11875.
155 D. Stone, L. K. Whalley and D. E. Heard, Tropospheric OH and HO2 radicals: field measurements and model comparisons, *Chem. Soc. Rev.*, 2012, **41**, 6348–6404.
156 T. B. Ryerson, A. E. Andrews, W. M. Angevine, T. S. Bates, C. A. Brock, B. Cairns, R. C. Cohen, O. R. Cooper, J. A. De Gouw, F. C. Fehsenfeld, R. A. Ferrare, M. L. Fischer, R. C. Flagan, A. H. Goldstein, J. W. Hair, R. M. Hardesty, C. A. Hostetler, J. L. Jimenez, A. O. Langford, E. McCauley, S. A. McKeen, L. T. Molina, A. Nenes, S. J. Oltmans, D. D. Parrish, J. R. Pederson, R. B. Pierce, K. Prather, P. K. Quinn, J. H. Seinfeld, C. J. Senff, A. Sorooshian, J. Stutz, J. D. Surratt, M. Trainer, R. Volkamer, E. J. Williams and S. C. Wofsy, The 2010 California Research at the Nexus of Air Quality and Climate Change (CalNex) field study, *J. Geophys. Res.: Atmos.*, 2013, **118**, 5830–5866.
157 V. F. McNeill, R. L. N. Yatavelli, J. A. Thornton, C. B. Stipe and O. Landgrebe, Heterogeneous OH oxidation of palmitic acid in single component and internally mixed aerosol particles: vaporization and the role of particle phase, *Atmos. Chem. Phys.*, 2008, **8**, 5465–5476.
158 A. A. Wiegel, K. R. Wilson, W. D. Hinsberg and F. A. Houle, Stochastic methods for aerosol chemistry: a compact molecular description of functionalization and fragmentation in the heterogeneous oxidation of squalane aerosol by OH radicals, *Phys. Chem. Chem. Phys.*, 2015, **17**, 4398–4411.
159 F. A. Houle, W. D. Hinsberg and K. R. Wilson, Oxidation of a model alkane aerosol by OH radical: the emergent nature of reactive uptake, *Phys. Chem. Chem. Phys.*, 2015, **17**, 4412–4423.
160 Y. Rudich, N. M. Donahue and T. F. Mentel, Aging of Organic Aerosol: Bridging the Gap Between Laboratory and Field Studies, *Annu. Rev. Phys. Chem.*, 2007, **58**, 321–352.
161 J. D. Blando and B. J. Turpin, Secondary organic aerosol formation in cloud and fog droplets: a literature evaluation of plausibility, *Atmos. Environ.*, 2000, **34**, 1623–1632.
162 V. F. McNeill, J. L. Woo, D. D. Kim, A. N. Schwier, N. J. Wannell, A. J. Sumner and J. M. Barakat, Aqueous-phase secondary organic aerosol and organosulfate formation in atmospheric aerosols: A modeling study, *Environ. Sci. Technol.*, 2012, **46**, 8075–8081.
163 J. H. Kroll, N. L. Ng, S. M. Murphy, V. Varutbangkul, R. C. Flagan and J. H. Seinfeld, Chamber studies of secondary organic aerosol growth by reactive uptake of simple carbonyl compounds, *J. Geophys. Res.*, 2005, **110**, D23207.
164 J. Liggio, S.-M. Li and R. McLaren, Reactive uptake of glyoxal by particulate matter, *J. Geophys. Res.*, 2005, **110**, D10304.
165 F. Paulot, J. D. Crounse, H. G. Kjaergaard, A. Kurten, J. M. St. Clair, J. H. Seinfeld and P. O. Wennberg, Unexpected Epoxide Formation in the Gas-Phase Photooxidation of Isoprene, *Science*, 2009, **325**, 730–733.
166 K. T. Malecha, Z. Cai and S. A. Nizkorodov, Photodegradation of Secondary Organic Aerosol Material Quantified with a Quartz Crystal Microbalance, *Environ. Sci. Technol. Lett.*, 2018, **5**, 366–371.
167 A. Hodzic, P. S. Kasibhatla, D. S. Jo, C. D. Cappa, J. L. Jimenez, S. Madronich and R. J. Park, Rethinking the global secondary organic aerosol (SOA) budget: stronger production, faster removal, shorter lifetime, *Atmos. Chem. Phys.*, 2016, **16**, 7917–7941.
168 K. T. Malecha and S. A. Nizkorodov, Photodegradation of Secondary Organic Aerosol Particles as a Source of Small, Oxygenated Volatile Organic Compounds, *Environ. Sci. Technol.*, 2016, **50**, 9990–9997.
169 J. P. S. Wong, S. Zhou and J. P. D. Abbatt, Changes in Secondary Organic Aerosol Composition and Mass due to Photolysis: Relative Humidity Dependence, *J. Phys. Chem. A*, 2015, **119**, 4309–4316.
170 L. H. Renbaum and G. D. Smith, Artifacts in measuring aerosol uptake kinetics: the roles of time, concentration and adsorption, *Atmos. Chem. Phys.*, 2011, **11**, 6881–6893.
171 E. Ahlberg, J. Falk, A. Eriksson, T. Holst, W. H. Brune, A. Kristensson, P. Roldin and B. Svenningsson, Secondary organic aerosol from VOC mixtures in an oxidation flow reactor, *Atmos. Environ.*, 2017, **161**, 210–220.
172 H. Zhang, D. R. Worton, S. Shen, T. Nah, G. Isaacman-VanWertz, K. R. Wilson and A. H. Goldstein, Fundamental Time Scales Governing Organic Aerosol Multiphase Partitioning and Oxidative Aging, *Environ. Sci. Technol.*, 2015, **49**, 9768–9777.
173 J. H. Slade and D. A. Knopf, Heterogeneous OH oxidation of biomass burning organic aerosol surrogate compounds: Assessment of volatilisation products and the role of OH concentration on the reactive uptake kinetics, *Phys. Chem. Chem. Phys.*, 2013, **15**, 5898–5915.
174 F. A. Houle, A. A. Wiegel and K. R. Wilson, Changes in Reactivity as Chemistry Becomes Confined to an Interface.

The Case of Free Radical Oxidation of C 30 H 62 Alkane by OH, *J. Phys. Chem. Lett.*, 2018, **9**, 1053–1057.

175 F. A. Houle, A. A. Wiegel and K. R. Wilson, Predicting Aerosol Reactivity Across Scales: from the Laboratory to the Atmosphere, *Environ. Sci. Technol.*, 2018, **52**, 13774–13781.

176 S. Gao, N. L. Ng, M. Keywood, V. Varutbangkul, R. Bahreini, A. Nenes, J. He, K. Y. Yoo, J. L. Beauchamp, R. P. Hodyss, R. C. Flagan and J. H. Seinfeld, Particle Phase Acidity and Oligomer Formation in Secondary Organic Aerosol, *Environ. Sci. Technol.*, 2004, **38**, 6582–6589.

177 A. Maisels, F. Jordan, F. E. Kruis and H. Fissan, A study of nanoparticle aerosol charging by Monte Carlo simulations, *J. Nanopart. Res.*, 2003, **5**, 225–235.

178 S. M. Charan, W. Kong, R. C. Flagan and J. H. Seinfeld, Effect of particle charge on aerosol dynamics in Teflon environmental chambers, *Aerosol Sci. Technol.*, 2018, **52**, 854–871.

179 NIST Chemistry Webbook, https://webbook.nist.gov/chemistry/.

180 D. M. Wood, Classical size dependence of the work function of small metallic spheres, *Phys. Rev. Lett.*, 1981, **46**, 749.

181 D. Matter, M. Mohr, W. Fendel, A. Schmidt-Ott and H. Burtscher, Multiple wavelength aerosol photoemission by excimer lamps, *J. Aerosol Sci.*, 1995, **26**, 1101–1115.

182 K. R. Wilson, D. S. Peterka, M. Jimenez-Cruz, S. R. Leone and M. Ahmed, VUV photoelectron imaging of biological nanoparticles: Ionization energy determination of nanophase glycine and phenylalanine-glycine-glycine, *Phys. Chem. Chem. Phys.*, 2006, **8**, 1884–1890.

183 B. Federer, H. Burtscher, A. Schimidt-Ott and H. C. Siegmann, Photoelectric charging and detection of ultrafine particles, *Atmos. Environ.*, 1983, **17**, 655–657.

184 H. Burtscher, L. Scherrer, H. C. Siegmann, A. Schmidt-Ott and B. Federer, Probing aerosols by photoelectric charging, *J. Appl. Phys.*, 1982, **53**, 3787–3791.

185 C. Y. Lim, D. H. Hagan, M. M. Coggon, A. R. Koss, K. Sekimoto, J. de Gouw, C. Warneke, C. D. Cappa and J. H. Kroll, Secondary organic aerosol formation from biomass burning emissions, *Atmos. Chem. Phys.*, 2019, **19**, 12797–12809.

186 S. A. Epstein, I. Riipinen and N. M. Donahue, A semiempirical correlation between enthalpy of vaporization and saturation concentration for organic aerosol, *Environ. Sci. Technol.*, 2010, **44**, 743–748.

187 K. Kristensen, Å. K. Watne, J. Hammes, A. Lutz, T. Petäjä, M. Hallquist, M. Bilde and M. Glasius, High-Molecular Weight Dimer Esters Are Major Products in Aerosols from α-Pinene Ozonolysis and the Boreal Forest, *Environ. Sci. Technol. Lett.*, 2016, **3**, 280–285.

188 A. C. Aiken, P. F. DeCarlo, J. H. Kroll, D. R. Worsnop, J. A. Huffman, K. S. Docherty, I. M. Ulbrich, C. Mohr, J. R. Kimmel, D. Sueper, Y. Sun, Q. Zhang, A. Trimborn, M. Northway, P. J. Ziemann, M. R. Canagaratna, T. B. Onasch, M. R. Alfarra, A. S. H. Prevot, J. Dommen, J. Duplissy, A. Metzger, U. Baltensperger and J. L. Jimenez, O/C and OM/OC Ratios of Primary, Secondary, and Ambient Organic Aerosols with High-Resolution Time-of-Flight Aerosol Mass Spectrometry, *Environ. Sci. Technol.*, 2008, **42**, 4478–4485.

189 J. H. Kroll, N. M. Donahue, J. L. Jimenez, S. H. Kessler, M. R. Canagaratna, K. R. Wilson, K. E. Altieri, L. R. Mazzoleni, A. S. Wozniak, H. Bluhm, E. R. Mysak, J. D. Smith, C. E. Kolb and D. R. Worsnop, Carbon oxidation state as a metric for describing the chemistry of atmospheric organic aerosol, *Nat. Chem.*, 2011, **3**, 133–139.

190 J. L. Jimenez, M. R. Canagaratna, N. M. Donahue, A. S. H. Prevot, Q. Zhang, J. H. Kroll, P. F. DeCarlo, J. D. Allan, H. Coe, N. L. Ng, A. C. Aiken, K. S. Docherty, I. M. Ulbrich, A. P. Grieshop, A. L. Robinson, J. Duplissy, J. D. Smith, K. R. Wilson, V. A. Lanz, C. Hueglin, Y. L. Sun, J. Tian, A. Laaksonen, T. Raatikainen, J. Rautiainen, P. Vaattovaara, M. Ehn, M. Kulmala, J. M. Tomlinson, D. R. Collins, M. J. Cubison, E. J. Dunlea, J. A. Huffman, T. B. Onasch, M. R. Alfarra, P. I. Williams, K. Bower, Y. Kondo, J. Schneider, F. Drewnick, S. Borrmann, S. Weimer, K. Demerjian, D. Salcedo, L. Cottrell, R. Griffin, A. Takami, T. Miyoshi, S. Hatakeyama, A. Shimono, J. Y. Sun, Y. M. Zhang, K. Dzepina, J. R. Kimmel, D. Sueper, J. T. Jayne, S. C. Herndon, A. M. Trimborn, L. R. Williams, E. C. Wood, A. M. Middlebrook, C. E. Kolb, U. Baltensperger and D. R. Worsnop, Evolution of organic aerosols in the atmosphere, *Science*, 2009, **326**, 1525–1529.

191 W. Xu, P. Croteau, L. Williams, M. Canagaratna, T. Onasch, E. Cross, X. Zhang, W. Robinson, D. Worsnop and J. Jayne, Laboratory characterization of an aerosol chemical speciation monitor with PM 2.5 measurement capability, *Aerosol Sci. Technol.*, 2017, **51**, 69–83.

192 A. Virtanen, J. Joutsensaari, T. Koop, J. Kannosto, P. Yli-Pirila, J. Leskinen, J. M. Makela, J. K. Holopainen, U. Poschl, M. Kulmala, D. R. Worsnop and A. Laaksonen, An amorphous solid state of biogenic secondary organic aerosol particles, *Nature*, 2010, **467**, 824–827.

193 D. A. Knopf, P. A. Alpert and B. Wang, The Role of Organic Aerosol in Atmospheric Ice Nucleation: A Review, *ACS Earth Space Chem.*, 2018, **2**, 168–202.

194 N. M. Donahue, J. H. Kroll, S. N. Pandis and A. L. Robinson, A two-dimensional volatility basis set – Part 2: Diagnostics of organic-aerosol evolution, *Atmos. Chem. Phys.*, 2012, **12**, 615–634.

195 J. A. Huffman, K. S. Docherty, C. Mohr, M. J. Cubison, I. M. Ulbrich, P. J. Ziemann, T. B. Onasch and J. L. Jimenez, Chemically-resolved volatility measurements of organic aerosol from different sources, *Environ. Sci. Technol.*, 2009, **43**, 5351–5357.

196 I. M. Ulbrich, M. R. Canagaratna, Q. Zhang, D. R. Worsnop and J. L. Jimenez, Interpretation of organic components from Positive Matrix Factorization of aerosol mass spectrometric data, *Atmos. Chem. Phys.*, 2009, **9**, 2891–2918.

197 Q. Zhang, J. L. Jimenez, M. R. Canagaratna, I. M. Ulbrich, N. L. Ng, D. R. Worsnop and Y. Sun, Understanding atmospheric organic aerosols *via* factor analysis of aerosol mass spectrometry: A review, *Anal. Bioanal. Chem.*, 2011, **401**, 3045–3067.

198 M. Kulmala, H. Vehkamaki, T. Petajda, M. Dal Maso, A. Lauri, V.-M. M. Kerminen, W. Birmili, P. H. H. McMurry,

H. Vehkamäki, T. Petäjä, M. Dal Maso, A. Lauri, V.-M. M. Kerminen, W. Birmili and P. H. H. McMurry, Formation and growth rates of ultrafine atmospheric particles: a review of observations, *J. Aerosol Sci.*, 2004, **35**, 143–176.

199 T. Moise, J. M. Flores and Y. Rudich, Optical Properties of Secondary Organic Aerosols and Their Changes by Chemical Processes, *Chem. Rev.*, 2015, **115**, 4400–4439.

200 P. H. Chowdhury, Q. He, T. Lasitza Male, W. H. Brune, Y. Rudich and M. Pardo, Exposure of Lung Epithelial Cells to Photochemically Aged Secondary Organic Aerosol Shows Increased Toxic Effects, *Environ. Sci. Technol. Lett.*, 2018, **5**, 424–430.

201 X. Zhang, A. T. Lambe, M. A. Upshur, W. A. Brooks, A. Gray Bé, R. J. Thomson, F. M. Geiger, J. D. Surratt, Z. Zhang, A. Gold, S. Graf, M. J. Cubison, M. Groessl, J. T. Jayne, D. R. Worsnop and M. R. Canagaratna, Highly Oxygenated Multifunctional Compounds in α-Pinene Secondary Organic Aerosol, *Environ. Sci. Technol.*, 2017, **51**, 5932–5940.

202 A. R. Whitehill, B. Jiang, H. Guo and S. Ono, SO_2 photolysis as a source for sulfur mass-independent isotope signatures in stratospehric aerosols, *Atmos. Chem. Phys.*, 2015, **15**, 1843–1864.

203 A. T. Lambe, P. S. Chhabra, T. B. Onasch, W. H. Brune, J. F. Hunter, J. H. Kroll, M. J. Cummings, J. F. Brogan, Y. Parmar, D. R. Worsnop, C. E. Kolb and P. Davidovits, Effect of oxidant concentration, exposure time, and seed particles on secondary organic aerosol chemical composition and yield, *Atmos. Chem. Phys.*, 2015, **15**, 3063–3075.

204 E. A. Bruns, I. El Haddad, A. Keller, F. Klein, N. K. Kumar, S. M. Pieber, I. El Haddad, A. Keller, F. Klein, N. K. Kumar, S. M. Pieber, J. C. Corbin, J. G. Slowik, W. H. Brune, U. Baltensperger and A. S. H. Prévôt, Inter-comparison of laboratory smog chamber and flow reactor systems on organic aerosol yield and composition, *Atmos. Meas. Tech.*, 2015, **8**, 2315–2332.

205 A. T. Lambe, A. T. Ahern, J. P. Wright, D. R. Croasdale, P. Davidovits and T. B. Onasch, Oxidative aging and cloud condensation nuclei activation of laboratory combustion soot, *J. Aerosol Sci.*, 2015, **79**, 31–39.

206 W.-S. W. DeRieux, Y. Li, P. Lin, J. Laskin, A. Laskin, A. K. Bertram, S. A. Nizkorodov and M. Shiraiwa, Predicting the glass transition temperature and viscosity of secondary organic material using molecular composition, *Atmos. Chem. Phys.*, 2018, **18**, 6331–6351.

207 M. Shiraiwa, Y. Li, A. P. Tsimpidi, V. A. Karydis, T. Berkemeier, S. N. Pandis, J. Lelieveld, T. Koop and U. Pöschl, Global distribution of particle phase state in atmospheric secondary organic aerosols, *Nat. Commun.*, 2017, **8**, 15002.

208 B. Wang, A. T. Lambe, P. Massoli, T. B. Onasch, P. Davidovits, D. R. Worsnop and D. A. Knopf, The deposition ice nucleation and immersion freezing potential of amorphous secondary organic aerosol: Pathways for ice and mixed-phase cloud formation, *J. Geophys. Res.*, 2012, **117**, D16209.

209 A. L. Hodshire, B. B. Palm, M. L. Alexander, Q. Bian, P. Campuzano-Jost, E. S. Cross, D. A. Day, S. S. de Sá, A. B. Guenther, A. Hansel, J. F. Hunter, W. Jud, T. Karl, S. Kim, J. H. Kroll, J. Park, Z. Peng, R. Seco, J. N. Smith, J. L. Jimenez and J. R. Pierce, Constraining nucleation, condensation, and chemistry in oxidation flow reactors using size-distribution measurements and aerosol microphysical modeling, *Atmos. Chem. Phys.*, 2018, **18**, 12433–12460.

210 C. D. Cappa, D. L. Che, S. H. Kessler, J. H. Kroll and K. R. Wilson, Variations in organic aerosol optical and hygroscopic properties upon heterogeneous OH oxidation, *J. Geophys. Res.*, 2011, **116**, D15204.

211 Q. Chen, F. Ikemori and M. Mochida, Light Absorption and Excitation–Emission Fluorescence of Urban Organic Aerosol Components and Their Relationship to Chemical Structure, *Environ. Sci. Technol.*, 2016, **50**, 10859–10868.

212 S. M. Phillips and G. D. Smith, Light Absorption by Charge Transfer Complexes in Brown Carbon Aerosols, *Environ. Sci. Technol. Lett.*, 2014, **1**, 382–386.

213 P. Lin, L. T. Fleming, S. A. Nizkorodov, J. Laskin and A. Laskin, Comprehensive Molecular Characterization of Atmospheric Brown Carbon by High Resolution Mass Spectrometry with Electrospray and Atmospheric Pressure Photoionization, *Anal. Chem.*, 2018, **90**, 12493–12502.

214 W. Y. Tuet, Y. Chen, L. Xu, S. Fok, D. Gao, R. J. Weber and N. L. Ng, Chemical oxidative potential of secondary organic aerosol (SOA) generated from the photooxidation of biogenic and anthropogenic volatile organic compounds, *Atmos. Chem. Phys.*, 2017, **17**, 839–853.

215 A. J. Kramer, W. Rattanavaraha, Z. Zhang, A. Gold, J. D. Surratt and Y. H. Lin, Assessing the oxidative potential of isoprene-derived epoxides and secondary organic aerosol, *Atmos. Environ.*, 2016, **130**, 211–218.

216 J. T. Bates, T. Fang, V. Verma, L. Zeng, R. J. Weber, P. E. Tolbert, J. Y. Abrams, S. E. Sarnat, M. Klein, J. A. Mulholland and A. G. Russell, Review of Acellular Assays of Ambient Particulate Matter Oxidative Potential: Methods and Relationships with Composition, Sources, and Health Effects, *Environ. Sci. Technol.*, 2019, **53**, 4003–4019.

217 U. Pöschl and M. Shiraiwa, Multiphase Chemistry at the Atmosphere–Biosphere Interface Influencing Climate and Public Health in the Anthropocene, *Chem. Rev.*, 2015, **115**, 4440–4475.

218 J. L. Jimenez, Z. Peng and B. B. Palm, PAM Wiki: Estimation Equations, https://sites.google.com/site/pamwiki/hardware/estimation-equations, accessed 6 April 2019.

219 Z. Peng and J. L. Jimenez, KinSim: A Research-Grade, User-Friendly, Visual Kinetics Simulator for Chemical-Kinetics and Environmental-Chemistry Teaching, *J. Chem. Educ.*, 2019, **96**, 806–811.

220 N. Wang, S. D. Jorga, J. R. Pierce, N. M. Donahue and S. N. Pandis, Particle wall-loss correction methods in smog chamber experiments, *Atmos. Meas. Tech.*, 2018, **11**, 6577–6588.

221 Y. Huang, R. Zhao, S. M. Charan, C. M. Kenseth, X. Zhang and J. H. Seinfeld, Unified Theory of Vapor–Wall Mass Transport in Teflon-Walled Environmental Chambers, *Environ. Sci. Technol.*, 2018, **52**, 2134–2142.

222 J. C. Rivera-Rios, T. B. Nguyen, J. D. Crounse, W. Jud, J. M. St. Clair, T. Mikoviny, J. B. Gilman, B. M. Lerner,

J. B. Kaiser, J. de Gouw, A. Wisthaler, A. Hansel, P. O. Wennberg, J. H. Seinfeld and F. N. Keutsch, Conversion of hydroperoxides to carbonyls in field and laboratory instrumentation: Observational bias in diagnosing pristine versus anthropogenically controlled atmospheric chemistry, *Geophys. Res. Lett.*, 2014, **41**, 8645–8651.

223 M. K. Bernett and W. A. Zisman, Effect of adsorbed water on wetting properties of borosilicate glass, quartz, and sapphire, *J. Colloid Interface Sci.*, 1969, **29**, 413–423.

224 X. Liu, B. Deming, D. Pagonis, D. A. Day, B. B. Palm, R. Talukdar, J. M. Roberts, P. R. Veres, J. E. Krechmer, J. A. Thornton, J. A. de Gouw, P. J. Ziemann and J. L. Jimenez, Effects of gas–wall interactions on measurements of semivolatile compounds and small polar molecules, *Atmos. Meas. Tech.*, 2019, **12**, 3137–3149.

225 K. L. Pereira, G. Rovelli, Y. C. Song, A. W. Mayhew, J. P. Reid and J. F. Hamilton, A new aerosol flow reactor to study secondary organic aerosol, *Atmos. Meas. Tech.*, 2019, **12**, 4519–4541.

226 A. T. Lambe, T. B. Onasch, D. R. Croasdale, J. P. Wright, A. T. Martin, J. P. Franklin, P. Massoli, J. H. Kroll, M. R. Canagaratna, W. H. Brune, D. R. Worsnop and P. Davidovits, Transitions from Functionalization to Fragmentation Reactions of Laboratory Secondary Organic Aerosol (SOA) Generated from the OH Oxidation of Alkane Precursors, *Environ. Sci. Technol.*, 2012, **46**, 5430–5437.

227 P. F. Liu, N. Abdelmalki, H.-M. Hung, Y. Wang, W. H. Brune and S. T. Martin, Ultraviolet and visible complex refractive indices of secondary organic material produced by photooxidation of the aromatic compounds toluene and m-Xylene, *Atmos. Chem. Phys.*, 2015, **15**, 1435–1446.

228 Q. Zhang, M. R. Canagaratna, J. T. Jayne, D. R. Worsnop and J.-L. Jimenez, Time- and size-resolved chemical composition of submicron particles in Pittsburgh: Implications for aerosol sources and processes, *J. Geophys. Res.*, 2005, **110**, D07S09.

229 C. Reche, M. Viana, T. Moreno, X. Querol, A. Alastuey, J. Pey, M. Pandolfi, A. Prévôt, C. Mohr, A. Richard, B. Artiñano, F. J. Gomez-Moreno and N. Cots, Peculiarities in atmospheric particle number and size-resolved speciation in an urban area in the western Mediterranean: Results from the DAURE campaign, *Atmos. Environ.*, 2011, **45**, 5282–5293.

230 W. Hu, M. Hu, W. Hu, J. L. Jimenez, B. Yuan, W. Chen, M. Wang, Y. Wu, C. Chen, Z. Wang, J. Peng, L. Zeng and M. Shao, Chemical composition, sources, and aging process of submicron aerosols in Beijing: Contrast between summer and winter, *J. Geophys. Res.: Atmos.*, 2016, **121**, 1955–1977.

231 D. Mitroo, J. Wu, P. F. Colletti, S. S. Lee, M. J. Walker, W. H. Brune, B. J. Williams and J. D. Fortner, Atmospheric Reactivity of Fullerene (C_{60}) Aerosols, *ACS Earth Space Chem.*, 2018, **2**, 95–102.

232 M. F. Link, J. Kim, G. Park, T. Lee, T. Park, Z. Bin Babar, K. Sung, P. Kim, S. Kang, J. S. Kim, Y. Choi, J. Son, H.-J. Lim and D. K. Farmer, Elevated production of NH4NO3 from the photochemical processing of vehicle exhaust: Implications for air quality in the Seoul Metropolitan Region, *Atmos. Environ.*, 2017, **156**, 95–101.

233 E. Saukko, A. T. Lambe, P. Massoli, T. Koop, J. P. Wright, D. R. Croasdale, D. A. Pedernera, T. B. Onasch, A. Laaksonen, P. Davidovits, D. R. Worsnop and A. Virtanen, Humidity-dependent phase state of SOA particles from biogenic and anthropogenic precursors, *Atmos. Chem. Phys.*, 2012, **12**, 7517–7529.

234 R. Li, B. B. Palm, A. Borbon, M. Graus, C. Warneke, A. M. Ortega, D. A. Day, W. H. Brune, J. L. Jimenez and J. A. de Gouw, Laboratory Studies on Secondary Organic Aerosol Formation from Crude Oil Vapors, *Environ. Sci. Technol.*, 2013, **47**, 12566–12574.

235 A. T. Lambe, C. D. Cappa, P. Massoli, T. B. Onasch, S. D. Forestieri, A. T. Martin, M. J. Cummings, D. R. Croasdale, W. H. Brune, D. R. Worsnop and P. Davidovits, Relationship between Oxidation Level and Optical Properties of Secondary Organic Aerosol, *Environ. Sci. Technol.*, 2013, **47**, 6349–6357.

236 B. Friedman, P. Brophy, W. H. Brune and D. K. Farmer, Anthropogenic Sulfur Perturbations on Biogenic Oxidation: SO 2 Additions Impact Gas-Phase OH Oxidation Products of α- and β-Pinene, *Environ. Sci. Technol.*, 2016, **50**, 1269–1279.

237 P. S. Chhabra, A. T. Lambe, M. R. Canagaratna, H. Stark, J. T. Jayne, T. B. Onasch, P. Davidovits, J. R. Kimmel and D. R. Worsnop, Application of high-resolution time-of-flight chemical ionization mass spectrometry measurements to estimate volatility distributions of α-pinene and naphthalene oxidation products, *Atmos. Meas. Tech.*, 2015, **8**, 1–18.

238 R. Bahreini, A. M. Middlebrook, C. A. Brock, J. A. de Gouw, S. A. McKeen, L. R. Williams, K. E. Daumit, A. T. Lambe, P. Massoli, M. R. Canagaratna, R. Ahmadov, A. J. Carrasquillo, E. S. Cross, B. Ervens, J. S. Holloway, J. F. Hunter, T. B. Onasch, I. B. Pollack, J. M. Roberts, T. B. Ryerson, C. Warneke, P. Davidovits, D. R. Worsnop and J. H. Kroll, Mass spectral analysis of organic aerosol formed downwind of the Deepwater Horizon oil spill: field studies and laboratory confirmations, *Environ. Sci. Technol.*, 2012, **46**, 8025–8034.

239 J. C. Charnawskas, P. A. Alpert, A. T. Lambe, T. Berkemeier, R. E. O'Brien, P. Massoli, T. B. Onasch, M. Shiraiwa, R. C. Moffet, M. K. Gilles, P. Davidovits, D. R. Worsnop and D. A. Knopf, Condensed-phase biogenic–anthropogenic interactions with implications for cold cloud formation, *Faraday Discuss.*, 2017, **200**, 165–194.

240 B. Friedman, M. F. Link, S. R. Fulgham, P. Brophy, A. Galang, W. H. Brune, S. H. Jathar and D. K. Farmer, Primary and Secondary Sources of Gas-Phase Organic Acids from Diesel Exhaust, *Environ. Sci. Technol.*, 2017, **51**, 10872–10880.

241 B. J. Sumlin, A. Pandey, M. J. Walker, R. S. Pattison, B. J. Williams and R. K. Chakrabarty, Atmospheric Photooxidation Diminishes Light Absorption by Primary Brown Carbon Aerosol from Biomass Burning, *Environ. Sci. Technol. Lett.*, 2017, **4**, 540–545.

242 C. F. Fortenberry, M. J. Walker, Y. Zhang, D. Mitroo, W. H. Brune and B. J. Williams, Bulk and molecular-level characterization of laboratory-aged biomass burning organic aerosol from oak leaf and heartwood fuels, *Atmos. Chem. Phys.*, 2018, **18**, 2199–2224.

243 S. M. Pieber, N. K. Kumar, F. Klein, P. Comte, D. Bhattu, J. Dommen, E. A. Bruns, D. Kılıç, I. El Haddad, A. Keller, J. Czerwinski, N. Heeb, U. Baltensperger, J. G. Slowik and A. S. H. Prévôt, Gas-phase composition and secondary organic aerosol formation from standard and particle filter-retrofitted gasoline direct injection vehicles investigated in a batch and flow reactor, *Atmos. Chem. Phys.*, 2018, **18**, 9929–9954.

244 D. Sengupta, V. Samburova, C. Bhattarai, E. Kirillova, L. Mazzoleni, M. Iaukea-Lum, A. Watts, H. Moosmüller and A. Khlystov, Light absorption by polar and non-polar aerosol compounds from laboratory biomass combustion, *Atmos. Chem. Phys.*, 2018, **18**, 10849–10867.

245 Q. He, N. Bluvshtein, L. Segev, D. Meidan, J. M. Flores, S. S. Brown, W. Brune and Y. Rudich, Evolution of the Complex Refractive Index of Secondary Organic Aerosols during Atmospheric Aging, *Environ. Sci. Technol.*, 2018, **52**, 3456–3465.

246 A. Buchholz, A. T. Lambe, A. Ylisirniö, Z. Li, O.-P. Tikkanen, C. Faiola, E. Kari, L. Hao, O. Luoma, W. Huang, C. Mohr, D. R. Worsnop, S. A. Nizkorodov, T. Yli-Juuti, S. Schobesberger and A. Virtanen, Insights into the O:C-dependent mechanisms controlling the evaporation of α-pinene secondary organic aerosol particles, *Atmos. Chem. Phys.*, 2019, **19**, 4061–4073.

247 J. Martinsson, A. C. Eriksson, I. E. Nielsen, V. B. Malmborg, E. Ahlberg, C. Andersen, R. Lindgren, R. Nyström, E. Z. Nordin, W. H. Brune, B. Svenningsson, E. Swietlicki, C. Boman and J. H. Pagels, Impacts of Combustion Conditions and Photochemical Processing on the Light Absorption of Biomass Combustion Aerosol, *Environ. Sci. Technol.*, 2015, **49**, 14663–14671.

248 P. Karjalainen, H. Timonen, E. Saukko, H. Kuuluvainen, S. Saarikoski, P. Aakko-Saksa, T. Murtonen, M. Bloss, M. Dal Maso, P. Simonen, E. Ahlberg, B. Svenningsson, W. H. Brune, R. Hillamo, J. Keskinen and T. Rönkkö, Time-resolved characterization of primary particle emissions and secondary particle formation from a modern gasoline passenger car, *Atmos. Chem. Phys.*, 2016, **16**, 8559–8570.

249 S. H. Jathar, B. Friedman, A. A. Galang, M. F. Link, P. Brophy, J. Volckens, S. Eluri and D. K. Farmer, Linking Load, Fuel, and Emission Controls to Photochemical Production of Secondary Organic Aerosol from a Diesel Engine, *Environ. Sci. Technol.*, 2017, **51**, 1377–1386.

250 H. Timonen, P. Karjalainen, E. Saukko, S. Saarikoski, P. Aakko-Saksa, P. Simonen, T. Murtonen, M. Dal Maso, H. Kuuluvainen, M. Bloss, E. Ahlberg, B. Svenningsson, J. Pagels, W. H. Brune, J. Keskinen, D. R. Worsnop, R. Hillamo and T. Rönkkö, Influence of fuel ethanol content on primary emissions and secondary aerosol formation potential for a modern flex-fuel gasoline vehicle, *Atmos. Chem. Phys.*, 2017, **17**, 5311–5329.

251 S. M. Pieber, A. Kambolis, D. Ferri, D. Bhattu, E. A. Bruns, M. Elsener, O. Kröcher, A. S. H. Prévôt and U. Baltensperger, Mitigation of Secondary Organic Aerosol Formation from Log Wood Burning Emissions by Catalytic Removal of Aromatic Hydrocarbons, *Environ. Sci. Technol.*, 2018, **52**, 13381–13390.

252 N. J. Janechek, R. F. Marek, N. Bryngelson, A. Singh, R. L. Bullard, W. H. Brune and C. O. Stanier, Physical properties of secondary photochemical aerosol from OH oxidation of a cyclic siloxane, *Atmos. Chem. Phys.*, 2019, **19**, 1649–1664.

253 A. Pajunoja, A. T. Lambe, J. Hakala, N. Rastak, M. J. Cummings, J. F. Brogan, L. Hao, M. Paramonov, J. Hong, N. L. Prisle, J. Malila, S. Romakkaniemi, K. E. J. Lehtinen, A. Laaksonen, M. Kulmala, P. Massoli, T. B. Onasch, N. M. Donahue, I. Riipinen, P. Davidovits, D. R. Worsnop, T. Petäjä and A. Virtanen, Adsorptive uptake of water by semisolid secondary organic aerosols, *Geophys. Res. Lett.*, 2015, **42**, 3063–3068.

254 D. M. Lienhard, A. J. Huisman, U. K. Krieger, Y. Rudich, C. Marcolli, B. P. Luo, D. L. Bones, J. P. Reid, A. T. Lambe, M. R. Canagaratna, P. Davidovits, T. B. Onasch, D. R. Worsnop, S. S. Steimer, T. Koop and T. Peter, Viscous organic aerosol particles in the upper troposphere: diffusivity-controlled water uptake and ice nucleation?, *Atmos. Chem. Phys.*, 2015, **15**, 13599–13613.

255 G. P. Schill, S. H. Jathar, J. K. Kodros, E. J. T. Levin, A. M. Galang, B. Friedman, M. F. Link, D. K. Farmer, J. R. Pierce, S. M. Kreidenweis and P. J. DeMott, Ice-nucleating particle emissions from photochemically aged diesel and biodiesel exhaust, *Geophys. Res. Lett.*, 2016, **43**, 5524–5531.

256 Å. K. Watne, J. Westerlund, Å. M. Hallquist, W. H. Brune and M. Hallquist, Ozone and OH-induced oxidation of monoterpenes: Changes in the thermal properties of secondary organic aerosol (SOA), *J. Aerosol Sci.*, 2017, **114**, 31–41.

257 M. F. Link, B. Friedman, R. Fulgham, P. Brophy, A. Galang, S. H. Jathar, P. Veres, J. M. Roberts and D. K. Farmer, Photochemical processing of diesel fuel emissions as a large secondary source of isocyanic acid (HNCO), *Geophys. Res. Lett.*, 2016, **43**, 4033–4041.

258 J. E. Krechmer, M. Groessl, X. Zhang, H. Junninen, P. Massoli, A. T. Lambe, J. R. Kimmel, M. J. Cubison, S. Graf, Y.-H. Lin, S. H. Budisulistiorini, H. Zhang, J. D. Surratt, R. Knochenmuss, J. T. Jayne, D. R. Worsnop, J.-L. Jimenez and M. R. Canagaratna, Ion mobility spectrometry–mass spectrometry (IMS–MS) for on- and offline analysis of atmospheric gas and aerosol species, *Atmos. Meas. Tech.*, 2016, **9**, 3245–3262.

